

Winter 12-15-2014

Kinetic Analysis and Inhibition Studies of Iron-Dependent Histone Demethylases

Barbara Gordon Cascella
Washington University in St. Louis

Follow this and additional works at: https://openscholarship.wustl.edu/art_sci_etds

 Part of the [Chemistry Commons](#)

Recommended Citation

Cascella, Barbara Gordon, "Kinetic Analysis and Inhibition Studies of Iron-Dependent Histone Demethylases" (2014). *Arts & Sciences Electronic Theses and Dissertations*. 349.
https://openscholarship.wustl.edu/art_sci_etds/349

This Dissertation is brought to you for free and open access by the Arts & Sciences at Washington University Open Scholarship. It has been accepted for inclusion in Arts & Sciences Electronic Theses and Dissertations by an authorized administrator of Washington University Open Scholarship. For more information, please contact digital@wumail.wustl.edu.

WASHINGTON UNIVERSITY IN ST. LOUIS

Department of Chemistry

Dissertation Examination Committee:

Liviu M. Mirica, Chair

Michael Gross

Joseph Jez

John-Stephen Taylor

Timothy Wencewicz

Kinetic Analysis and Inhibition Studies of Iron-Dependent Histone Demethylases

by

Barbara Gordon Cascella

A dissertation presented to the
Graduate School of Arts and Sciences
of Washington University in
partial fulfillment of the
requirements for the degree
of Doctor of Philosophy

December 2014
St. Louis, Missouri

© 2014, Barbara Gordon Casella

Table of Contents

List of Figures.....	v
List of Schemes	viii
List of Tables.....	ix
List of Abbreviations.....	x
Acknowledgments.....	xii
Abstract	xiv
Chapter 1: Introduction	1
1.1 Covalent Modification of Chromatin.....	1
1.2 Dynamic Methylation and Demethylation of Histone Lysine Residues	6
1.3 Catalytic Mechanisms of Histone Lysine Demethylation	7
1.3.1 Flavin-Dependent Histone Demethylases	7
1.3.2 Iron-Dependent Histone Demethylases.....	10
1.4 HDMs in DNA Repair.....	15
1.5 HDMs in Cancer	16
1.5.1 Flavin-Dependent Histone Demethylases	16
1.5.2 Iron-Dependent Histone Demethylases.....	17
1.6 Project Goals.....	19
1.7 References	20
Chapter 2: Kinetic Analysis of Iron-Dependent Histone Demethylases: α -Ketoglutarate Substrate Inhibition and Potential Relevance to the Regulation of Histone Demethylation in Cancer Cells	28
2.1 Introduction	28
2.2 Methods	29
2.2.1 Protein Expression and Purification.....	29
2.2.2 Formaldehyde Dehydrogenase Coupled Fluorescence Assay.....	31
2.2.3 Dioxygen Consumption Assay.....	33
2.2.4 MALDI-TOF Mass Spectrometry Assay	34
2.2.5 Docking Studies of KDM4A and KDM4C with α KG	35
2.2.6 Crystallography.....	35

2.3	Results and Discussion	36
2.4	Conclusions	54
2.5	References	55
Chapter 3: Survey of Simple Primary- and Secondary-Substrate Analog Inhibitors of Iron-Dependent Histone Demethylases		61
3.1	Introduction	61
3.2	Methods	66
3.2.1	Synthesis of Primary Substrate Analogs	66
3.2.2	Synthesis of Secondary Substrate Analogs	70
3.2.3	MALDI-TOF Mass Spectrometry Inhibition Assay	74
3.2.4	Enzyme-Templated Cycloaddition Reaction	75
3.3	Results and Discussion	75
3.4	Conclusions	84
3.5	References	85
Chapter 4: Inhibition of JmjC-Histone Demethylases with a Modified Histone H3 Peptide.....		89
4.1	Introduction	89
4.2	Methods	92
4.2.1	Synthesis of a Modified Histone H3 Peptide.....	92
4.2.2	MALDI-TOF Mass Spectrometry Assays.....	93
4.2.3	Docking Studies of ARK(N ^ε - bis(propargyl))ST with KDM4A	95
4.3	Results and Discussion	96
4.4	Conclusions	107
4.5	References	108
Chapter 5: Inhibition and Crystallography Studies of KDM4A with the Small Molecule JIB-04....		112
5.1	Introduction	112
5.2	Methods	114
5.2.1	Synthesis of JIB-04	114
5.2.2	Inhibition of KDM4A by JIB-04.....	115
5.2.3	Docking Studies of KDM4A with JIB-04 Isomers	117
5.2.4	Crystallography.....	117
5.2.5	Stability of JIB-04 in Aqueous Solution	118

5.3	Results and Discussion	119
5.4	Conclusions	130
5.5	References	131
Chapter 6: Conclusions and Future Directions		133
Appendix A: Supplementary Information for Chapter 2		137
Appendix B: Supplementary Information for Chapter 4		144
Appendix C: Supplementary Information for Chapter 5		154
Curriculum Vitae		159

List of Figures

1.1	The nucleosome, with the four core histones in different colors (PDB 1AOI)	2
1.2	HP1's interaction with H3K9me ₃ via cation- π interactions	3
1.3	Epigenetic events and their effects on chromatin condensation	4
1.4	Acetylation of lysine residues leads to neutralization of charge	4
1.5	Histone lysine methylation as carried out by SAM-dependent KMTs	5
1.6	Proposed mechanism of flavin-dependent HDMs	8
1.7	The oxidation of formaldehyde to formate	9
1.8	A model of KDM1A in complex with H3K4me ₂	10
1.9	The KDM4A active site, with iron coordinated to N-oxalylglycine and O ₂	11
1.10	Mechanism of iron-dependent HDMs, where Lys-CH ₃ is the histone lysine substrate	12
1.11	Tranylcypromine and a tranylcypromine-FAD adduct	17
1.12	Two specific inhibitors of JmjC-HDMs	18
2.1	Coomassie Blue stained 4-20% SDS-PAGE gel of purified KDM4A, KDM4E, and KDM4C	30
2.2	Observed lag phase in NADH production at high peptide substrate concentrations	32
2.3	Variable H3 ₍₇₋₁₄₎ K9me ₃ K _m plots obtained using the FDH-coupled assay	39
2.4	Variable H3 ₍₇₋₁₄₎ K9me ₃ K _m plots obtained from the O ₂ consumption assay for 1.6 μ M KDM4A, 3 μ M KDM4C, and 2.1 μ M KDM4E	40
2.5	Variable O ₂ K _m plots obtained using the O ₂ electrode assay for 2 μ M KDM4A, 3 μ M KDM4C, and 2.1 μ M KDM4E	41
2.6	Variable α KG K _m plots obtained for KDM4A and KDM4E using the O ₂ consumption and FDH coupled assays	43
2.7	Inhibition of KDM4C by α KG, as measured by the O ₂ consumption and FDH coupled assays	44
2.8	Variable O ₂ K _m plots for 3 μ M KDM4C obtained at varying α KG concentrations	45
2.9	Double reciprocal plot of 1/rate of O ₂ consumed vs. 1/[O ₂] obtained using the O ₂ consumption assay, suggesting α KG competitive inhibition of KDM4C with respect to O ₂	46
2.10	Variable H3 ₍₇₋₁₄₎ K9me ₃ K _m plots obtained using the FDH coupled assay for KDM4C at α KG concentrations of 300 μ M, 2 mM, and 5 mM, and double reciprocal plots for	

	KDM4C inhibition by α KG with respect to H3K9me ₃ , showing a mixed-mode, nonlinear type of inhibition	47
2.11	Variable H3 ₍₇₋₁₄₎ K9me ₃ K _m plots obtained using the O ₂ electrode assay for 3 μ M KDM4C at α KG concentrations of 300 μ M, 2 mM, and 5 mM, and double reciprocal plots for KDM4C inhibition by α KG with respect to H3K9me ₃ , showing a mixed-mode, nonlinear type of inhibition	48
2.12	The activity of KDM4C is optimized at 300 μ M α KG in vitro	49
2.13	Docking studies of <i>N</i> -oxalylglycine and α KG in the active sites of KDM4A (PDB 2OQ7) and KDM4C (PDB 2XML)	50
2.14	A comparison of docked α KG – Ni(II) distances in the active sites of KDM4A and KDM4C	51
2.15	The predicted polar contacts for a second molecule of α KG in the active sites of KDM4A and KDM4C	52
2.16	The experimental $2F_o - F_c$ electron density, displayed as blue mesh, is shown for the α KG ligand, which coordinates in a bidentate fashion to Ni(II) (substituting for Fe(II))	53
2.17	KDM4A in complex with Ni(II) and α -ketoglutarate or <i>N</i> -oxalylglycine (distances in Å; (<i>left</i>) unpublished structure, (<i>right</i>) PDB 2OQ7).....	53
2.18	Resonance of <i>N</i> -oxalylglycine	54
3.1	Two primary-substrate competitors of JmjC-HDMs	62
3.2	Catalytic mechanism of JmjC-HDMs	63
3.3	Compounds tested as inhibitors of JmjC-HDMs	65
3.4	Recognition of H3K9me ₃ and NOG in the KDM4A active site	76
3.5	KDM4E inhibition by primary substrate analogs at two concentrations of H3 ₍₇₋₁₄₎ K9me ₃	78
3.6	KDM4E inhibition by secondary substrate analogs at two concentrations of α KG	81
3.7	ESI-MS of 5 with excess N ₃ ⁻ in water at 0 minutes and 30 minutes. The peak at m/z of 156 corresponds to the alkyne starting material 5 , m/z at 199 corresponds to the triazole product 6	84
4.1	A substrate-based inhibitor, selective for KDM4C over PHF8	90
4.2	The novel histone H3 peptide, ARK ⁺ (N ^E -methyl bis(propargyl))ST, designed to selectively inhibit KDM4C over KDM4A	97
4.3	(<i>left</i>) H3 ₍₇₋₁₄₎ K9me ₃ crystallized in the KDM4A active site; (<i>right</i>) H3 ₍₇₋₁₄₎ K9(bis(propargyl)) docked into the KDM4A active site	98
4.4	Selective inhibition of KDM4C over KDM4A by ARK(N ^E -bis(propargyl))ST	99

4.5	Inhibition of KDM4A and KDM4C by $\text{ARK}^+(\text{N}^\text{e}\text{-methyl bis(propargyl)})\text{ST}$	100
4.6	Minimal inhibition of KDM4A and KDM4C using a methyl iodide solution	102
4.7	MALDI-TOF spectra obtained from KDM4C incubation with ARK^+ST for 0 minutes and 60 minutes	103
4.8	N_3^- is a weak inhibitor of KDM4A and KDM4C, as shown by MALDI-TOF MS	104
4.9	MALDI-TOF MS results for KDM4C-Fe-azide and KDM4C-Ni-azide incubations with $\text{ARK}^+(\text{N}^\text{e}\text{-methyl bis(propargyl)})\text{ST}$	106
5.1	JIB-04 E- and Z- isomers	113
5.2	Mild inhibition of KDM4A by JIB-04 as shown by the O_2 consumption assay	120
5.3	Inhibition of KDM4A by JIB-04 following pre-incubation with holoenzyme, as found by MALDI-TOF MS	121
5.4	Inhibition of KDM4A by JIB-04 as tested at three concentrations of O_2	123
5.5	JIB-04 E-isomer (pink sticks) competes with the histone peptide substrate (green sticks) in the KDM4A active site, with H_2O shown as red sphere (PDB 2Q8C); JIB-04 Z-isomer is a weak inhibitor of KDM4 enzymes	125
5.6	(a) View of JIB-04 E-isomer as modeled in the KDM4A active site. KDM4A shown as transparent ribbons and green sticks; JIB-04 shown as pink sticks, with the chlorine colored green. Ni(II) (orange sphere) replaces Fe(II) in the active site, and structural Zn(II) is shown as a blue sphere. (b) Close-up view of JIB-04 modeled in the KDM4A active site, showing predicted polar contacts with Asp 191 and Lys 241	126
5.7	The experimental $2F_o - F_c$ electron density, displayed as blue mesh, is shown for the ligand fragment in two alternate views	127
5.8	(a) View of the KDM4A:JIB-04 fragment crystal structure. KDM4A shown as transparent ribbons and green sticks; the JIB-04 fragment shown as gray sticks, with the chlorine colored green. Ni(II) (orange sphere) replaces Fe(II) in the active site, and structural Zn(II) is shown as a blue sphere. (b) Close-up view of the JIB-04 fragment in the KDM4A active site, showing hydrogen bonding to Tyr 132 and chelation to Ni(II)	129
6.1	Two inhibitors of KDM4E, as described in Chapter 3	134

List of Schemes

2.1	Oxidation of formaldehyde is coupled with the reduction of NAD^+	31
2.2	Histone demethylation by JmjC-HDMs, shown for a trimethyllysine substrate	37
3.1	In situ HDM-templated click-chemistry	64
4.1	Huisgen 1, 3-dipolar cycloaddition of $\text{ARK}^+(\text{N}^{\text{E}}\text{-methyl bis(propargyl)})\text{ST}$ with a KDM4- M^{2+} -azide adduct	91

List of Tables

1.1	JmjC-HDMs and their substrate specificities	13
2.1	Kinetic parameters for the three JmjC-HDMs with respect to the primary histone analog substrate	40
2.2	Kinetic parameters for the three JmjC-HDMs with respect to the secondary substrate O ₂	41
2.3	Kinetic parameters for the three JmjC-HDMs with respect to the secondary substrate αKG	42
4.1	Inhibition data for KDM4A and KDM4C with modified H3K9 peptides	101
4.2	ARK ⁺ (N ^e - methyl bis(propargyl))ST peaks of interest in the enzyme-templated cycloaddition experiment	105

List of Abbreviations

ACN:	Acetonitrile
α KG:	Alpha-ketoglutarate
AR:	Androgen receptor
CAM:	Chloramphenicol
CID:	Collision-induced dissociation
DMAP:	Dimethylaminopyridine
DMSO:	Dimethylsulfoxide
EDTA:	Ethylenediaminetetraacetic acid
ESI:	Electrospray ionization
EtOH:	Ethanol
FDH:	Formaldehyde dehydrogenase
HDM:	Histone demethylase
HEPES:	a Good's buffer with a pKa of 7.5 at 25 °C
HIF:	Hypoxia-inducible factor
HMT:	Histone methyltransferase
IC ₅₀ :	Half-maximal inhibitory concentration
JmjC:	Jumonji-C domain
k_{cat} :	Turnover number
KDM:	Lysine-specific demethylase
K_i :	Inhibitory binding constant
K_m :	Michaelis-Menten constant
KM:	Kanamycin
LB:	Luria broth

Lys, K:	Lysine
MALDI:	Matrix assisted light desorption ionization
MeOH:	Methanol
MS:	Mass spectrometry
NAD ⁺ :	Nicotinamide adenine dinucleotide (oxidized)
NOG:	<i>N</i> -oxalyglycine
PEG:	Polyethylene glycol
PHD:	Plant homeodomain or Prolyl hydroxylase
PMSF:	Phenylmethylsulfonyl fluoride (protease inhibitor)
SCX:	Strong cation exchange
TB:	Terrific broth
TCEP:	Tris(2-carboxyethyl)phosphine (reducing agent)
TLC:	Thin layer chromatography
TOF:	Time of flight
TFA:	Trifluoroacetic acid

Acknowledgements

First and foremost, I would like to thank Professor Liviu Mirica for welcoming me into his group six years ago. As he started a lab with three distinct projects, I am unsure how Liviu was able to give each of his students the attention that we and our projects needed, but he did, and I am so grateful for his patience and guidance over the years. I would also like to thank my committee members, Professors Michael Gross and John-Stephen Taylor, for their encouragement and advice during our annual meetings.

To past and present members of the Mirica group, I am grateful for the insight you offered into my project, as well as your friendship. In particular, I need to acknowledge the other original members of the group, Drs. Fengzhi Tang, Fengrui Qu, and Jia Luo. I have learned much from each of you. The advice, encouragement, and friendship I received from Dr. Hannah Malcolm is invaluable to me. Thank you.

I would like to thank Professor Joseph Jez and Dr. Soon Goo Lee for their generosity and patience, as I spent a good portion of my last year in the Jez lab setting up protein crystal trays. Thank you, Soon, for staying up all night to collect diffraction data and for resolving the structures. I am forever grateful. I also need to thank Sukrit Singh, formerly of the Marshall lab, for his help with the molecular modeling studies.

This work would not have been possible without funding from the Department of Defense Breast Cancer Research Program Concept Award BC097014 (W81XWH-10-1-0442) and the Dean's Dissertation Fellowship from Washington University. Additionally, I need to thank the Washington University Department of Chemistry for funding me through teaching assistantships for many years.

Finally, I am thankful for the encouragement my husband has given me the past ten years. He never stopped believing I would finish this degree. Thank you for our daughter, who is the most precious gift. I dedicate this to you both.

Barbara Gordon Cascella

Washington University in St. Louis

December 2014

ABSTRACT OF THE DISSERTATION

Kinetic Analysis and Inhibition Studies of Iron-Dependent Histone Demethylases

by

Barbara Gordon Cascella

Doctor of Philosophy in Chemistry

Washington University in St. Louis, 2014

Professor Liviu Mirica, Chair

The research presented herein focuses on the kinetics and inhibition of the KDM4 subfamily of Jumonji C (JmjC) domain-containing histone demethylases (HDMS). Belonging to the larger class of α -ketoglutarate (α KG)-dependent, non-heme iron monooxygenases, the JmjC-HDMS remove methyl groups from mono-, di-, and tri-methylated histone lysine residues through an Fe(IV)-oxo-catalyzed hydroxylation reaction. JmjC-HDMS have been found to play integral roles in the maintenance of genomic integrity as well as in the regulation of transcription. Three KDM4 members were studied: the mixed H3K9/H3K36 demethylases KDM4A and KDM4C, and the pure H3K9 demethylase KDM4E. *KDM4C* is a hypoxia-inducible factor 1 (HIF-1) target gene and a putative oncogene, while KDM4A is found to be overexpressed at the protein level in multiple cancers. KDM4E is closely related to KDM4D, which has been found to regulate the tumor suppressor p53.

Three in vitro enzyme activity assays, including a novel continuous O₂ consumption assay, were employed to determine the kinetics of the three HDMS. The kinetic parameters of the three substrates, with an H3K9me₃ peptide in place of the full histone substrate, were determined. All three HDMS were found to have low apparent affinities for O₂, suggesting that these enzymes may act as O₂ sensors in vivo. α KG was found to inhibit KDM4C competitively with respect to O₂, with KDM4C displaying optimal activity in vitro at α KG concentrations similar to those found in cancer cells. Additionally, a 2.1 Å structure of KDM4A in complex with Ni(II) and α KG was solved.

Various avenues were explored in the study of JmjC-HDM inhibition. First, a small library of simple primary- and secondary- substrate analogs was synthesized and screened against KDM4E. From this screen, two small molecules were identified as promising candidates for modification in future KDM4 inhibitor design studies. The analogs contained carbon-carbon triple bonds or 1,2,3-triazole groups. We find the triazole-containing compounds to be stronger inhibitors of KDM4E. Several of the alkyne-containing compounds were tested in KDM4-templated Huisgen 1,3-dipolar cycloaddition studies, with no evidence of enzyme-driven triazole formation.

Using a peptidomimetic approach, two novel, modified histone H3₍₇₋₁₁₎ peptides were synthesized and tested for inhibition against KDM4A and KDM4C. Lys residues were modified to incorporate two propargyl groups on the terminal nitrogen, with one of the peptides having an additional methyl group on the terminal nitrogen to make it quaternary. We find enhanced inhibition of KDM4A and KDM4C using the positively charged peptide vs. the neutral peptide. KDM4 members show no hydroxylase or demethylase activity toward the methylated peptide, suggesting that modification of this peptide could lead to enhanced specific inhibition of JmjC-HDMs. No evidence of HDM-driven triazole formation was found for either peptide in studies with KDM4A- and KDM4C- azide adducts.

The inhibition of KDM4A with respect to O₂ for the pan-selective JmjC-HDM inhibitor JIB-04 was explored. KDM4A inhibition by JIB-04 increases with decreasing O₂ concentration, suggesting that JIB-04 may inhibit KDM4A in part by disrupting the binding of O₂. JIB-04 isomers were modeled into the KDM4A active site, revealing the predicted basis for JIB-04 isomer-specific inhibition of JmjC-HDMs. Finally, a 3.1 Å structure of KDM4A in complex with JIB-04 was solved, revealing only a fragment of the inhibitor in the enzyme active site.

Chapter 1: Introduction

1.1 Covalent Modification of Chromatin

A nucleosome is an assembly of deoxyribonucleic acid (DNA) wound around an octamer protein core composed of four types of histones: H2A, H2B, H3, and H4 (Figure 1.1). Nucleosomes string together via linker histones, H1, to form chromatin. Though DNA is packaged into chromatin, it is necessary that the genetic information be accessible to cellular machinery for replication and transcription. The interplay between the condensed heterochromatin form and the transcriptionally active euchromatin form is facilitated through epigenetic events such as DNA methylation and covalent histone modification. DNA can be modified through methylation of cytosine residues, while histone protein tails, rich in basic residues and protruding from the nucleosome core, are subjected to various forms of chemical modification. Aside from the most common modifications of methylation and acetylation, basic histone residues can also be phosphorylated and ubiquitylated. The histone tail most subjected to modification is the N-terminus of histone H3, which is boxed in Figure 1.1.¹

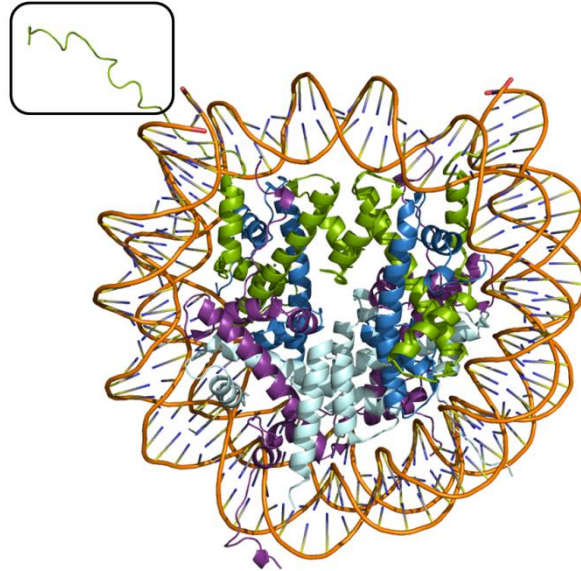


Figure 1.1. The nucleosome, with the four core histones in different colors (PDB 1AOI).²

There exists a vast network of proteins in the regulation of transcription that serve as “writers”, “readers”, and “erasers” of nucleosome modification. Writers are those enzymes that add a chemical group to a histone residue or cytosine. Writers include enzymes such as histone methyltransferases (HMTs), histone acetyltransferases (HATs), and DNA methyltransferases (DNMTs). Reader proteins function as the interpreters of the network. Methylated lysine residues are often recognized by proteins with chromodomains (e.g. heterochromatin protein 1 (HP1), which binds $H3K9me_{2/3}$)³ or plant homeodomains (PHDs, e.g. the tumor suppressor ING2). Such protein domains contain aromatic cages to stabilize binding to methyllysine, through cation- π interactions, as illustrated in Figure 1.2.⁴⁻⁸

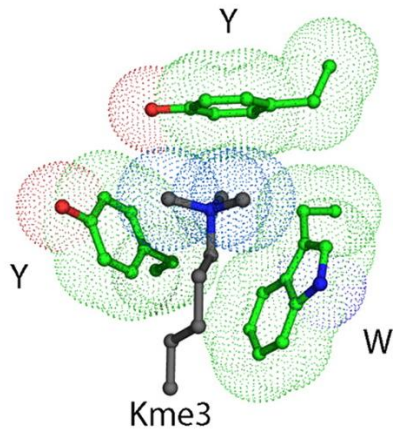


Figure 1.2. HP1's interaction with H3K9me₃ via cation- π interactions.⁹

Eraser proteins can be recruited to sites of nucleosome modification to remove the modification. Erasers include enzymes such as histone demethylases (HDMs), which are the focus of this dissertation work, and histone deacetylases (HDACs). A recent report illustrates a portion of the complex regulatory system of writers, readers, and erasers in *C. elegans* that serves to maintain proper heterochromatin and euchromatin boundaries.¹⁰ Working in concert in the euchromatin region are an H3K4me_{2/1} demethylase and two H3K4 methyltransferases, while in the heterochromatin region, the epigenetic memory antagonism protein 1 (EAP-1) reads and binds trimethylated H3K9, and subsequently moderates the activities of H3K9me₃ HDMs and HMTs.

Modification of histone termini contributes to the regulation of transcription by affecting accessibility of DNA sequences to transcription machinery (Figure 1.3).¹¹ Chromatin modification can disrupt the interaction between the negatively charged DNA and positively charged histone protein N-termini.

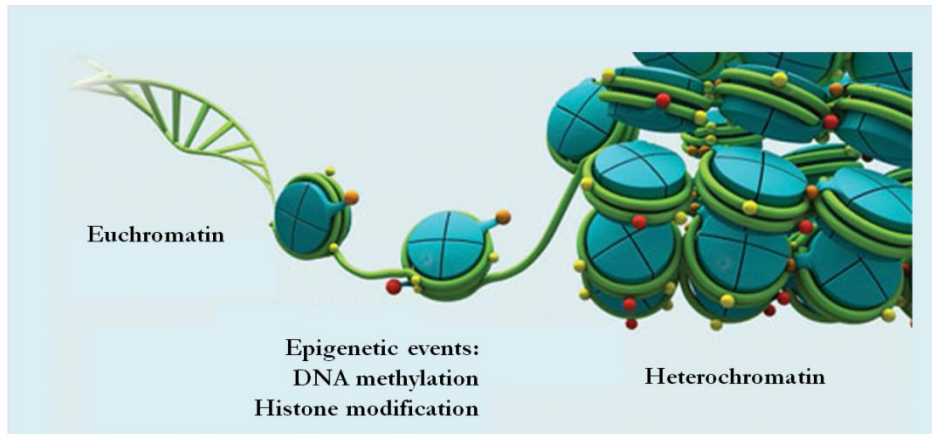


Figure 1.3. Epigenetic events and their effects on chromatin condensation. Adapted from a Bio-Rad Laboratories image.

Acetylation of lysine residues (Figure 1.4) generally leads to relaxation of chromatin and activation of transcription, as the modification neutralizes lysine and therefore reduces the overall charge of the histone. The reduction of positive charge is thought to lessen the affinity between the histone and surrounding DNA.^{12,13}

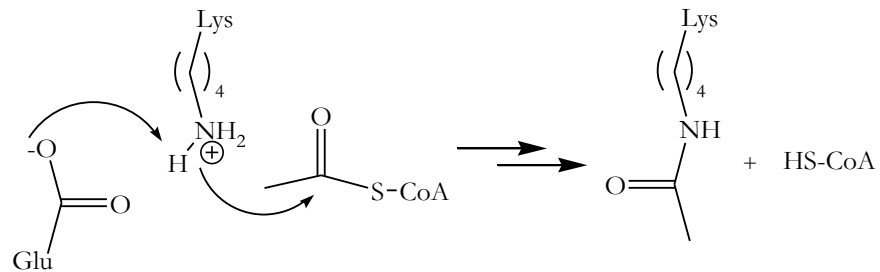


Figure 1.4. Acetylation of lysine residues leads to neutralization of charge.

Methylation of lysine histone residues is predominantly accomplished via methyl transfer by S-adenosylmethionine (SAM)-dependent histone lysine methyltransferases (KMTs).¹⁴ Following binding of SAM and deprotonation of the lysine substrate by a KMT, there is a proposed S_N2 attack of the lysine's ϵ nitrogen on the activated SAM cofactor (Figure 1.5).¹⁵ Addition of methyl groups to

lysine and arginine residues increases the hydrophobicity of the residue, thus enhancing the residue's interaction with hydrophobic regions of methyl-binding domains in various proteins.⁶ Because methylation of lysine residues does not affect the charge of the residue, this covalent modification can contribute to both transcriptional activation and repression. The position on the histone of the residue being modified, as well as surrounding residue modifications, determines whether the action will result in activation of transcription.

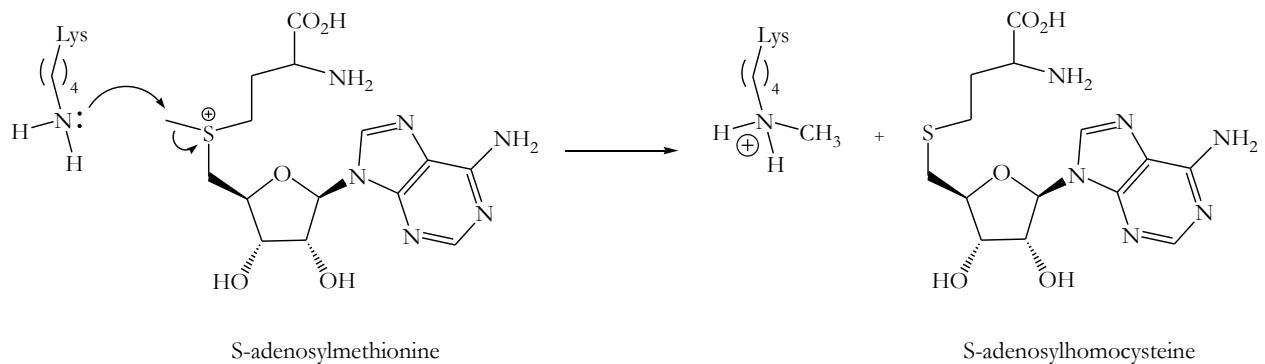


Figure 1.5. Histone lysine methylation as carried out by SAM-dependent KMTs.

Whereas the same histone can have multiple sites of modification, some histone marks prevent other histone modification events from taking place owing to what is known as histone crosstalk. For example, methylation of H3K9 is associated with the heterochromatin state, while methylation of H3K4 is associated with active gene expression. Studies show that these two modifications have an inverse relationship, whereby H3K9 cannot be methylated if H3K4 is methylated, and vice versa.¹⁶ Another example of histone crosstalk is found in the antagonistic relationship between H3R2 and H3K4; trimethylation of H3K4 prevents demethylation of H3R2, while dimethylation of H3R2 inhibits H3K4 methylation.^{17, 18}

1.2 Dynamic Methylation and Demethylation of Histone

Lysine Residues

Histone lysine methylation is an interesting post-translational modification with integral roles in gene regulation, genomic integrity, and epigenetic inheritance. The C-N bond formed upon lysine methylation confers stability, which is critical to certain biological events, and interestingly, the mark is removable in response to stimuli, owing to the presence of histone lysine demethylases (HDMs). The role of histone methylation in epigenetic inheritance is not yet completely understood. Although research suggests that histone methylation is stable across generations, the inheritance of methyl groups on histones through cell divisions is a rare event, and the propagation of post-translational modifications of histones is an area of active study.¹⁹ One theory proposes the immediate modification of histones associating with newly synthesized DNA to maintain an epigenetic memory.²⁰

There exists a dynamic relationship between histone lysine methylation and demethylation that enriches the overall epigenetic regulatory system of the cell. Disruption to the activities of HMTs or HDMs has been shown to lead to aging, developmental defects, and cancer cell formation.¹⁹ There exist two classes of HDMs with distinct mechanisms of lysine demethylation: the amine-oxidase domain-containing HDMs, and the Jumonji C (JmjC)-domain containing HDMs.

1.3 Catalytic Mechanisms of Histone Lysine Demethylation

Although histone methylation was once believed to be a static modification, two classes of demethylases have been discovered that work through distinctly different mechanisms: the earlier discovered amine oxidase-domain containing, and a larger class of JmjC-domain containing, O₂-activating enzymes. The two classes of lysine demethylases are highly conserved from yeast to humans.^{19, 21}

1.3.1 Flavin-Dependent Histone Demethylases

The earliest discovered class of HDMs includes just two members: LSD1 and LSD2 (KDM1A and KDM1B). Demethylase activity is dependent on the amine-oxidase domain, and the cofactor flavin-adenine dinucleotide (FAD) is reduced in the demethylation reaction. KDM1A and B work through a mechanism that requires a lone electron pair on the lysine ϵ -nitrogen atom, as shown in Figure 1.6. Thus, the demethylase activity of KDM1A and KDM1B is limited to monomethylated lysine (Kme₁) and dimethylated lysine (Kme₂) residues.²² After proceeding through iminium and hemiaminal intermediates, formaldehyde is released as a side product. Note that in Figure 1.6, only the flavin portion of FAD is shown.

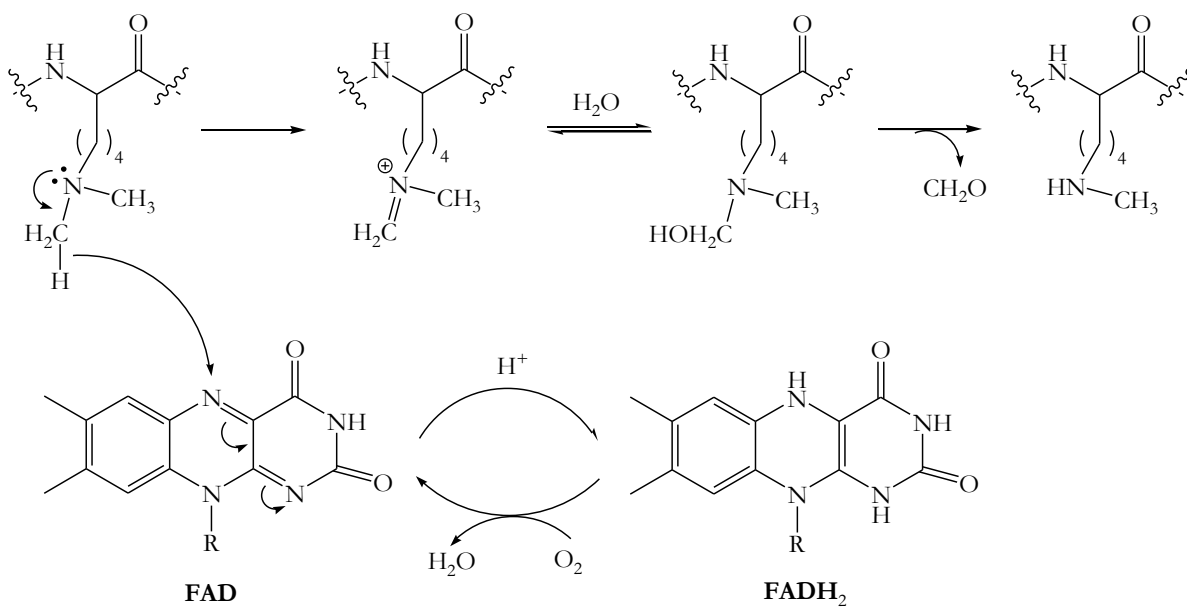


Figure 1.6. Proposed mechanism of flavin-dependent HDMs.

In the cell, formaldehyde that is produced from the demethylation reaction is continually oxidized as shown in Figure 1.7. Human formaldehyde dehydrogenase (FDH) is found in nearly every tissue of the body, and the enzyme works in conjunction with *S*-formylglutathione hydrolase to carry out the oxidation.

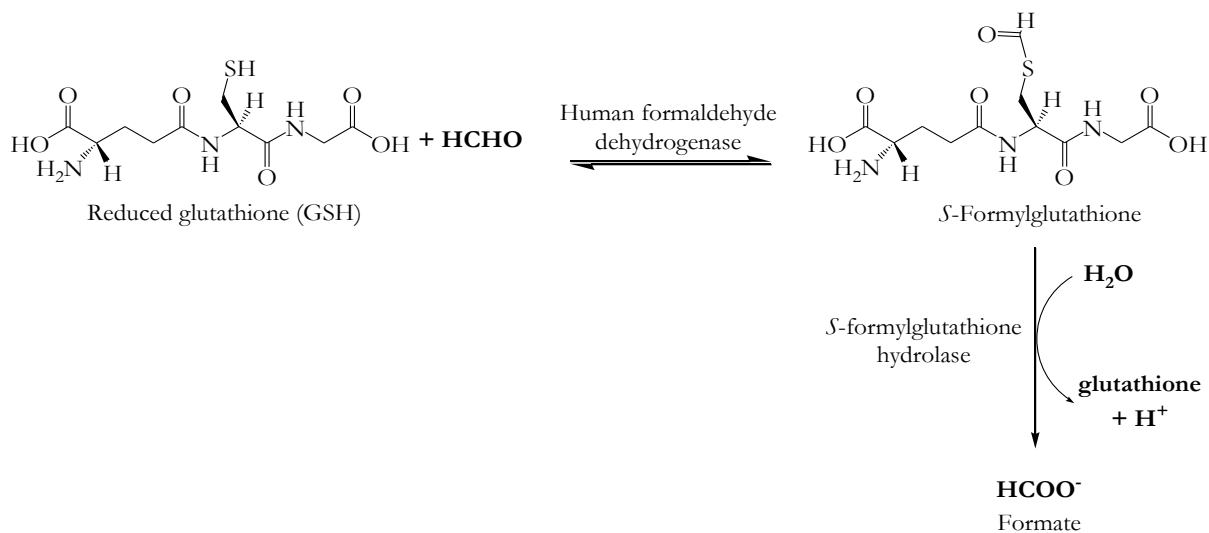


Figure 1.7. The oxidation of formaldehyde to formate.

The histone lysine substrate-binding subdomain in the KDM1 enzymes is composed of multiple acidic residues that complement the basic histone tail.²³ KDM1A is part of a protein complex named CoREST, and while in complex, the demethylase activity of KDM1A is specific for H3K4me_{2/1}.^{24,25} Figure 1.8 shows how FAD is positioned for the hydride transfer from H3K4me₂. Interestingly, when KDM1A associates with androgen receptor (AR), its specificity changes to H3K9me₂.²⁶

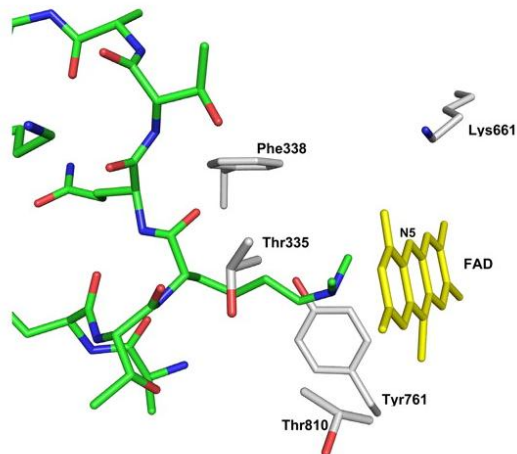


Figure 1.8. A model of KDM1A (gray residues) in complex with H3K4me₂ (green residues).²⁷

1.3.2 Iron-Dependent Histone Demethylases

Chemistry of the Iron Active Site

JmjC-domain containing HDMs contain conserved N-terminal JmjC and JmjN catalytic domains, grouping the demethylases in the cupin superfamily of metalloenzymes.²⁸ These demethylases are iron-dependent monooxygenases that utilize the cosubstrate α -ketoglutarate (α KG) for enzymatic activity. As shown in Figure 1.9, the active site iron in JmjC-HDMs coordinates to a conserved His₂(Asp/Glu)₁ facial triad. The remaining coordination sites are taken by an α KG analog and dioxygen, with the histone lysine substrate (H3K36me₃) binding in a separate pocket.

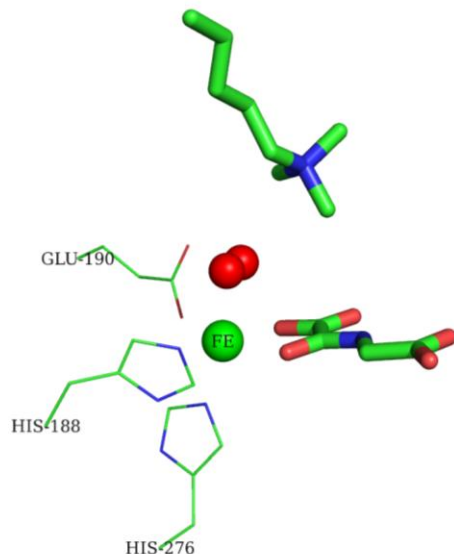


Figure 1.9. The KDM4A active site, with iron coordinated to *N*-oxalylglycine and O₂ (PDB 2P5B).²⁹

Mechanism of Lysine Demethylation

A six-coordinate Fe(II) is held in the enzyme active site through a conserved 2-histidine 1-carboxylate binding motif (Figure 1.10).³⁰ As shown through steady state kinetics experiments, α KG binds iron first in a bidentate fashion, displacing two H₂O molecules. Next, an additional H₂O molecule is lost as the histone lysine substrate binds in a pocket away from the iron center, resulting in a 5-coordinate Fe(II) species. Primary substrate binding facilitates the binding of O₂ to the metal center, giving rise to an Fe(III)-superoxide radical. Superoxide acts as a nucleophile to attack the alpha-keto carbonyl of α KG, leading to rearrangement of a highly reactive Fe(IV)-oxo species.³¹ This species is responsible for hydroxylation of the primary substrate methyl group. Finally, the hydroxylated substrate converts non-enzymatically to the product. Side products of the reaction include formaldehyde, CO₂, and succinate.

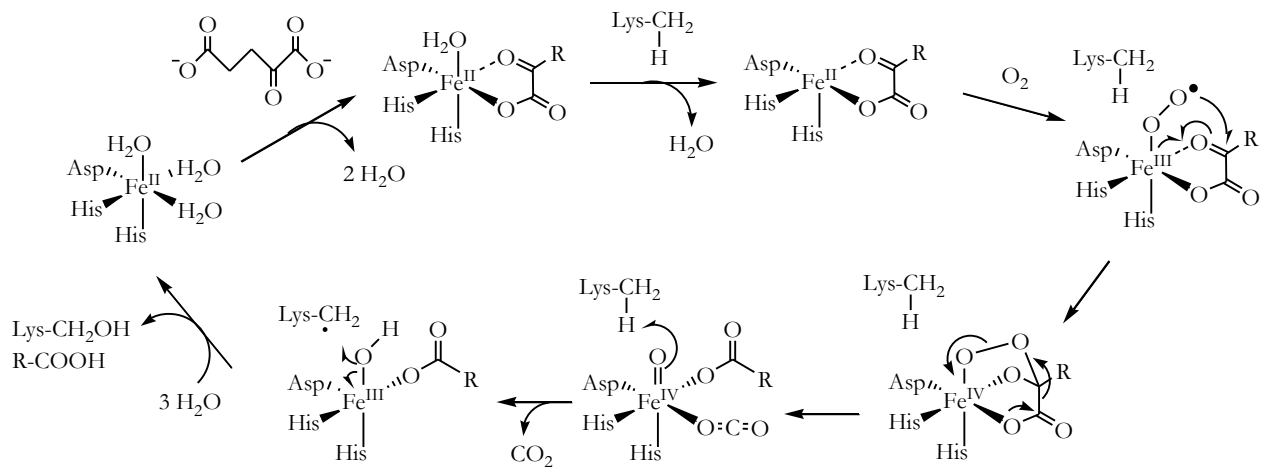


Figure 1.10. Mechanism of iron-dependent HDMs, where Lys-CH₃ is the histone lysine substrate.

Classification of JmjC-HDMs

The 18 identified JmjC-HDMs have varying histone lysine substrate specificities and are grouped into five subfamilies: KDM2/7, KDM3, KDM4, KDM5, and KDM6 (Table 1.1). The focus of my research was on three members of the KDM4 subfamily: KDM4A, KDM4C, and the pseudogene-encoded KDM4E, as a substitute for KDM4D.

Table 1.1. JmjC-HDMs and their substrate specificities.³²

JmjC-HDM Subfamily	Members	Substrate Specificity
KDM2/KDM7	KDM2A KDM2B KDM7A PHF8	H3K36me _{2/1} , H3K4me ₃ H3K36me _{2/1} H3K27me _{2/1} H3K9me _{2/1} , H3K27me _{2/1} , H3K36me ₂ , H4K20me ₁
KDM3	KDM3A, KDM3B KDM3C	H3K9me _{2/1} MDC1 at Lys45 ³³
KDM4	KDM4A, KDM4B, KDM4C KDM4D, KDM4E	H3K9me _{3/2} , H3K36me _{3/2} H3K9me _{3/2}
KDM5	KDM5A, KDM5B, KDM5C, KDM5D	H3K4me _{3/2}
KDM6	KDM6A, KDM6B	H3K27me _{2/1}

Although the JmjC and JmjN domains are required for all JmjC-HDMs' catalytic activity, only certain enzymes contain PHD and Tudor domains, which are proposed to have essential roles in enzymatic binding to chromatin.³⁴⁻³⁷ For instance, in the KDM4 subfamily, KDM4D lacks the PHD and Tudor domains, whereas KDM4A and KDM4C do not, and this difference may contribute to KDM4D being limited to a single substrate. Moreover, studies have shown KDM4C, and not KDM4A-B, to play a role in mitotic chromosome separation, and the Tudor domains of KDM4C are essential for its association with chromatin for this fidelity process.³⁸

The KDM4 subfamily contains five members: KDM4A-E, of which one (KDM4E) is encoded by a pseudogene, with the protein being catalytically active.³⁴ KDM4 enzymes have putative

roles in a wide variety of cellular processes such as DNA replication, regulation of gene expression, and the DNA damage response.

KDM4 Dual-Substrate Specificities

Although one study has shown KDM4 enzymes to be capable of hydroxylating and dealkylating substrates other than N^{ϵ} -methyl,³⁹ KDM4 enzymes are highly selective, owing in large part to residues surrounding the methylated lysine of interest. Through competition experiments, it was found that KDM4A-C display highest catalytic activity toward H3K9 in the trimethylated state, but can also recognize H3K9me₂. In addition, these enzymes act on H3K36me_{3/2}, albeit at significantly lower rates. KDM4D-E activities are limited to H3K9me_{3/2}.^{34, 40} Crystal structures of KDM4A, C, and E have been obtained and reveal that these enzymes share remarkably similar active site structures, owing to highly conserved residues which make up the methylammonium-binding pocket. Because KDM4D/E cannot recognize H3K36, variants of KDM4A with residues thought to determine sequence selectivity in KDM4E were studied. None of the KDM4A variants studied displayed catalytic activity toward H3K36.³⁴

An octapeptide commonly used in in vitro studies of KDM4 enzymes includes a trimethylated lysine 9, and the sequence is as follows: ARK(me₃)STGGK (H3₍₇₋₁₄₎K9me₃). Certain residues surrounding K9 on histone H3 have been found to be important for KDM4 recognition. Alanine at the -2 position was shown to be significant for peptide recognition by KDM4C, but not as important for KDM4A.^{41, 42} Serine at +1 and glycine at +3 are necessary for recognition by KDM4A, as the side chain of the former forms an intra-molecular hydrogen bond with the amide of the latter; interestingly, the Gly-Gly motif is not necessary for recognition by KDM4C.⁴³ While their

H3 lysine specificities are the same, KDM4A and KDM4C differ in the length of H3K9 peptide necessary for recognition. KDM4A can demethylate an H3K9me₃ peptide no shorter than eight residues (H3₍₇₋₁₄₎K9me₃), while KDM4C recognizes peptides as short as four residues (H3₍₇₋₁₀₎K9me₃).⁴²

1.4 HDMs in DNA Repair

HDMs have been found to play important roles in the maintenance of genomic integrity.⁴⁴⁻⁴⁶ Double-stranded breaks (DSB) in DNA lead to a coordinated cellular effort to recognize and repair the lesion efficiently, a process known as the DNA damage response (DDR). Recognition of lesions is done by Poly(ADP-ribose) polymerase (PARP) family proteins PARP1 and PARP2. If the DSB occurs in heterochromatin, decondensation of the chromatin is necessary.⁴⁷ Rapid expansion of heterochromatin is characterized by displacement of HP1 β from lesion sites without changes in H3K9 methylation status.^{48, 49}

Multiple HDMs have been found to be integral in the DDR. KDM1A has been implicated in the pathway, as H3K4 dimethylation is reduced at DNA lesion sites following irradiation in a KDM1A-dependent manner.⁴⁶ At least two members of the KDM4 JmjC-HDM subfamily play putative roles in the maintenance of genomic integrity: KDM4B and KDM4D. One study found KDM4D to be recruited to lesion sites in a PARP1-dependent manner. Additionally, KDM4D is implicated in DSB repair, as the demethylase promotes the phosphorylation of early DNA damage markers such as checkpoint kinase 2 (CHK2).⁴⁴ KDM4B overexpression has been found to improve the DDR by enhancing DSB repair following laser microirradiation.⁴⁵

1.5 HDMs in Cancer

It is widely known that inappropriate gene expression can lead to the development of disease. Chromatin modification is thought to contribute to the control of gene expression through influencing chromatin compaction or signaling to other protein complexes. One characteristic of tumors is the local and global changes in chromatin structure compared with healthy tissue, suggesting epigenetic deregulation as the culprit.⁵⁰ Much research suggests that the regulation of histone methylation becomes askew in cancer, as well as in aging and intellectual disability.^{19, 51}

1.5.1 Flavin-Dependent Histone Demethylases

Because KDM1A associates with both the functional corepressor complex CoREST and androgen receptor, this enzyme can act as a transcriptional co-repressor (by demethylating H3K4me_{2/1}) or co-activator (by demethylating H3K9me_{2/1}), depending on its association at the time. KDM1A is reported to be oncogenic and/or overexpressed in multiple cancers, including leukemias and solid tumors.^{52, 53} KDM1A is required for the maintenance of acute myeloid leukemia (AML)-containing MLL translocations. Inhibition of KDM1A is found to significantly inhibit the colony-forming ability of AML cells.⁵⁴ In human prostate cancer cells, KDM1A cooperates with the JmjC-HDM KDM4C to activate AR-mediated gene expression. KDM4C removes a methyl group from H3K9me₃ at the promoter of AR target genes, while KDM1A finishes the demethylation of H3K9 to activate transcription.^{55, 56} Mechanism-based inhibitors tranylcypromine and its derivatives have proven to be effective inhibitors of KDM1A, as they form adducts with FAD, and, thus, prevent

amine-oxidase activity of the enzyme (Figure 1.11). Tranylcypromine was first identified as a monoamine oxidase inhibitor (MAOI) for the treatment of depression.

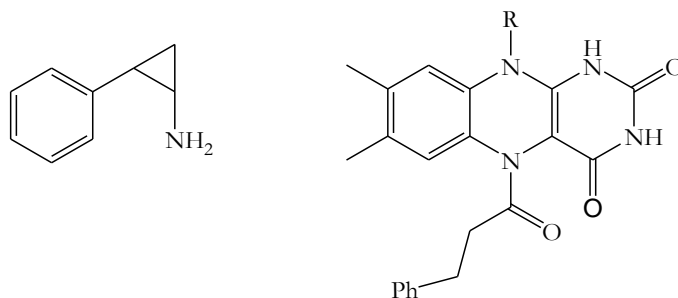


Figure 1.11. Tranylcypromine (*left*) and a tranylcypromine-FAD adduct (*right*).⁵⁷

1.5.2 Iron-Dependent Histone Demethylases

KDM4C is the KDM4 subfamily member implicated in the greatest number of cancers. *KDM4C* is a hypoxia-inducible factor 1 (HIF-1) target gene, which may explain KDM4C's mRNA and protein overexpression in breast and colon cancers, medulloblastoma, and squamous cell carcinoma.⁵⁸⁻⁶⁰ HIF target gene products play putative roles in various steps of cancer progression.⁶¹ In addition to working in concert with KDM1A to stimulate AR- mediated gene expression in human prostate cancer cells, KDM4C demethylates H3K9me₃ at hypoxia response elements (HREs) of HIF-1 target genes, which enhances HIF-1 binding to HREs, promoting transcription.⁶² Interestingly, increased KDM4C mRNA expression is linked to elevated tumor grade in human breast cancers.⁶²

KDM4A has been found to be overexpressed at the protein level in lung cancer, prostate cancer, and about 60% of breast tumors.^{63,64} However, overexpression of KDM4A does not enhance tumor growth in all cancers, as studies of KDM4A in HeLa cervical carcinoma or 293T embryonal kidney cells have shown.⁶⁵ In certain cell lines, overexpression of KDM4A reduces

recruitment and/or binding of HP1 to chromatin, as HP1 localizes upon trimethylation of H3K9.⁶⁶ Recent studies detail the complicated and cell line-specific nature of JmjC-HDM involvement in cancer. For instance, H3K9 trimethylation was found to be increased in certain breast and colon cancer cell lines during hypoxia.⁶⁷ This recent finding may be partly explained by the low apparent affinity of KDM4 enzymes for O₂ in vitro, with O₂ K_m values ranging from 60 – 200 μM, far above the cellular concentration of O₂ during times of hypoxia.⁶⁸ Human breast cancers have intratumoral hypoxic regions with median pO₂ values of 5 -10 mm Hg (<1.5% or ~10 - 20 μM O₂), compared with ~ 35 mm Hg O₂ in normal breast tissue.^{62, 69}

Whereas the inhibition of KDM1A has proven to be fairly straightforward, the inhibition of JmjC-HDMs is complicated by several factors. First, these enzymes share an active-site motif with a much larger group of enzymes, making selective inhibition difficult. Second, primary substrate selectivities stem from multiple main-chain interactions of the histone with the HDM. Lastly, of the three JmjC-HDM substrates, αKG is the highest affinity. However, designing inhibitors that bind like αKG is less than ideal owing to the promiscuous nature of such metal-binding compounds. Thus far, only two compounds have been identified that act as specific inhibitors of JmjC-HDMs without competing with αKG (Figure 1.12).^{70, 71}

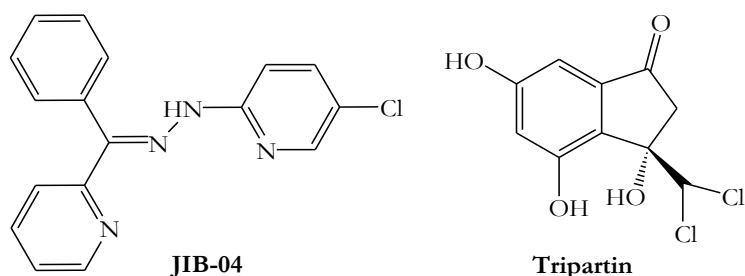


Figure 1.12. Two specific inhibitors of JmjC-HDMs.

1.6 Project Goals

At the start of this dissertation work, the kinetics of the JmjC-HDM KDM4 subfamily had not been fully elucidated. Moreover, very little was known of the enzymology of KDM4C, an enzyme encoded by a putative oncogene, with the protein implicated in multiple cancers.^{62, 72-74} An early goal of this dissertation work was to gain a thorough understanding of the *in vitro* kinetics of three JmjC-HDMs with respect to all three substrates: a histone lysine substrate analog (H3₍₇₋₁₄₎K9me₃) and the two cosubstrates O₂ and α KG. As the concentration of O₂ in healthy cells and cancerous cells is dramatically different, it was of particular interest to determine how the KDM4 enzymes behave toward O₂ *in vitro*.

The second goal of this dissertation work was the development of a continuous, real-time *in vitro* enzymatic assay to study the activity of JmjC-HDMs. At the beginning of this work, the only published *in vitro* assays were discontinuous or coupled in nature, which can lead to distorted K_m , k_{cat} , K_i , and IC₅₀ values.

The final goal of this work was broad in scope: the development of small molecule inhibitors of JmjC-HDMs. As these enzymes are part of a much larger group of α KG-dependent oxygenases, the problem of target selectivity arises when designing inhibitors. At the time of this writing, only two of the hundreds of published JmjC-HDM inhibitors have been shown to selectively inhibit JmjC-HDMs without an α KG analog chelating the metal center.^{70, 71} This work describes two HDM inhibition strategies: the first, simple substrate analogs bearing di- or tri-methylammonium groups or analogs that include an amide oxalyl group; the second, a peptidomimetic approach to achieve isoform selectivity.

1.7 References

1. Thinnes, C. C., England, K. S., Kawamura, A., Chowdhury, R., Schofield, C. J., Hopkinson, R. J., Targeting Histone Lysine Demethylases—Progress, Challenges, and the Future. *Biochimica et Biophysica Acta (BBA)-Gene Regulatory Mechanisms* **1839**, 1416-1432 (2014).
2. Luger, K., Mäder, A. W., Richmond, R. K., Sargent, D. F., Richmond, T. J., Crystal Structure of the Nucleosome Core Particle at 2.8 Å Resolution. *Nature* **389**, 251-260 (1997).
3. James, T. C., Elgin, S., Identification of a Nonhistone Chromosomal Protein Associated with Heterochromatin in *Drosophila Melanogaster* and Its Gene. *Molecular and Cellular Biology* **6**, 3862-3872 (1986).
4. Pena, P. V., Davrazou, F., Shi, X., Walter, K. L., Verkhusha, V. V., Gozani, O., Zhao, R., Kutateladze, T. G., Molecular Mechanism of Histone H3k4me3 Recognition by Plant Homeodomain of Ing2. *Nature* **442**, 100-103 (2006).
5. Li, H., Ilin, S., Wang, W., Duncan, E. M., Wysocka, J., Allis, C. D., Patel, D. J., Molecular Basis for Site-Specific Read-out of Histone H3k4me3 by the Bptf Phd Finger of Nurf. *Nature* **442**, 91-95 (2006).
6. Nielsen, P. R., Nietlispach, D., Mott, H. R., Callaghan, J., Bannister, A., Kouzarides, T., Murzin, A. G., Murzina, N. V., Laue, E. D., Structure of the Hp1 Chromodomain Bound to Histone H3 Methylated at Lysine 9. *Nature* **416**, 103-107 (2002).
7. Flanagan, J. F., Mi, L.-Z., Chruszcz, M., Cymborowski, M., Clines, K. L., Kim, Y., Minor, W., Rastinejad, F., Khorasanizadeh, S., Double Chromodomains Cooperate to Recognize the Methylated Histone H3 Tail. *Nature* **438**, 1181-1185 (2005).
8. Jacobs, S. A., Khorasanizadeh, S., Structure of Hp1 Chromodomain Bound to a Lysine 9-Methylated Histone H3 Tail. *Science* **295**, 2080-2083 (2002).
9. Hughes, R. M., Wiggins, K. R., Khorasanizadeh, S., Waters, M. L., Recognition of Trimethyllysine by a Chromodomain Is Not Driven by the Hydrophobic Effect. *Proceedings of the National Academy of Sciences* **104**, 11184-11188 (2007).

10. Greer, Eric L., Beese-Sims, Sara E., Brookes, E., Spadafora, R., Zhu, Y., Rothbart, Scott B., Aristizábal-Corrales, D., Chen, S., Badeaux, Aimee I., Jin, Q., Wang, W., Strahl, Brian D., Colaiácovo, Monica P., Shi, Y., A Histone Methylation Network Regulates Transgenerational Epigenetic Memory in *C. elegans*. *Cell reports* **7**, 113-126 (2014).
11. Zentner, G. E., Henikoff, S., Regulation of Nucleosome Dynamics by Histone Modifications. *Nature Structural & Molecular Biology* **20**, 259-266 (2013).
12. Chi, P., Allis, C. D., Wang, G. G., Covalent Histone Modifications—Miswritten, Misinterpreted and Mis-Erased in Human Cancers. *Nature reviews cancer* **10**, 457-469 (2010).
13. Suganuma, T., Workman, J. L., Signals and Combinatorial Functions of Histone Modifications. *Annual Review of Biochemistry* **80**, 473-499 (2011).
14. Xiao, B., Jing, C., Wilson, J. R., Walker, P. A., Vasisht, N., Kelly, G., Howell, S., Taylor, I. A., Blackburn, G. M., Gamblin, S. J., Structure and Catalytic Mechanism of the Human Histone Methyltransferase Set7/9. *Nature* **421**, 652-656 (2003).
15. Helin, K., Dhanak, D., Chromatin Proteins and Modifications as Drug Targets. *Nature* **502**, 480-488 (2013).
16. Noma, K.-i., Allis, C. D., Grewal, S. I., Transitions in Distinct Histone H3 Methylation Patterns at the Heterochromatin Domain Boundaries. *Science* **293**, 1150-1155 (2001).
17. Guccione, E., Bassi, C., Casadio, F., Martinato, F., Cesaroni, M., Schuchlantz, H., Lüscher, B., Amati, B., Methylation of Histone H3r2 by Prmt6 and H3k4 by an Mll Complex Are Mutually Exclusive. *Nature* **449**, 933-937 (2007).
18. Kirmizis, A., Santos-Rosa, H., Penkett, C. J., Singer, M. A., Vermeulen, M., Mann, M., Bähler, J., Green, R. D., Kouzarides, T., Arginine Methylation at Histone H3r2 Controls Deposition of H3k4 Trimethylation. *Nature* **449**, 928-932 (2007).
19. Greer, E. L., Shi, Y., Histone Methylation: A Dynamic Mark in Health, Disease and Inheritance. *Nature Reviews Genetics* **13**, 343-357 (2012).
20. Margueron, R., Reinberg, D., Chromatin Structure and the Inheritance of Epigenetic Information. *Nature Reviews Genetics* **11**, 285-296 (2010).

21. Mosammaparast, N., Shi, Y., Reversal of Histone Methylation: Biochemical and Molecular Mechanisms of Histone Demethylases. *Annual Review of Biochemistry* **79**, 155-179 (2010).
22. Shi, Y., Lan, F., Matson, C., Mulligan, P., Whetstine, J. R., Cole, P. A., Casero, R. A., Shi, Y., Histone Demethylation Mediated by the Nuclear Amine Oxidase Homolog Lsd1. *Cell* **119**, 941-953 (2004).
23. Chen, Y., Yang, Y., Wang, F., Wan, K., Yamane, K., Zhang, Y., Lei, M., Crystal Structure of Human Histone Lysine-Specific Demethylase 1 (Lsd1). *Proceedings of the National Academy of Sciences* **103**, 13956-13961 (2006).
24. Yang, M., Gocke, C. B., Luo, X., Borek, D., Tomchick, D. R., Machius, M., Otwinowski, Z., Yu, H., Structural Basis for Corest-Dependent Demethylation of Nucleosomes by the Human Lsd1 Histone Demethylase. *Molecular cell* **23**, 377-387 (2006).
25. Stavropoulos, P., Blobel, G., Hoelz, A., Crystal Structure and Mechanism of Human Lysine-Specific Demethylase-1. *Nature Structural & Molecular Biology* **13**, 626-632 (2006).
26. Metzger, E., Wissmann, M., Yin, N., Müller, J. M., Schneider, R., Peters, A. H., Günther, T., Buettner, R., Schüle, R., Lsd1 Demethylates Repressive Histone Marks to Promote Androgen-Receptor-Dependent Transcription. *Nature* **437**, 436-439 (2005).
27. Forneris, F., Binda, C., Adamo, A., Battaglioli, E., Mattevi, A., Structural Basis of Lsd1-Corest Selectivity in Histone H3 Recognition. *Journal of Biological Chemistry* **282**, 20070-20074 (2007).
28. Tsukada, Y., Fang, J., Erdjument-Bromage, H., Warren, M. E., Borchers, C. H., Tempst, P., Zhang, Y., Histone Demethylation by a Family of JmjC Domain-Containing Proteins. *Nature* **439**, 811-816 (2006).
29. Chen, Z., Zang, J., Kappler, J., Hong, X., Crawford, F., Wang, Q., Lan, F., Jiang, C., Whetstine, J., Dai, S., Structural Basis of the Recognition of a Methylated Histone Tail by Jmjd2a. *Proceedings of the National Academy of Sciences* **104**, 10818-10823 (2007).
30. Bollinger, J. M., Krebs, C., Enzymatic C-H Activation by Metal-Superoxo Intermediates. *Current Opinion in Chemical Biology* **11**, 151-158 (2007).

31. Price, J. C., Barr, E. W., Tirupati, B., Bollinger, J. M., Krebs, C., The First Direct Characterization of a High-Valent Iron Intermediate in the Reaction of an Alpha-Ketoglutarate-Dependent Dioxygenase: A High-Spin Fe(IV) Complex in Taurine/Alpha-Ketoglutarate Dioxygenase (Taud) from Escherichia Coli. *Biochemistry* **42**, 7497-7508 (2003).
32. Woon, E. C. Y., Tumber, A., Kawamura, A., Hillringhaus, L., Ge, W., Rose, N. R., Ma, J. H. Y., Chan, M. C., Walport, L. J., Che, K. H., Ng, S. S., Marsden, B. D., Oppermann, U., McDonough, M. A., Schofield, C. J., Linking of 2-Oxoglutarate and Substrate Binding Sites Enables Potent and Highly Selective Inhibition of Jmjc Histone Demethylases. *Angewandte Chemie International Edition* **51**, 1631-1634 (2012).
33. Watanabe, S., Watanabe, K., Akimov, V., Bartkova, J., Blagoev, B., Lukas, J., Bartek, J., Jmjd1c Demethylates Mdc1 to Regulate the Rnf8 and Brca1-Mediated Chromatin Response to DNA Breaks. *Nature Structural & Molecular Biology* **20**, 1425-1433 (2013).
34. Hillringhaus, L., Yue, W. W., Rose, N. R., Ng, S. S., Gileadi, C., Loenarz, C., Bello, S. H., Bray, J. E., Schofield, C. J., Oppermann, U., Structural and Evolutionary Basis for the Dual Substrate Selectivity of Human Kdm4 Histone Demethylase Family. *Journal of Biological Chemistry* **286**, 41616-41625 (2011).
35. Yu, L., Wang, Y., Huang, S., Wang, J., Deng, Z., Zhang, Q., Wu, W., Zhang, X., Liu, Z., Gong, W., Structural Insights into a Novel Histone Demethylase Phf8. *Cell research* **20**, 166-173 (2010).
36. Horton, J. R., Upadhyay, A. K., Qi, H. H., Zhang, X., Shi, Y., Cheng, X., Enzymatic and Structural Insights for Substrate Specificity of a Family of Jumonji Histone Lysine Demethylases. *Nature Structural & Molecular Biology* **17**, 38-43 (2010).
37. Shin, S., Janknecht, R., Diversity within the Jmjd2 Histone Demethylase Family. *Biochemical and Biophysical Research Communications* **353**, 973-977 (2007).
38. Kupershmit, I., Khoury-Haddad, H., Awwad, S. W., Guttmann-Raviv, N., Ayoub, N., Kdm4c (Gasc1) Lysine Demethylase Is Associated with Mitotic Chromatin and Regulates Chromosome Segregation During Mitosis. *Nucleic Acids Research*, (2014).
39. Hopkinson, R. J., Walport, L. J., Münzel, M., Rose, N. R., Smart, T. J., Kawamura, A., Claridge, T. D., Schofield, C. J., Is Jmjc Oxygenase Catalysis Limited to Demethylation? *Angewandte Chemie* **125**, 7863-7867 (2013).

40. Krishnan, S., Trievel, Raymond C., Structural and Functional Analysis of Jmjd2d Reveals Molecular Basis for Site-Specific Demethylation among Jmjd2 Demethylases. *Structure* **21**, 98-108 (2013).
41. Couture, J. F., Collazo, E., Ortiz-Tello, P. A., Brunzelle, J. S., Trievel, R. C., Specificity and Mechanism of Jmjd2a, a Trimethyllysine-Specific Histone Demethylase. *Nature Structural & Molecular Biology* **14**, 689-695 (2007).
42. Lohse, B., Nielsen, A. L., Kristensen, J. B. L., Helgstrand, C., Cloos, P. A. C., Olsen, L., Gajhede, M., Clausen, R. P., Kristensen, J. L., Targeting Histone Lysine Demethylases by Truncating the Histone 3 Tail to Obtain Selective Substrate-Based Inhibitors. *Angewandte Chemie, International Edition in English* **123**, 9266-9269 (2011).
43. Ng, S. S., Kavanagh, K. L., McDonough, M. A., Butler, D., Pilka, E. S., Lienard, B. M. R., Bray, J. E., Savitsky, P., Gileadi, O., von Delft, F., Rose, N. R., Offer, J., Scheinost, J. C., Borowski, T., Sundstrom, M., Schofield, C. J., Oppermann, U., Crystal Structures of Histone Demethylase Jmjd2a Reveal Basis for Substrate Specificity. *Nature* **448**, 87-U88 (2007).
44. Khoury-Haddad, H., Guttmann-Raviv, N., Ipenberg, I., Huggins, D., Jeyasekharan, A. D., Ayoub, N., Parp1-Dependent Recruitment of Kdm4d Histone Demethylase to DNA Damage Sites Promotes Double-Strand Break Repair. *Proceedings of the National Academy of Sciences* **111**, E728-E737 (2014).
45. Young, L. C., McDonald, D. W., Hendzel, M. J., Kdm4b Histone Demethylase Is a DNA Damage Response Protein and Confers a Survival Advantage Following Γ -Irradiation. *Journal of Biological Chemistry* **288**, 21376-21388 (2013).
46. Mosammaparast, N., Kim, H., Laurent, B., Zhao, Y., Lim, H. J., Majid, M. C., Dango, S., Luo, Y., Hempel, K., Sowa, M. E., The Histone Demethylase Lsd1/Kdm1a Promotes the DNA Damage Response. *The Journal of cell biology* **203**, 457-470 (2013).
47. Deem, A. K., Li, X., Tyler, J. K., Epigenetic Regulation of Genomic Integrity. *Chromosoma* **121**, 131-151 (2012).
48. Ayoub, N., Jeyasekharan, A. D., Bernal, J. A., Venkitaraman, A. R., Hp1-&Bgr; Mobilization Promotes Chromatin Changes That Initiate the DNA Damage Response. *Nature* **453**, 682-686 (2008).

49. Goodarzi, A. A., Noon, A. T., Deckbar, D., Ziv, Y., Shiloh, Y., Löbrich, M., Jeggo, P. A., Atm Signaling Facilitates Repair of DNA Double-Strand Breaks Associated with Heterochromatin. *Molecular cell* **31**, 167-177 (2008).
50. Berry, W. L., Janknecht, R., Kdm4/Jmjd2 Histone Demethylases: Epigenetic Regulators in Cancer Cells. *Cancer Research* **73**, 2936-2942 (2013).
51. Tan, M., Luo, H., Lee, S., Jin, F., Yang, J. S., Montellier, E., Buchou, T., Cheng, Z., Rousseaux, S., Rajagopal, N., Identification of 67 Histone Marks and Histone Lysine Crotonylation as a New Type of Histone Modification. *Cell* **146**, 1016-1028 (2011).
52. Shi, Y., Histone Lysine Demethylases: Emerging Roles in Development, Physiology and Disease. *Nature Reviews Genetics* **8**, 829-833 (2007).
53. Hayami, S., Kelly, J. D., Cho, H. S., Yoshimatsu, M., Unoki, M., Tsunoda, T., Field, H. I., Neal, D. E., Yamaue, H., Ponder, B. A., Overexpression of Lsd1 Contributes to Human Carcinogenesis through Chromatin Regulation in Various Cancers. *International Journal of Cancer* **128**, 574-586 (2011).
54. Harris, W. J., Huang, X., Lynch, J. T., Spencer, G. J., Hitchin, J. R., Li, Y., Ciceri, F., Blaser, J. G., Greystoke, B. F., Jordan, A. M., The Histone Demethylase Kdm1a Sustains the Oncogenic Potential of Mll-Af9 Leukemia Stem Cells. *Cancer cell* **21**, 473-487 (2012).
55. Wissmann, M., Yin, N., Muller, J. M., Greschik, H., Fodor, B. D., Jenuwein, T., Vogler, C., Schneider, R., Gunther, T., Buettner, R., Metzger, E., Schule, R., Cooperative Demethylation by Jmjd2c and Lsd1 Promotes Androgen Receptor-Dependent Gene Expression. *Nature Cell Biology* **9**, 347-U176 (2007).
56. Wissmann, M., Yin, N., Muller, J. M., Greschik, H., Gunther, T., Friedrichs, N., Buettner, R., Metzger, E., Schule, R., Androgen Receptor Function Is Regulated by Histone Demethylases: Implication for Prostate Cancer. *Febs Journal* **275**, 16-16 (2008).
57. Mimasu, S., Sengoku, T., Fukuzawa, S., Umehara, T., Yokoyama, S., Crystal Structure of Histone Demethylase Lsd1 and Tranylcypromine at 2.25 Å. *Biochemical and Biophysical Research Communications* **366**, 15-22 (2008).
58. Ehrbrecht, A., Müller, U., Wolter, M., Hoischen, A., Koch, A., Radlwimmer, B., Actor, B., Mincheva, A., Pietsch, T., Lichter, P., Comprehensive Genomic Analysis of Desmoplastic

- Medulloblastomas: Identification of Novel Amplified Genes and Separate Evaluation of the Different Histological Components. *The Journal of pathology* **208**, 554-563 (2006).
59. Liu, G., Bollig-Fischer, A., Kreike, B., van de Vijver, M. J., Abrams, J., Ethier, S. P., Yang, Z. Q., Genomic Amplification and Oncogenic Properties of the Gasc1 Histone Demethylase Gene in Breast Cancer. *Oncogene* **28**, 4491-4500 (2009).
 60. Yang, Z.-Q., Imoto, I., Fukuda, Y., Pimkhaokham, A., Shimada, Y., Imamura, M., Sugano, S., Nakamura, Y., Inazawa, J., Identification of a Novel Gene, Gasc1, within an Amplicon at 9p23–24 Frequently Detected in Esophageal Cancer Cell Lines. *Cancer Research* **60**, 4735-4739 (2000).
 61. Semenza, G. L., Defining the Role of Hypoxia-Inducible Factor 1 in Cancer Biology and Therapeutics. *Oncogene* **29**, 625-634 (2010).
 62. Luo, W., Chang, R., Zhong, J., Pandey, A., Semenza, G. L., Histone Demethylase Jmjd2c Is a Coactivator for Hypoxia-Inducible Factor 1 That Is Required for Breast Cancer Progression. *Proceedings of the National Academy of Sciences* **109**, E3367-E3376 (2012).
 63. Berry, W. L., Shin, S., Lightfoot, S. A., Janknecht, R., Oncogenic Features of the Jmjd2a Histone Demethylase in Breast Cancer. *International Journal of Oncology* **41**, 1701-1706 (2012).
 64. Mallette, F. A., Richard, S., Jmjd2a Promotes Cellular Transformation by Blocking Cellular Senescence through Transcriptional Repression of the Tumor Suppressor Chd5. *Cell reports* **2**, 1233-1243 (2012).
 65. Black, J. C., Allen, A., Van Rechem, C., Forbes, E., Longworth, M., Tschöp, K., Rinehart, C., Quiton, J., Walsh, R., Smallwood, A., Conserved Antagonism between Jmjd2a/Kdm4a and Hp1 γ During Cell Cycle Progression. *Molecular cell* **40**, 736-748 (2010).
 66. Klose, R. J., Yamane, K., Bae, Y. J., Zhang, D. Z., Erdjument-Bromage, H., Tempst, P., Wong, J. M., Zhang, Y., The Transcriptional Repressor Jhdm3a Demethylates Trimethyl Histone H3 Lysine 9 and Lysine 36. *Nature* **442**, 312-316 (2006).
 67. Lu, Y., Wajapeyee, N., Turker, M. S., Glazer, P. M., Silencing of the DNA Mismatch Repair Gene *Mlh1* Induced by Hypoxic Stress in a Pathway Dependent on the Histone Demethylase Lsd1. *Cell reports* **8**, 501-513 (2014).

68. Cascella, B., Mirica, L. M., Kinetic Analysis of Iron-Dependent Histone Demethylases: A-Ketoglutarate Substrate Inhibition and Potential Relevance to the Regulation of Histone Demethylation in Cancer Cells. *Biochemistry* **51**, 8699-8701 (2012).
69. Lengner, C. J., Gimelbrant, A. A., Erwin, J. A., Cheng, A. W., Guenther, M. G., Welstead, G. G., Alagappan, R., Frampton, G. M., Xu, P., Muffat, J., Derivation of Pre-X Inactivation Human Embryonic Stem Cells under Physiological Oxygen Concentrations. *Cell* **141**, 872-883 (2010).
70. Kim, S.-H., Kwon, S. H., Park, S.-H., Lee, J. K., Bang, H.-S., Nam, S.-J., Kwon, H. C., Shin, J., Oh, D.-C., Tripartin, a Histone Demethylase Inhibitor from a Bacterium Associated with a Dung Beetle Larva. *Organic Letters* **15**, 1834-1837 (2013).
71. Wang, L., Chang, J., Varghese, D., Dellinger, M., Kumar, S., Best, A. M., Ruiz, J., Bruick, R., Peña-Llopis, S., Xu, J., A Small Molecule Modulates Jumonji Histone Demethylase Activity and Selectively Inhibits Cancer Growth. *Nature communications* **4**, (2013).
72. Cloos, P. A. C., Christensen, J., Agger, K., Maiolica, A., Rappsilber, J., Antal, T., Hansen, K. H., Helin, K., The Putative Oncogene Gasc1 Demethylates Tri- and Dimethylated Lysine 9 on Histone H3. *Nature* **442**, 307-311 (2006).
73. Liu, G., Bollig-Fischer, A., Kreike, B., van de Vijver, M. J., Abrams, J., Ethier, S. P., Yang, Z. Q., Genomic Amplification and Oncogenic Properties of the Gasc1 Histone Demethylase Gene in Breast Cancer. *Oncogene*, (2009).
74. Suikki, H. E., Kujala, P. M., Tammela, T. L. J., van Weerden, W. M., Vessella, R. L., Visakorpi, T., Genetic Alterations and Changes in Expression of Histone Demethylases in Prostate Cancer. *Prostate* **70**, 889-898 (2010).

Chapter 2: Kinetic Analysis of Iron-Dependent Histone Demethylases: α -Ketoglutarate Substrate Inhibition and Potential Relevance to the Regulation of Histone Demethylation in Cancer Cells

A portion of this work was published as a communication in *Biochemistry* on October 15, 2012.

DOI:10.1021/bi3012466

2.1 Introduction

Covalent modification of chromatin by histone methylation has wide-ranging effects on nuclear functions, such as transcriptional regulation, genome integrity, and epigenetic inheritance.¹⁻³ Until recently, histone methylation was believed to be a static modification, however the identification of histone demethylase (HDM) enzymes has revealed that this epigenetic mark is dynamically controlled.⁴⁻⁶ The Jumonji C domain-containing HDMs (JmjC-HDMs) catalyze the demethylation of methylated lysine residues through a hydroxylation reaction and belong to the large class of α -ketoglutarate (α KG) dependent, O₂-activating, non-heme iron enzymes.⁷⁻⁹ To date, 18 JmjC-HDMs have been reported and grouped into five subfamilies, and the enzymes exhibit both residue and methylation state specificity.¹⁰⁻¹² In addition, JmjC-HDMs have been implicated in cancer and stem cell biology. For example, it has recently been shown that PLU-1 (KDM5B/JARID1B) is an H3K4 HDM that plays an important role in the proliferation of breast cancer cells through transcriptional repression of tumor suppressor genes,^{13,14} while the H3K9/H3K36 HDM GASC1

(or KDM4C/JMJ2C) was proposed to be linked to stem-cell phenotypes in breast cancer.¹⁵ Thus, it is of great interest to design specific inhibitors for the various HDM subfamilies by utilizing the enzymes' substrate specificities.¹⁶⁻²⁴ However, there is limited data available on the enzymology of HDMs. In this regard, we have successfully expressed and purified three HDMs of the KDM4 subfamily, including cancer-relevant KDM4A and KDM4C, and obtained a detailed enzyme kinetic analysis by employing three different assays (vide infra). Interestingly, a case of α KG substrate inhibition was observed, which could have important implications into the regulation of KDM4 activity in cancer biology.

2.2 Methods

2.2.1 Protein Expression and Purification

Truncated constructs of KDM4A,¹¹ KDM4E,¹¹ and KDM4C,¹⁹ containing the catalytic JmjC- and JmjN- domains, were obtained as gifts from Professors Schofield and Opperman (KDM4A and KDM4E) and Professor Mizukami (KDM4C), and were expressed and purified as reported,^{11,19} with minor modifications. Each plasmid was transformed into the Rosetta II (DE3) strain of *E. coli*, with colonies grown on LB agar + kanamycin (KM) plates. Single colonies were picked and allowed to grow overnight in Terrific Broth (TB) medium supplemented with 50 μ g/mL KM and 34 μ g/mL chloramphenicol (CAM). The overnight culture was split evenly into four flasks containing 600 mL TB with the appropriate antibiotics and 0.4% glycerol, and the inoculation was set to shake at 225 rpm at 37 °C. When the absorbance at 600 nm reached 0.5, the temperature was reduced to 18 °C. When OD₆₀₀ = 0.8, expression was induced with 0.2 mM IPTG, and the growth was continued for 18 hours at 18 °C, at which time the cells were collected via centrifugation (3500

rpm for 20 minutes, 4 °C) and lysed. *Lysis conditions:* 50 mM HEPES (pH 7.5), 500 mM NaCl, 5 mM imidazole, 0.5 mM phenylmethylsulfonyl fluoride (PMSF), 0.5 mM tris(2-carboxyethyl)phosphine (TCEP), 15 units/mL benzonase.

Following lysis, the cells were sonicated in 30 second intervals for approximately 30 min. The homogenized cells were spun at 10,000 rpm for 30 min at 4 °C, and the supernatant was collected and purified over a Ni-NTA superflow column using increasing concentrations of imidazole. The elution fractions rich in the protein of interest were exchanged into 50 mM Tris (pH 8.5) with 50 mM NaCl overnight. The protein solution was passed over 1 mL anion-exchange resin (Super-Q, Bio-Rad) using a step gradient of increasing concentrations of NaCl. Fractions of interest were combined and exchanged into a storage buffer (500 mM NaCl, 10 mM HEPES pH 7.5, 500 μ M TCEP, 5% glycerol), concentrated, and flash frozen in liquid nitrogen. The yield of >95% pure protein (Figure 2.1) varied from 3 mg/L (KDM4C) to 20 mg/L (KDM4E).

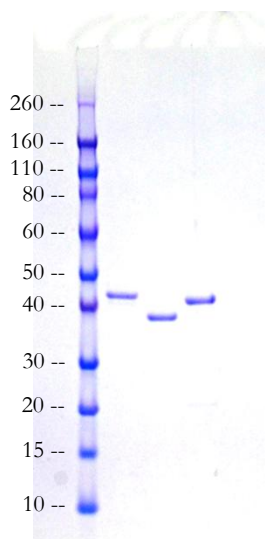
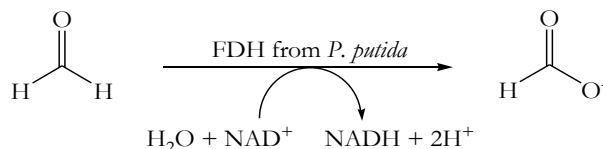


Figure 2.1. Coomassie Blue stained 4-20% SDS-PAGE gel of (left to right): MW marker (kDa) and purified KDM4A, KDM4E, and KDM4C.

2.2.2 Formaldehyde Dehydrogenase Coupled Fluorescence Assay

Scheme 2.1. Oxidation of formaldehyde is coupled with the reduction of NAD⁺.



All reactions were performed at room temperature. The fixed assay conditions were 50 mM HEPES (pH 7.5), 500 μ M sodium L-ascorbate, 50 mM NaCl, 0.04 units formaldehyde dehydrogenase (FDH) (*P. putida*, Sigma), and 1 mM NAD⁺. In H3₍₇₋₁₄₎K9me₃ variation assays (25-750 μ M), α KG was held constant at 300 μ M. In α KG variation assays (10-5000 μ M), H3₍₇₋₁₄₎K9me₃ was held constant at 250 μ M. All FDH coupled assays were performed at 258 μ M O₂ concentration. The reaction components (except H3₍₇₋₁₄₎K9me₃) were combined and added to a mixture of 50 μ M Fe^{II}(NH₄)₂SO₄·6H₂O and 8 μ M HDM. The reaction was started by addition of H3₍₇₋₁₄₎K9me₃ and fluorescence of NADH production was monitored for 10 minutes. In order to eliminate the possibility of artificially enhanced enzymatic activity due to uncoupling, the extent of demethylation of the peptide substrate was confirmed by MALDI-TOF MS (section 2.2.4). The apparent kinetic parameters k_{cat} and K_{m} were determined by fitting the kinetic data to the Michaelis-Menten equation (2-1) by using the program Kaleidagraph:

$$\text{rate} = \frac{V_{\text{max}}[S]}{K_{\text{m}} + [S]} \quad (2-1)$$

The apparent K_{i} values for α KG were determined by fitting the kinetic data to the following substrate inhibition equation (2-2) using the program Kaleidagraph:

$$\text{rate} = \frac{\frac{V_{\max}[S]}{K_m}}{1 + \frac{[S]}{K_m} + \frac{[S]^2}{K_m K_i}} \quad (2-2)$$

Although NAD^+ shows no inhibition of KDM4E up to 3 mM, the higher K_m (peptide) and lower k_{cat} values obtained through the FDH coupled assay (vide infra) are likely due to the less-than-optimal activity of *P. putida* FDH at high peptide concentrations, when a lag phase in NADH formation was observed. A lag phase in the formation of NADH was when the initial HDM initial rates were large (e.g., at high peptide substrate concentrations, Fig. 2.3). This could be due to either a less-than-optimal enzymatic rate for the FDH-catalyzed reaction that is lower than the HDM enzymatic rate, or a partial inhibition of FDH by the excess peptide. Overall, the observed lag phase could lead to overestimated K_m values and underestimated k_{cat} values, as observed experimentally (see Table 2.1). In addition, although slightly higher enzymatic HDM activities were observed at 37 °C and pH 8 vs. 25 °C and pH 7.5, we employed the latter conditions to allow a direct comparison with literature data.

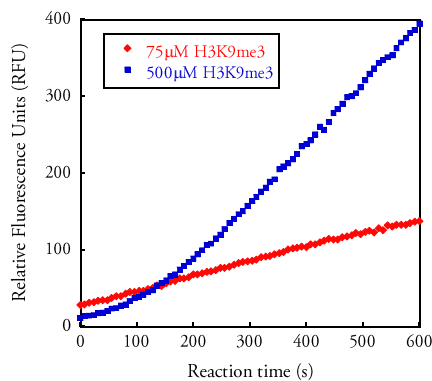


Figure 2.2. Observed lag phase in NADH formation at high peptide substrate concentrations.

2.2.3 Dioxygen Consumption Assay

All reactions were performed at 25 °C. A YSI model 5300 biological oxygen electrode was used to measure the initial rates of oxygen uptake, which were found to be linear for approximately 2 min. The instrument was calibrated by using air-saturated water, which contains 258 μM O_2 and was assigned to correspond to “100% Air”. The fixed assay conditions include 50 mM HEPES pH 7.5 (or 50 mM Tris pH 7.5) and 500 μM sodium L-ascorbate. The HDM concentration ranged from 1.6 to 3.0 μM , as given in Figures 2.4 and 2.5. In $\text{H3}_{(7-14)}\text{K9me}_3$ variation assays (5-500 μM), αKG was held constant at 300 μM . In αKG variation assays (2-6000 μM), $\text{H3}_{(7-14)}\text{K9me}_3$ was held constant at 100 μM . In O_2 variation experiments (15-1200 μM), the $\text{H3}_{(7-14)}\text{K9me}_3$ and αKG were held constant at 100-250 μM and 300 μM , respectively. The reaction mixture was allowed to equilibrate in the electrode chamber under an atmosphere containing various amounts of O_2 . The reaction was started by addition of the HDM enzyme reconstituted with 1 equivalent $\text{Fe}^{\text{II}}(\text{NH}_4)_2\text{SO}_4 \cdot 6\text{H}_2\text{O}$ to the O_2 electrode chamber. All rates were calculated subtracting background oxygen consumption due to ascorbate and/or $\text{Fe}(\text{II})$ in the absence of enzyme. Normally, these background rates of O_2 consumption due to the presence of both $\text{Fe}(\text{II})$ and ascorbate are negligible (less than 1%) vs. the typically measured enzymatic rates for HDMs. In addition, a similar negligible O_2 consumption background rate was observed in the presence of the holoenzyme and the absence of the peptide substrate, suggesting a very limited extent of enzyme uncoupling. The apparent kinetic parameters k_{cat} and K_{m} were determined by fitting the kinetic data to the Michaelis-Menten equation (2-1) using the program Kaleidagraph.

The apparent K_i values for αKG were determined by fitting the kinetic data to the substrate inhibition equation (2-2) using the program Kaleidagraph.

To eliminate the possibility of artificially enhanced enzymatic activity due to uncoupling, the extent of demethylation of the peptide substrate was confirmed by MALDI-TOF MS (see Section 2.2.4).

2.2.4 MALDI-TOF Mass Spectrometry Assay

In a typical assay, the purified HDM (8 μM) was incubated for 10 min at 37 $^{\circ}\text{C}$ with $\text{H3}_{(7-14)}\text{K9me}_3$ (80-250 μM) in 50 mM HEPES (pH 7.5), 50 μM $\text{Fe}^{\text{II}}(\text{NH}_4)_2\text{SO}_4 \cdot 6\text{H}_2\text{O}$, 500 μM sodium L-ascorbate, and varying αKG (50 μM , 100 μM , 300 μM , 1 mM, 3 mM, 5mM). The enzymatic demethylation was stopped by addition of MeOH and TFA, the precipitated protein was removed via centrifugation, and the resulting supernatant was collected. An aliquot of the reaction solution was added to 10 mg/mL α -cyano-4-hydroxycinnamic acid MALDI matrix in 50% acetonitrile/0.1% TFA and spotted directly onto the MALDI plate. For analysis, an ABI DE-STR MALDI TOF instrument was used.

In addition, MALDI-TOF MS assays were used to confirm the extent of demethylation of the peptide substrate for the FDH coupled assay or O_2 consumption assay experiments. MALDI-TOF MS studies were performed at both 37 $^{\circ}\text{C}$ and 25 $^{\circ}\text{C}$, and the results were similar, except that the reaction was slower at 25 $^{\circ}\text{C}$, and led to smaller amounts of demethylated product that were more difficult to quantify accurately. Thus, we chose to use the 37 $^{\circ}\text{C}$ data for confirming the αKG substrate inhibition behavior.

2.2.5 Docking Studies of KDM4A and KDM4C with α KG

Low energy conformers of α KG were generated using OMEGA following minimization by SZYBKI (both OpenEye software). The conformers were modeled into the KDM4A (PDB 2OQ7) and KDM4C (PDB 2XML) active sites with OpenEye's FRED fast exhaustive docking program using the Poisson-Boltzmann solvation method at 310 K, taking into account cavity solvation energies. All renderings were generated using PyMol.

2.2.6 Crystallography

Protein crystals were grown by the hanging drop vapor diffusion method at 4 °C. Crystals of the catalytic domains of KDM4A (residues 1-350; 11 mg/mL) in complex with α KG (100 mM) formed in drops of a 1 : 1.5 mixture of protein and crystallization buffer (0.1 M citrate pH 6.0, 17.5% PEG-3500, 4 mM NiCl₂). Crystals were harvested from the mother liquor with a nylon loop, mounted on a goniometer, and directly frozen in a liquid N₂ vapor stream at 100 K. Data were collected by Dr. Soon Goo Lee using 19ID beamline at Argonne National Laboratory Advanced Photon Source with a CCD detector at a distance of 361.69 mm from the crystal. Images (180 frames) were collected at 0.979 Å in 1.0° oscillations (a 180° hemisphere) indexed (P 2 21 21) and scaled using HKL 3000.²⁵ This resulted in 50,379 reflections in the 50 - 2.1 Å resolution range. Unit cell parameters and data reduction statistics are summarized in Table A.1 in Appendix A.

Detector	CCD
Type	ADSC QUANTUM 315r
Details	Rosenbaum-Rock high-resolution double-crystal monochromator

The structure of KDM4A was phased by using the molecular replacement method with Phaser, and a model of the crystal structure of KDM4A complexed with inhibitor (PDB: 3RVH) structure.²⁶ Based on the Matthew's coefficient, two protein monomers were expected in the asymmetric unit. The solution from Phaser had a top TFZ of 41.6. Manual fitting was initiated using COOT.²⁷ Refinement was performed using Phenix with 10% of the data excluded from refinement for the R_{free} calculation.²⁸ The structure models were analyzed at TLS Motion Determination Server and refined with eight TLS groups, yielding a model with an R_{cryst} of 18.1% and R_{free} of 22.4%.²⁹ The final model was analyzed by using the CCP4 programs SFCHECK and PROCHECK.^{30, 31, 32} Refinement statistics are listed in Table A.1 in Appendix A.

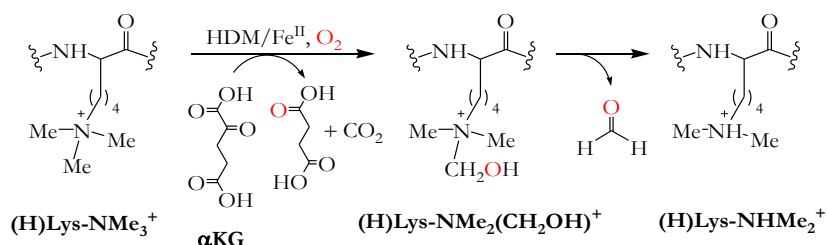
2.3 Results and Discussion

In the lysine demethylation reaction, JmjC-HDMs hydroxylate the *N*-methyl substrate to a hydroxymethyl group, which is converted non-enzymatically to formaldehyde and the demethylated product (Scheme 1).⁴⁻⁶ Our initial kinetic studies focused on KDM4A, the first HDM with a resolved crystal structure and one that has been used extensively in biochemical studies.¹⁰⁻¹² Moreover, KDM4A was recently found to be overexpressed at the protein level in lung cancer, prostate cancer,

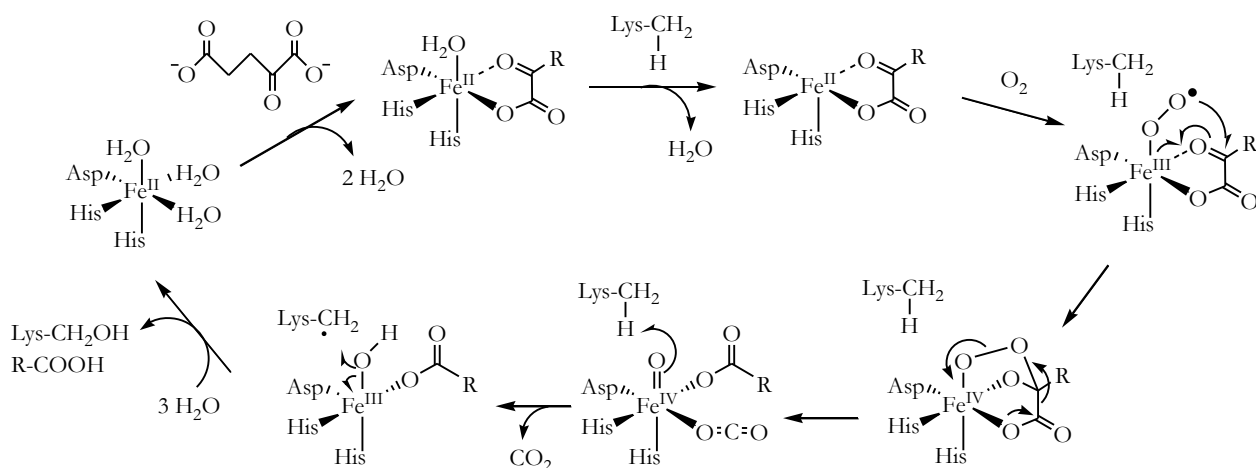
and about 60% of breast tumors.^{15, 33, 34} The pseudogene-encoded KDM4E, which shares greater than 80% sequence similarity to KDM4A, has been often employed in enzyme activity studies as it has the highest activity when compared to the other members of the KDM4 subfamily.¹⁶⁻²⁴ Finally, KDM4C is of great interest owing to its implications in brain, breast, prostate, and esophageal cancers,^{15, 35} although the kinetics of KDM4C has not been fully investigated to date.¹⁶⁻²⁴

Scheme 2.2. Histone demethylation by JmjC-HDMs, shown for a trimethyllysine substrate.

a. Overview of lysine demethylation



b. Proposed mechanism of lysine demethylation



Truncated constructs of KDM4A,¹⁰⁻¹² KDM4E,¹⁶⁻²⁴ and KDM4C,¹⁶⁻²⁴ containing the catalytic JmjN- and JmjC- domains, were transformed into the *E. coli* Rosetta II strain and expressed and purified using published procedures (see Section 2.2.1). The enzymatic activity of the three HDMs was monitored by three complimentary assays: a coupled formaldehyde dehydrogenase (FDH) NADH fluorescence assay, a discontinuous MALDI-TOF mass spectrometry (MS) assay, and a continuous O₂ consumption assay. Initially, kinetic parameters were obtained using an adapted version of the widely-employed FDH coupled assay,^{10-12, 36, 37} and a trimethylated H3₍₇₋₁₄₎K9me₃ octapeptide as the histone substrate analog. However, this coupled assay could yield altered kinetic data owing to the employment of a second enzyme and corresponding substrate in the reaction solution (vide infra). Demethylation of the peptide substrate was also confirmed by MALDI-TOF MS, and quantification of the amount of di- and mono-methylated peptide products was correlated to the extent of demethylation measured using the other enzymatic assays. However, no direct continuous assay to study the enzymatic activity of HDMs has been developed to date. In this regard, we have employed a continuous O₂ consumption assay that measures in real-time the HDM enzymatic activity through the use of a Clark oxygen electrode. To the best of our knowledge, this is the first kinetic study of HDMs using a continuous O₂ consumption assay, which could provide more physiologically relevant kinetic parameters.³⁸

Using the above enzyme activity assays, we determined the kinetic parameters for three JmjC-HDMs with respect to all three substrates: the H3₍₇₋₁₄₎K9me₃ peptide substrate, O₂, and α KG. For KDM4A and KDM4C, the FDH-coupled assay yielded K_m values for the peptide substrate (104 \pm 16 μ M for KDM4A, 76 \pm 11 μ M for KDM4C) that are similar to those found in the

literature,^{10-12, 16-24, 39, 40} while for KDM4E a slightly larger K_m value was obtained ($224 \pm 15 \mu\text{M}$, Table 2.1).¹ Figure 2.3 displays the $\text{H3}_{(7-14)}\text{K9me}_3$ K_m plots for the three HDMs.

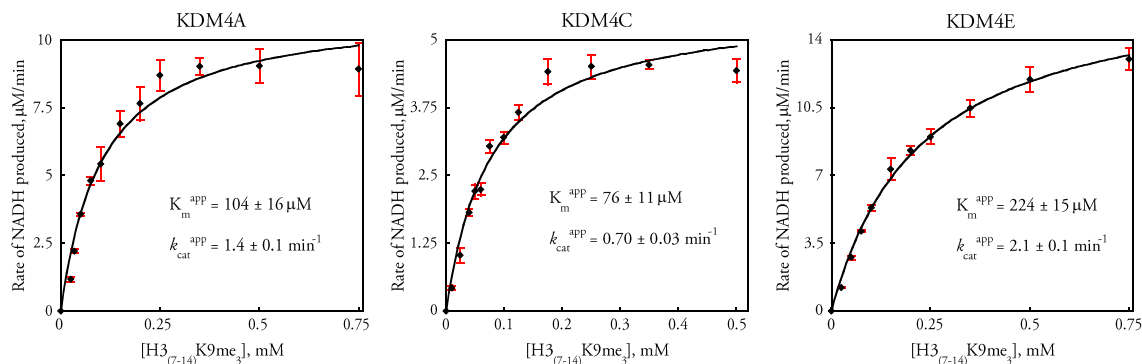


Figure 2.3. Variable $\text{H3}_{(7-14)}\text{K9me}_3$ K_m plots obtained using the FDH-coupled assay.

Interestingly, the use of the O_2 consumption assay reveals significantly reduced peptide K_m values for KDM4A ($31 \pm 3 \mu\text{M}$), KDM4C ($32 \pm 3 \mu\text{M}$), and KDM4E ($38 \pm 3 \mu\text{M}$), as well as turnover numbers that are similar or higher than those from other studies (Figure 2.4).^{10-12, 16-24, 39, 40} The O_2 consumption assay can be performed under saturating conditions for all substrates, and, thus, it provides a unique opportunity to obtain true k_{cat} values for the three HDMs (Table 2.1). Most importantly, the observed activity of KDM4C is higher than reported previously,¹⁶⁻²⁴ and comparable to the activities of KDM4A and KDM4E, the HDMs commonly employed in enzyme activity studies.¹⁶⁻²⁴ Thus, KDM4C can now be used in inhibition studies employing the O_2 consumption assay, especially given its direct implication in cancer biology.¹⁵ Overall, the O_2 consumption assay seems to allow for a superior characterization of HDMs vs. the FDH coupled

¹ While NAD^+ shows no inhibition of KDM4E up to 3 mM, the higher $K_m(\text{peptide})$ values obtained through the FDH coupled assay are likely due to the presence of a second enzyme and corresponding substrate in the reaction solution.

assay, because the obtained K_m values for the peptide substrate are more in line with the expected affinities for the natural substrate *in vivo*, whereas higher turnover numbers were also found for all three HDMs investigated.

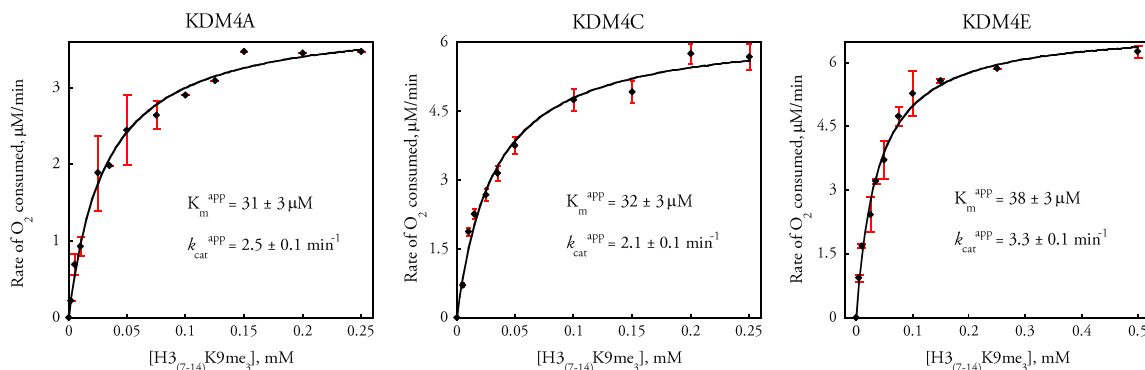


Figure 2.4. Variable H₃(₇₋₁₄)K₉me₃ K_m plots obtained from the O₂ consumption assay for 1.6 μM KDM4A, 3 μM KDM4C, and 2.1 μM KDM4E.

Table 2.1. Kinetic parameters for the three JmjC-HDMs with respect to the primary histone analog substrate.^a

HDM	Assay	H ₃ (₇₋₁₄)K ₉ me ₃ K_m^{app} (μM)	k_{cat}^{app} (min ⁻¹) ^b
KDM4A	O ₂ consumed	31 ± 3	2.5 ± 0.1
	coupled FDH	104 ± 16	1.4 ± 0.1
KDM4C	O ₂ consumed	32 ± 3	2.1 ± 0.1
	coupled FDH	76 ± 11	0.70 ± 0.03
KDM4E	O ₂ consumed	38 ± 3	3.3 ± 0.1
	coupled FDH	224 ± 15	2.1 ± 0.1

^a See section 2.2 for assay conditions. ^b k_{cat}^{app} values were determined at 258 μM O₂.

Though the majority of HDM inhibitors reported are αKG analogs,¹⁶⁻²⁴ it may be desirable to design inhibitors that compete in the enzyme active site not just with respect to αKG, but also

with respect to the peptide substrate or O₂. Using the O₂ consumption assay, we measured for the first time the K_m(O₂) values for HDMs and found that these enzymes have relatively low apparent affinities for O₂, with K_m values near or above normal cellular O₂ concentration (57 ± 10 μM for KDM4A; 158 ± 13 μM for KDM4C; 197 ± 16 μM for KDM4E; Figure 2.5 and Table 2.2).⁴¹ Such O₂ affinities suggest the enzymatic activity can be altered by small changes in O₂ concentration, and, thus, the JmjC-HDMs can act as oxygen sensors *in vivo*, as observed previously for other αKG-dependent non-heme iron oxygenases involved in the hypoxic response.⁴¹

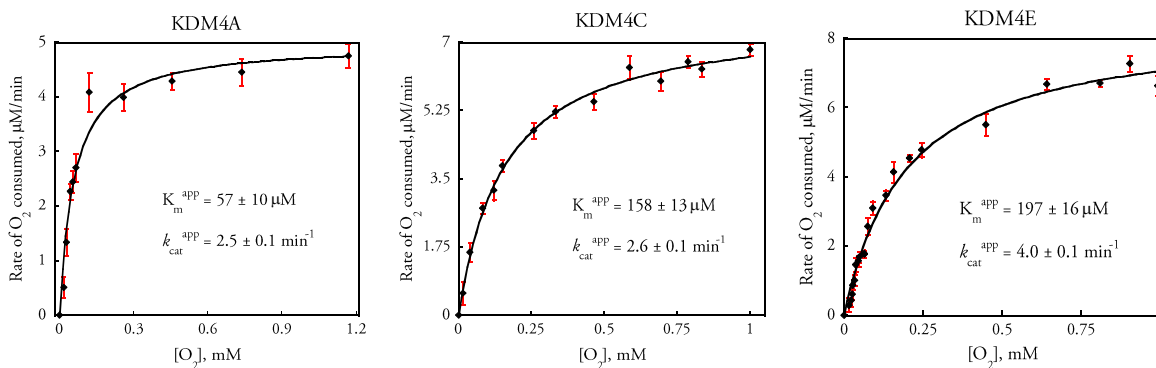


Figure 2.5. Variable O₂ K_m plots obtained using the O₂ electrode assay for 2 μM KDM4A, 3 μM KDM4C, and 2.1 μM KDM4E.

Table 2.2. Kinetic parameters for the three JmjC-HDMs with respect to the secondary substrate O₂.^a

HDM	Assay	O ₂ K _m ^{app} (μM)	k _{cat} ^{app} (min ⁻¹)
KDM4A	O ₂ consumed	57 ± 10	2.5 ± 0.1
KDM4C	O ₂ consumed	158 ± 13	2.6 ± 0.1
KDM4E	O ₂ consumed	197 ± 16	4.0 ± 0.1

^a See section 2.2 for assay conditions.

Contrastingly, the enzymes' affinities for α KG are high compared to those for O_2 , and in line with values reported previously.^{16-24, 42, 43} For all three HDMs investigated, the α KG K_m values are between 10 and 37 μ M and differ by less than two-fold between the FDH coupled assay and the O_2 consumption assay, with the latter technique providing slightly lower K_m values (Table 2.3).

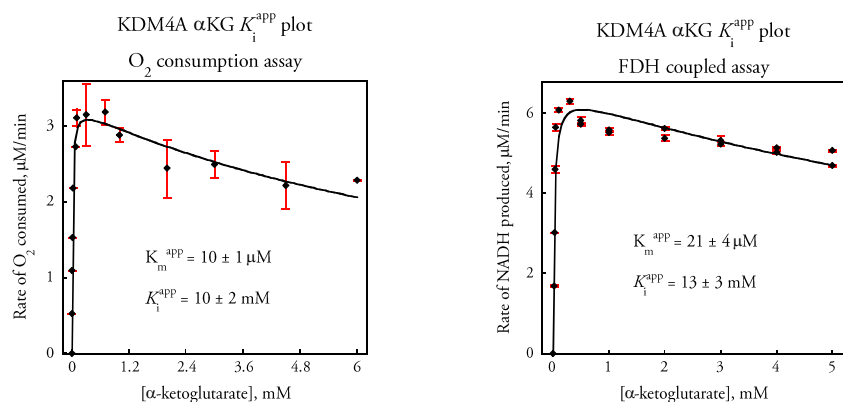
Table 2.3. Kinetic parameters for the three JmjC-HDMs with respect to the secondary substrate α KG.^a

HDM	Assay	α KG K_m^{app} (μ M)	K_i^{app} (mM) ^b
KDM4A	O_2 consumed	10 ± 1	10 ± 2
	coupled FDH	21 ± 4	13 ± 3
KDM4C	O_2 consumed	12 ± 2	4.3 ± 0.6
	coupled FDH	22 ± 5	3.4 ± 0.6
KDM4E	O_2 consumed	21 ± 2	12 ± 1
	coupled FDH	37 ± 7	11 ± 3

^a See section 2.2 for assay conditions. ^b α KG K_i^{app} values reported at 258 μ M O_2 .

While investigating the affinities of KDM4A and KDM4E for α KG, we found a mild substrate inhibition effect when α KG was present in high concentrations (>1 mM; the plots for KDM4A and KDM4E are given in Figure 2.6). The apparent K_i values were obtained using the FDH coupled assay (KDM4A, $K_i^{app} = 13 \pm 3$ mM; KDM4E, $K_i^{app} = 11 \pm 3$ mM) and the O_2 consumption assay (KDM4A, $K_i^{app} = 10 \pm 2$ mM; KDM4E, $K_i^{app} = 12 \pm 1$ mM, Table 2.3).

a)



b)

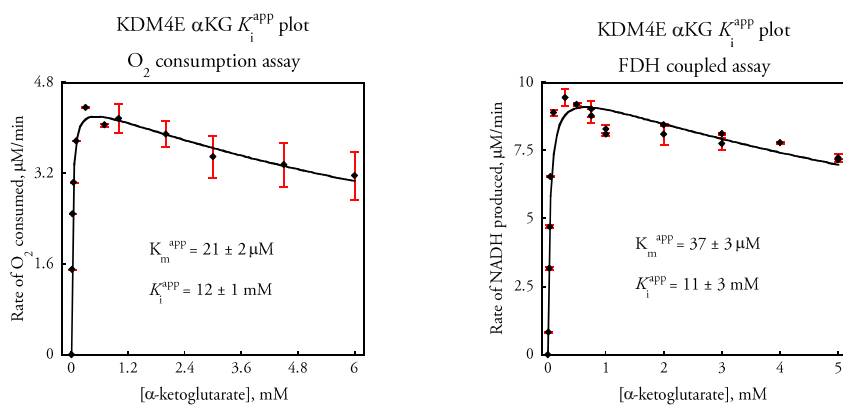


Figure 2.6. Variable α KG K_m plots obtained for a) KDM4A and b) KDM4E using the (*left*) O_2 consumption and (*right*) FDH coupled assays.

Interestingly, the α KG inhibitory effect is significantly stronger in the case of KDM4C (FDH coupled assay: $K_i^{app} = 3.4 \pm 0.6 \text{ mM}$; O_2 electrode assay: $K_i^{app} = 4.3 \pm 0.6 \text{ mM}$; Figure 2.7). Of note is that succinate, the product derived from α KG decarboxylation, was found to have no inhibitory effect on KDM4C up to 1mM. In addition, the variation of ionic strength (0 vs. 50 mM NaCl) or buffer (Tris vs. HEPES) has only a negligible effect on the measured enzymatic rates. Overall, these results suggest that the observed α KG substrate inhibition behavior is likely not due

to a generic ion or ionic strength effect. Moreover, the inhibition of KDM4C by α KG was confirmed by MALDI-TOF MS analysis (Figure A.1, Appendix A).

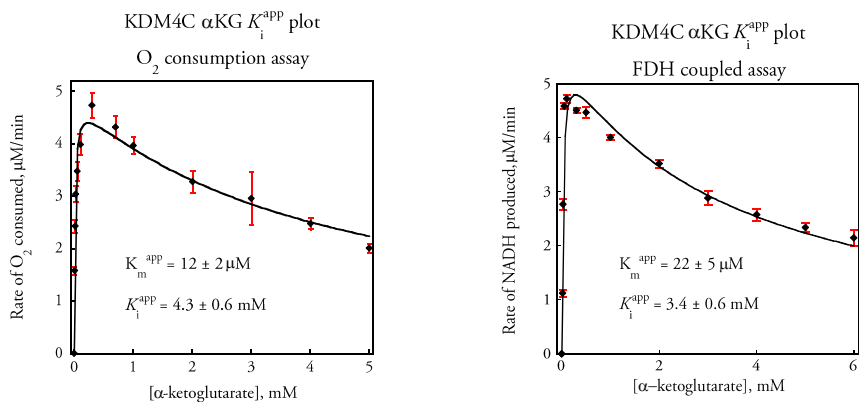


Figure 2.7. Inhibition of KDM4C by α KG, as measured by the (*left*) O₂ consumption and (*right*) FDH coupled assays. For reaction conditions, see section 2.2.

Although previous studies reported the inhibition of other α KG-dependent Fe(II) oxygenases by α KG,⁴⁴⁻⁴⁶ the type of inhibition with respect to the other substrates was not investigated in detail. In this regard, the inhibition of KDM4C by α KG was measured at constant α KG concentrations (300 μ M, 2 mM, 4 mM, 5 mM) and variable O₂ concentrations by using the O₂ consumption assay. It was found that the K_m value for O₂ increased with increasing α KG concentration, while the V_{max} value stayed relatively constant (Figure 2.8).

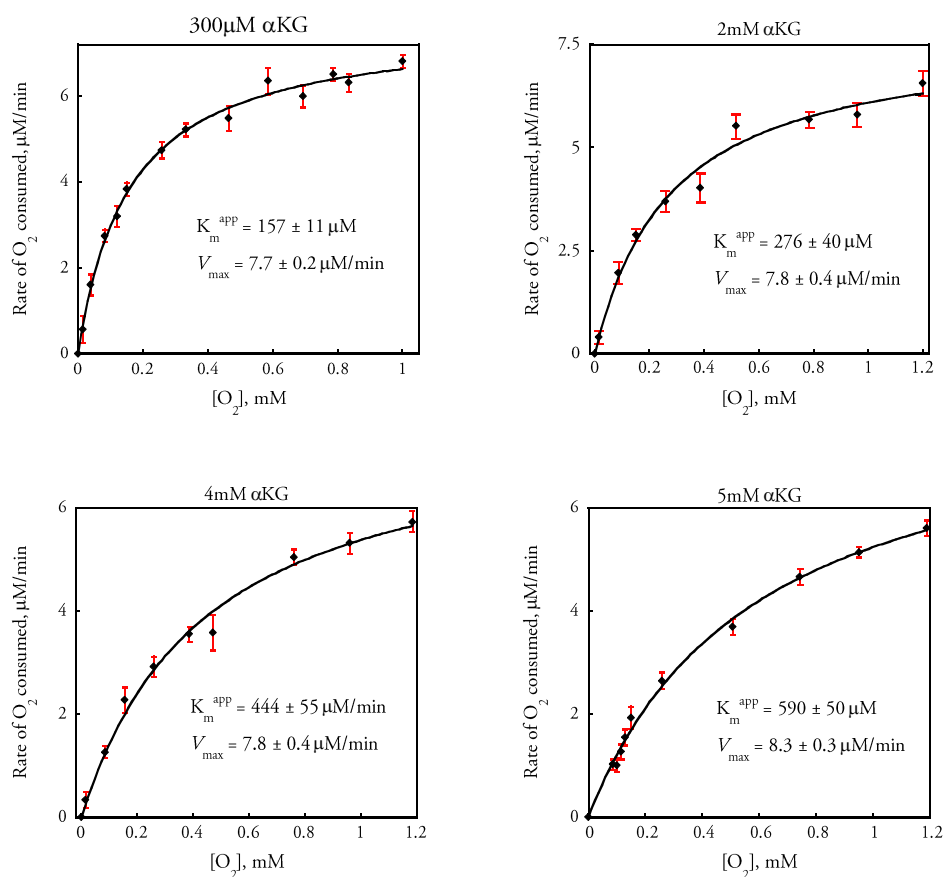


Figure 2.8. Variable O_2 K_m plots for 3 μM KDM4C obtained at varying αKG concentrations. For reaction conditions, see section 2.2.

In addition, a double reciprocal plot of the inverse of rate of reaction vs. the inverse of O_2 concentration reveals that the linear plots corresponding to the different αKG concentrations intersect on the y-axis, suggesting that αKG is a competitive inhibitor with respect to O_2 (Figure 2.9). Importantly, a competitive inhibition of O_2 by αKG has not been observed for any αKG -dependent oxygenase to date.^{16-24, 44-46} Moreover, the more pronounced αKG inhibition of KDM4C

vs. KDM4A and KDM4E is expected to impact the different activity profiles in vivo for these enzymes.

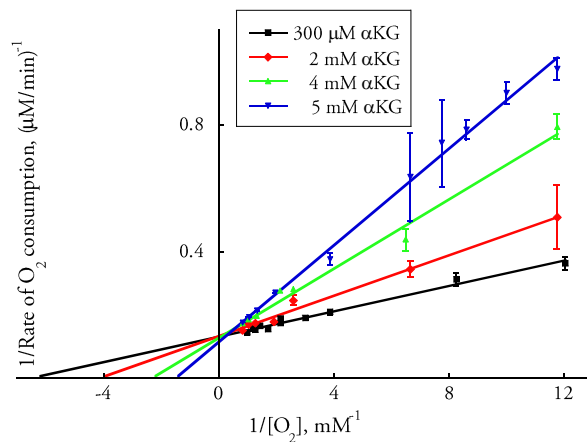


Figure 2.9. Double reciprocal plot of 1/rate of O₂ consumed vs. 1/[O₂] obtained using the O₂ consumption assay, suggesting αKG competitive inhibition of KDM4C with respect to O₂.

To test the mode of αKG inhibition of KDM4C with respect to H3₍₇₋₁₄₎K9me₃, H3₍₇₋₁₄₎K9me₃ K_m plots were generated at 300 μM, 2 mM, and 5 mM αKG concentrations by using both the FDH-coupled and O₂ consumption assays. From the FDH-coupled assay double-reciprocal plot shown in Figure 2.10, we find that αKG shows a weak, mixed-mode nonlinear inhibition of KDM4C with respect to the histone analog substrate.^{47, 48} Such a mode of inhibition is as expected, because the peptide substrate does not interact directly with the metal center and binds in the active site in a different pocket than O₂ and αKG.

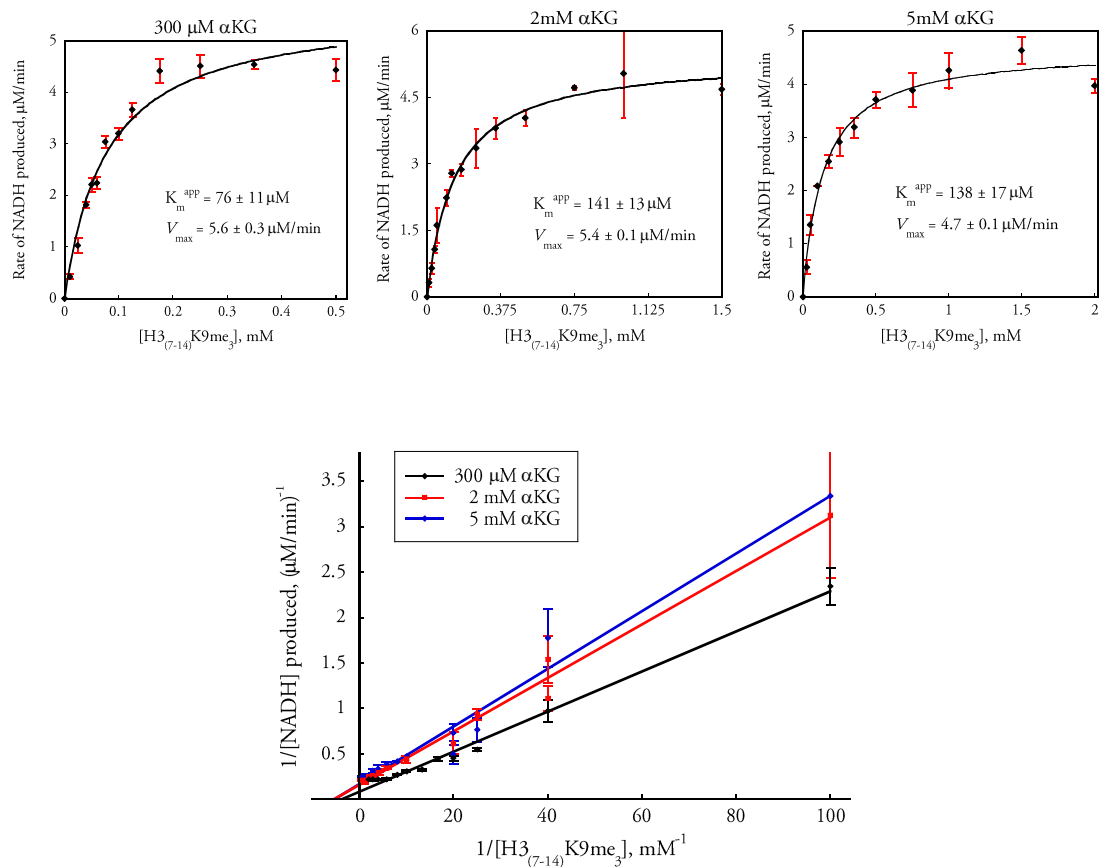


Figure 2.10. Variable $H3_{(7-14)}K9me_3$ K_m plots obtained using the FDH-coupled assay for KDM4C at α KG concentrations of 300 μ M, 2 mM, and 5 mM, and double reciprocal plots for KDM4C inhibition by α KG with respect to $H3K9me_3$, showing a mixed-mode, nonlinear type of inhibition (*bottom*).

When the mode of α KG inhibition of KDM4C with respect to $H3_{(7-14)}K9me_3$ was tested using the O_2 consumption assay, results similar to those from the FDH coupled assay were obtained. Although there is a modest increase in the apparent K_m as the α KG concentration increased, we find from the double reciprocal plots that the intersection does not occur on the y-axis, thus displaying a mixed-mode type of inhibition as expected (Figure 2.11).^{47, 48}

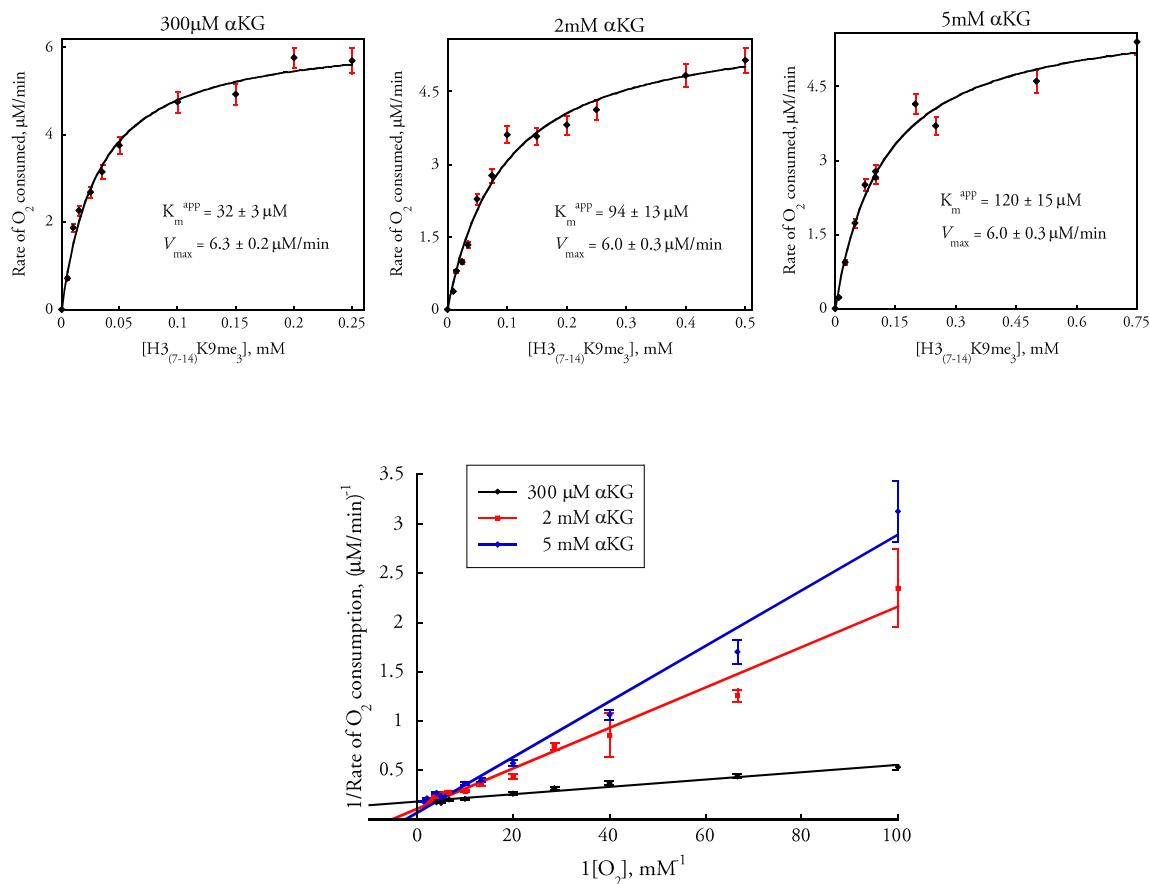


Figure 2.11. Variable H3₍₇₋₁₄₎K9me₃ K_m plots obtained using the O₂ electrode assay for 3 μ M KDM4C at α KG concentrations of 300 μ M, 2 mM, and 5 mM, and double reciprocal plots for KDM4C inhibition by α KG with respect to H3K9me₃, showing a mixed-mode, nonlinear type of inhibition (*bottom*).

The observed α KG substrate inhibition of KDM4C could have important implications in cancer biology, as KDM4C is encoded by the putative oncogene *GASC1* that is implicated in various types of cancer.³⁵ In normal healthy cells, the expression and activity of KDM4C is believed to be highly regulated.^{15, 35} Given the observed in vitro inhibition by α KG, the activity of KDM4C could be regulated in healthy tissue through a high cellular concentration of α KG, which does not allow for an optimal demethylase activity of KDM4C. Interestingly, there is a large difference in the level

of α KG in healthy brain cells and glioblastomas. Whereas in healthy brain tissue the α KG concentration ranges from 1 to 3 mM,⁴⁹ it has been reported that the α KG concentration in gliomas and glioblastoma multiformes is 100-300 μ M.^{50, 51} Indeed, we find that KDM4C displays its highest activity in vitro at an α KG concentration of \sim 300 μ M (Figure 2.12), suggesting that a decreased concentration of α KG could lead to an increased HDM activity in cancer vs. normal cells.⁵²

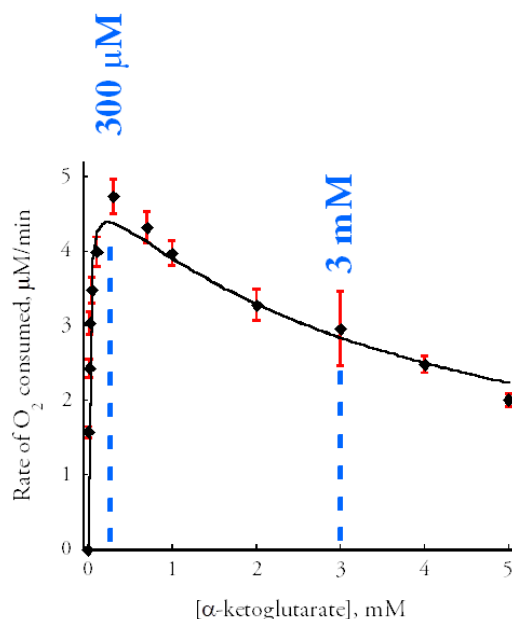


Figure 2.12. The activity of KDM4C is optimized at 300 μ M α KG in vitro.

Crystal structures of KDM4A and KDM4C in complex with Ni²⁺ and *N*-oxalylglycine were used in docking studies to visualize how a second molecule of α KG might potentially fit into the two active sites (Figure 2.13). We find a lower overall score or more energetically favorable fit for the second α KG in the KDM4C active site vs. the KDM4A active site.

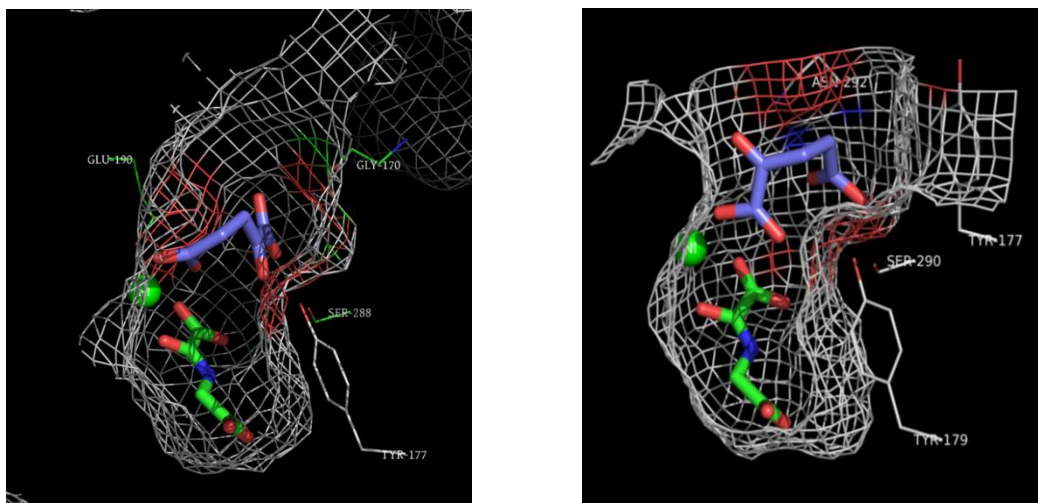


Figure 2.13. Docking studies of *N*-oxalylglycine (green) and α KG (blue) in the active sites of (*left*) KDM4A (PDB 2OQ7) and (*right*) KDM4C (PDB 2XML).

Interestingly, the orientation of α KG is flipped in the two active sites, with the α -keto oxygen closer to the metal center in the KDM4C model. Unlike the known mode of α KG binding, we find that the α -keto group of the second α KG molecule is not predicted to chelate the metal center in the KDM4C active site (Figure 2.14, *right*). We find that α KG is modeled closer to the metal center in the KDM4A active site (Figure 2.14, *left*).

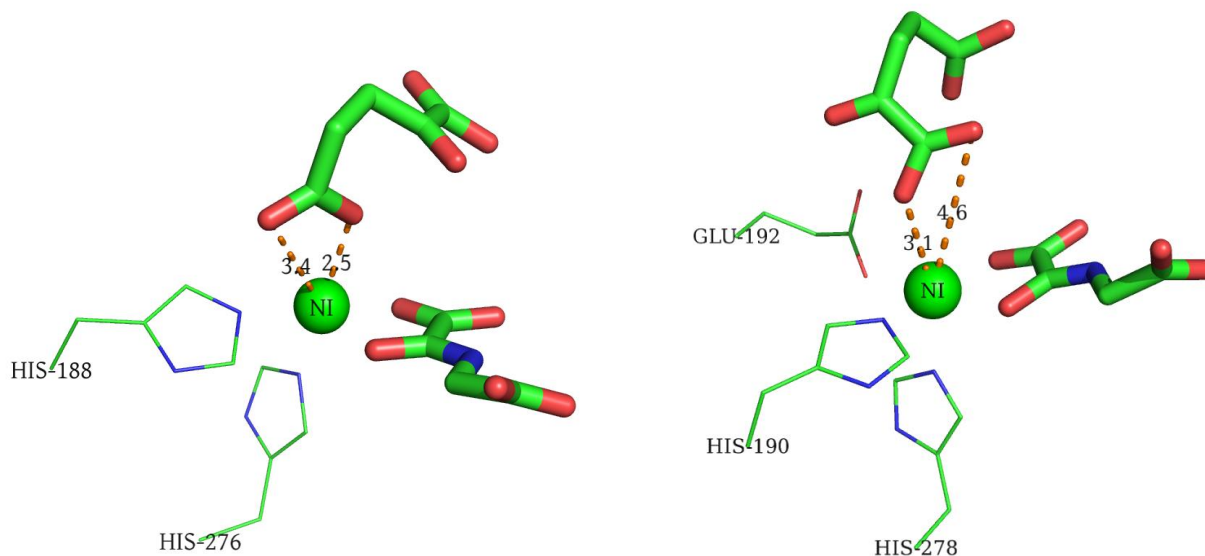


Figure 2.14. A comparison of docked α KG – Ni(II) distances in the active sites of KDM4A (*left*) and KDM4C (*right*); distances in Å.

The predicted polar contacts that a second molecule of α KG could make in each of the KDM4 active sites are shown in Figure 2.15. In both models, the second molecule of α KG is predicted to form a hydrogen bond with homologous serine and tyrosine residues (Ser 288 or 290, Tyr 177 or 179). However, only in the KDM4C is the second molecule of α KG predicted to make additional contact with a lysine side chain NH_3^+ group (Lys 243), as shown in Figure 2.15 (*right*). This additional stabilizing interaction contributes to the overall lower energy score we find when modeling the second molecule of α KG in the KDM4C vs. KDM4A active sites.

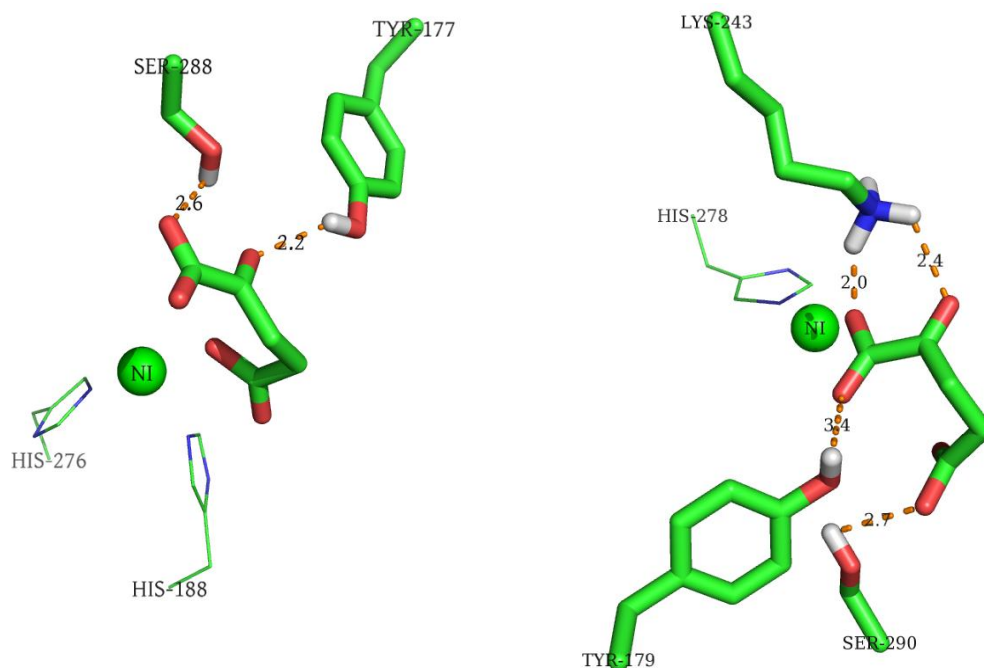


Figure 2.15. The predicted polar contacts for a second molecule of α KG in the active sites of KDM4A (*left*) and KDM4C (*right*).

Finally, we attempted to obtain a crystal structure of KDM4A in complex with two molecules of α KG, despite the high K_i^{app} value obtained from both the coupled FDH and O_2 consumption assays (Table 2.3). Protein expression limitations prevented us from attempting to obtain the structure with KDM4C. Briefly, KDM4A (11 mg/mL, 262 μM) was incubated with NiCl_2 , PEG-3500, and 100 mM α KG in citrate buffer to generate crystals via the hanging drop diffusion method at 4 $^\circ\text{C}$. Ni(II) is used in the crystallization, as it coordinates in place of Fe(II) and prevents enzymatic activity. The resulting 2.10 \AA data set obtained from a single crystal reveals KDM4A in complex with a single molecule of α KG (Figure 2.16). As this binary complex has not been solved before, we can compare it to the published KDM4A-Ni-NOG 2.15 \AA structure (Figure 2.17).

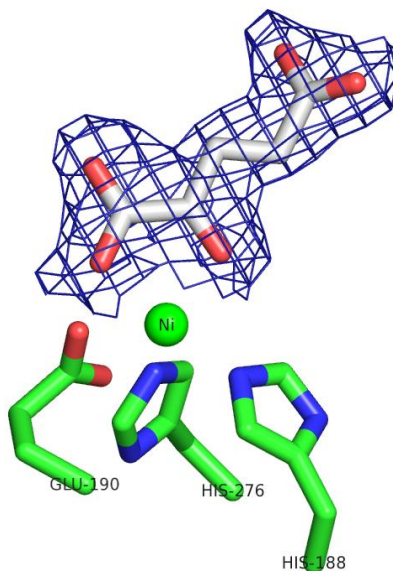


Figure 2.16. The experimental $2F_o - F_c$ electron density, displayed as blue mesh, is shown for the α KG ligand, which coordinates in a bidentate fashion to Ni(II) (substituting for Fe(II)).

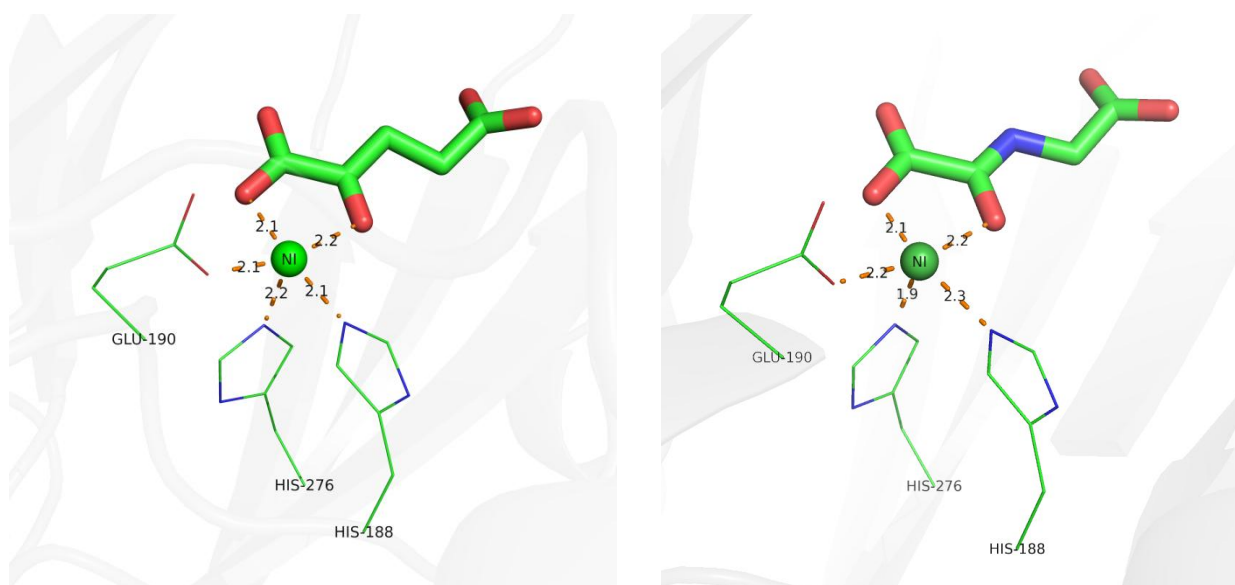


Figure 2.17. KDM4A in complex with Ni(II) and α -ketoglutarate (*left*) or *N*-oxalylglycine (*right*) (distances in Å; (*left*) unpublished structure, (*right*) PDB 2OQ7).

We find that the distances between the metal center and the facial triad (2 His, 1 Glu) are slightly different in the two complexes, while the Ni – NOG and Ni – α KG distances are the same. This is in contrast to what would be expected owing to the resonance of NOG (Figure 2.18). From the resonance contribution, one might anticipate a stronger Ni – NOG interaction than Ni – α KG. Moreover, one might anticipate a weaker Ni – His interaction in the NOG complex, but instead we find the Ni – His₂₇₆ interaction stronger than in the α KG complex.

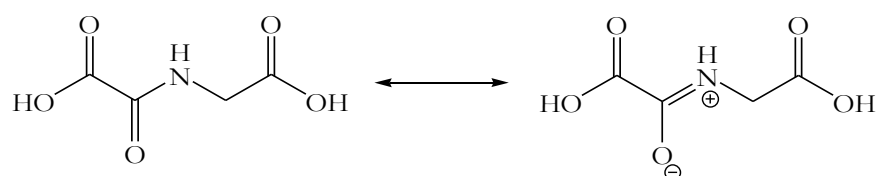


Figure 2.18. Resonance of *N*-oxalylglycine.

2.4 Conclusions

In conclusion, a detailed kinetic analysis of three JmjC-HDMs, including cancer-relevant KDM4A and KDM4C, was achieved by employing three enzyme activity assays. Using a continuous O₂ consumption assay, we found that HDMs have affinities for O₂ near or above the cellular O₂ concentration, suggesting that HDMs can act as oxygen sensors *in vivo*. Importantly, we have observed a case of α KG substrate inhibition, and the kinetic data suggest that α KG inhibits KDM4C competitively with respect to O₂. The concentration of α KG at which KDM4C displays optimal activity *in vitro* is similar to the concentration of α KG in cancer cells, which has direct implications for the increased activity of KDM4C in cancer vs. normal cells. Future studies will focus on probing the effect of α KG concentration on the activity of HDMs *in vivo*, as well as the implication of α KG concentration variation in the epigenetic control of cancer vs. normal cells.

Lastly, a new KDM4A crystal structure was solved, with the protein in a binary complex with Ni(II) and α KG.

2.5 References

1. Klose, R. J., Kallin, E. M., Zhang, Y., Jmjc-Domain-Containing Proteins and Histone Demethylation. *Nature Reviews Genetics* **7**, 715-727 (2006).
2. Bhaumik, S. R., Smith, E., Shilatifard, A., Covalent Modifications of Histones During Development and Disease Pathogenesis. *Nature Structural & Molecular Biology* **14**, 1008-1016 (2007).
3. Mosammamarast, N., Shi, Y., Reversal of Histone Methylation: Biochemical and Molecular Mechanisms of Histone Demethylases. *Annual Review of Biochemistry* **79**, 155-179 (2010).
4. Klose, R. J., Yamane, K., Bae, Y. J., Zhang, D. Z., Erdjument-Bromage, H., Tempst, P., Wong, J. M., Zhang, Y., The Transcriptional Repressor Jhdm3a Demethylates Trimethyl Histone H3 Lysine 9 and Lysine 36. *Nature* **442**, 312-316 (2006).
5. Tsukada, Y., Fang, J., Erdjument-Bromage, H., Warren, M. E., Borchers, C. H., Tempst, P., Zhang, Y., Histone Demethylation by a Family of Jmjc Domain-Containing Proteins. *Nature* **439**, 811-816 (2006).
6. Zhang, Y., Klose, R. J., Regulation of Histone Methylation by Demethylimination and Demethylation. *Nature Reviews Molecular Cell Biology* **8**, 307-318 (2007).
7. Costas, M., Mehn, M. P., Jensen, M. P., Que, L., Jr., Dioxygen Activation at Mononuclear Nonheme Iron Active Sites: Enzymes, Models, and Intermediates. *Chemical Reviews* **104**, 939-986 (2004).
8. Krebs, C., Fujimori, D. G., Walsh, C. T., Bollinger, J. M., Jr., Non-Heme Fe(IV)-Oxo Intermediates. *Accounts of Chemical Research* **40**, 484-492 (2007).

9. Loenarz, C., Schofield, C. J., Physiological and Biochemical Aspects of Hydroxylations and Demethylations Catalyzed by Human 2-Oxoglutarate Oxygenases. *Trends in Biochemical Sciences* **36**, 7-18 (2011).
10. Chen, Z., Zang, J., Whetstine, J., Hong, X., Davrazou, F., Kutateladze, T. G., Simpson, M., Mao, Q., Pan, C. H., Dai, S., Hagman, J., Hansen, K., Shi, Y., Zhang, G., Structural Insights into Histone Demethylation by Jmjd2 Family Members. *Cell* **125**, 691-702. (2006).
11. Ng, S. S., Kavanagh, K. L., McDonough, M. A., Butler, D., Pilka, E. S., Lienard, B. M. R., Bray, J. E., Savitsky, P., Gileadi, O., von Delft, F., Rose, N. R., Offer, J., Scheinost, J. C., Borowski, T., Sundstrom, M., Schofield, C. J., Oppermann, U., Crystal Structures of Histone Demethylase Jmjd2a Reveal Basis for Substrate Specificity. *Nature* **448**, 87-U88 (2007).
12. Couture, J. F., Collazo, E., Ortiz-Tello, P. A., Brunzelle, J. S., Trievel, R. C., Specificity and Mechanism of Jmjd2a, a Trimethyllysine-Specific Histone Demethylase. *Nature Structural & Molecular Biology* **14**, 689-695 (2007).
13. Lu, P. J., Sundquist, K., Baeckstrom, D., Poulsom, R., Hanby, A., Meier-Ewert, S., Jones, T., Mitchell, M., Pitha-Rowe, P., Freemont, P., Taylor-Papadimitriou, J., A Novel Gene (Plu-1) Containing Highly Conserved Putative DNA/Chromatin Binding Motifs Is Specifically up-Regulated in Breast Cancer. *Journal of Biological Chemistry* **274**, 15633-15645 (1999).
14. Yamane, K., Tateishi, K., Klose, R. J., Fang, J., Fabrizio, L. A., Erdjument-Bromage, H., Taylor-Papadimitriou, J., Tempst, P., Zhang, Y., Plu-1 Is an H3k4 Demethylase Involved in Transcriptional Repression and Breast Cancer Cell Proliferation. *Molecular cell* **25**, 801-812 (2007).
15. Cloos, P. A. C., Christensen, J., Agger, K., Maiolica, A., Rappsilber, J., Antal, T., Hansen, K. H., Helin, K., The Putative Oncogene Gasc1 Demethylates Tri- and Dimethylated Lysine 9 on Histone H3. *Nature* **442**, 307-311 (2006).
16. Rose, N. R., Ng, S. S., Mecinovic, J., Lienard, B. M. R., Bello, S. H., Sun, Z., McDonough, M. A., Oppermann, U., Schofield, C. J., Inhibitor Scaffolds for 2-Oxoglutarate-Dependent Histone Lysine Demethylases. *Journal of Medicinal Chemistry* **51**, 7053-7056 (2008).
17. Rose, N. R., Woon, E. C. Y., Kingham, G. L., King, O. N. F., Mecinovic, J., Clifton, I. J., Ng, S. S., Talib-Hardy, J., Oppermann, U., McDonough, M. A., Schofield, C. J., Selective Inhibitors of the Jmjd2 Histone Demethylases: Combined Nondenaturing Mass Spectrometric Screening and Crystallographic Approaches. *Journal of Medicinal Chemistry* **53**, 1810-1818 (2010).

18. Hamada, S., Kim, T. D., Suzuki, T., Itoh, Y., Tsumoto, H., Nakagawa, H., Janknecht, R., Miyata, N., Synthesis and Activity of N-Oxalylglycine and Its Derivatives as Jumonji C-Domain-Containing Histone Lysine Demethylase Inhibitors. *Bioorganic & Medicinal Chemistry Letters* **19**, 2852-2855 (2009).
19. Hamada, S., Suzuki, T., Mino, K., Kosek, K., Oehme, F., Flamme, I., Ozasa, H., Itoh, Y., Ogasawara, D., Komarashi, H., Kato, A., Tsumoto, H., Nakagawa, H., Hasegawa, M., Sasaki, R., Mizukami, T., Miyata, N., Design, Synthesis, Enzyme-Inhibitory Activity, and Effect on Human Cancer Cells of a Novel Series of Jumonji Domain-Containing Protein 2 Histone Demethylase Inhibitors. *Journal of Medicinal Chemistry* **53**, 5629-5638 (2010).
20. Chang, K.-H., King, O. N. F., Tumber, A., Woon, E. C. Y., Heightman, T. D., McDonough, M. A., Schofield, C. J., Rose, N. R., Inhibition of Histone Demethylases by 4-Carboxy-2,2'-Bipyridyl Compounds. *ChemMedChem* **6**, 759-764 (2011).
21. Lohse, B., Nielsen, A. L., Kristensen, J. B. L., Helgstrand, C., Cloos, P. A. C., Olsen, L., Gajhede, M., Clausen, R. P., Kristensen, J. L., Targeting Histone Lysine Demethylases by Truncating the Histone 3 Tail to Obtain Selective Substrate-Based Inhibitors. *Angewandte Chemie, International Edition in English* **123**, 9266-9269 (2011).
22. Luo, X., Liu, Y., Kubicek, S., Myllyharju, J., Tumber, A., Ng, S., Che, K. H., Podoll, J., Heightman, T. D., Oppermann, U., Schreiber, S. L., Wang, X., A Selective Inhibitor and Probe of the Cellular Functions of Jumonji C Domain-Containing Histone Demethylases. *Journal of the American Chemical Society* **133**, 9451-9456 (2011).
23. Woon, E. C. Y., Tumber, A., Kawamura, A., Hillringhaus, L., Ge, W., Rose, N. R., Ma, J. H. Y., Chan, M. C., Walport, L. J., Che, K. H., Ng, S. S., Marsden, B. D., Oppermann, U., McDonough, M. A., Schofield, C. J., Linking of 2-Oxoglutarate and Substrate Binding Sites Enables Potent and Highly Selective Inhibition of Jmjc Histone Demethylases. *Angewandte Chemie International Edition* **51**, 1631-1634 (2012).
24. Rose, N. R., McDonough, M. A., King, O. N. F., Kawamura, A., Schofield, C. J., Inhibition of 2-Oxoglutarate Dependent Oxygenases. *Chemical Society Reviews* **40**, 4364-4397 (2011).
25. Minor, W., Cymborowski, M., Otwinowski, Z., Chruszcz, M., Hkl-3000: The Integration of Data Reduction and Structure Solution-from Diffraction Images to an Initial Model in Minutes. *Acta Crystallographica Section D: Biological Crystallography* **62**, 859-866 (2006).
26. McCoy, A. J., Grosse-Kunstleve, R. W., Adams, P. D., Winn, M. D., Storoni, L. C., Read, R. J., Phaser Crystallographic Software. *Journal of Applied Crystallography* **40**, 658-674 (2007).

27. Emsley, P., Cowtan, K., Coot: Model-Building Tools for Molecular Graphics. *Acta Crystallographica Section D: Biological Crystallography* **60**, 2126-2132 (2004).
28. Adams, P. D., Afonine, P. V., Bunkóczi, G., Chen, V. B., Davis, I. W., Echols, N., Headd, J. J., Hung, L.-W., Kapral, G. J., Grosse-Kunstleve, R. W., Phenix: A Comprehensive Python-Based System for Macromolecular Structure Solution. *Acta Crystallographica Section D: Biological Crystallography* **66**, 213-221 (2010).
29. Painter, J., Merritt, E. A., Optimal Description of a Protein Structure in Terms of Multiple Groups Undergoing Tls Motion. *Acta Crystallographica Section D: Biological Crystallography* **62**, 439-450 (2006).
30. Collaborative Computational Project, N., The Ccp4 Suite: Programs for Protein Crystallography. *Acta Crystallographica* **D50**, 760-763 (1994).
31. Vaguine, A. A., Richelle, J., Wodak, S. J., Sfccheck: A Unified Set of Procedures for Evaluating the Quality of Macromolecular Structure-Factor Data and Their Agreement with the Atomic Model. *Acta Crystallographica* **D55 (Pt 1)**, 191-205 (1999).
32. Laskowsky, R. A., W., M. M., Moss, D. S., Thornton, J. M., Procheck: A Program to Check Stereochemical Quality of Protein Structure Coordinates. *J Applied Crystallography* **26**, 283-291 (1993).
33. Mallette, F. A., Richard, S., Jmjd2a Promotes Cellular Transformation by Blocking Cellular Senescence through Transcriptional Repression of the Tumor Suppressor Chd5. *Cell reports* **2**, 1233-1243 (2012).
34. Berry, W. L., Shin, S., Lightfoot, S. A., Janknecht, R., Oncogenic Features of the Jmjd2a Histone Demethylase in Breast Cancer. *International Journal of Oncology* **41**, 1701-1706 (2012).
35. Liu, G., Bollig-Fischer, A., Kreike, B., van de Vijver, M. J., Abrams, J., Ethier, S. P., Yang, Z. Q., Genomic Amplification and Oncogenic Properties of the Gasc1 Histone Demethylase Gene in Breast Cancer. *Oncogene*, (2009).
36. Shi, Y., Lan, F., Matson, C., Mulligan, P., Whetstine, J. R., Cole, P. A., Casero, R. A., Shi, Y., Histone Demethylation Mediated by the Nuclear Amine Oxidase Homolog Lsd1. *Cell* **119**, 941-953 (2004).

37. Roy, T. W., Bhagwat, A. S., Kinetic Studies of Escherichia Coli Alkb Using a New Fluorescence-Based Assay for DNA Demethylation. *Nucleic Acids Research* **35**, (2007).
38. Mirica, L. M., Klinman, J. P., The Nature of O₂ Activation by the Ethylene-Forming Enzyme Acc Oxidase. *Proceedings of the National Academy of Sciences U. S. A.* **105**, 1814-1819 (2008).
39. Krishnan, S., Collazo, E., Ortiz-Tello, P. A., Trievel, R. C., Purification and Assay Protocols for Obtaining Highly Active Jumonji C Demethylases. *Analytical Biochemistry* **420**, 48-53 (2012).
40. Kristensen, L. H., Nielsen, A. L., Helgstrand, C., Lees, M., Cloos, P., Kastrup, J. S., Helin, K., Olsen, L., Gajhede, M., Studies of H3k4me3 Demethylation by Kdm5b/Jarid1b/Plu1 Reveals Strong Substrate Recognition in Vitro and Identifies 2,4-Pyridine-Dicarboxylic Acid as an in Vitro and in Cell Inhibitor. *FEBS J.* **279**, 1905-1914 (2012).
41. Hirsila, M., Koivunen, P., Gunzler, V., Kivirikko, K. I., Myllyharju, J., Characterization of the Human Prolyl 4-Hydroxylases That Modify the Hypoxia-Inducible Factor. *Journal of Biological Chemistry* **278**, 30772-30780 (2003).
42. Chowdhury, R., Yeoh, K. K., Tian, Y. M., Hillringhaus, L., Bagg, E. A., Rose, N. R., Leung, I. K., Li, X. S., Woon, E. C., Yang, M., McDonough, M. A., King, O. N., Clifton, I. J., Klose, R. J., Claridge, T. D., Ratcliffe, P. J., Schofield, C. J., Kawamura, A., The Oncometabolite 2-Hydroxyglutarate Inhibits Histone Lysine Demethylases. *EMBO Rep.* **12**, 463-469 (2011).
43. Sakurai, M., Rose, N. R., Schultz, L., Quinn, A. M., Jadhav, A., Ng, S. S., Oppermann, U., Schofield, C. J., Simeonov, A., A Miniaturized Screen for Inhibitors of Jumonji Histone Demethylases. *Molecular Biosystems* **6**, 357-364 (2010).
44. Holme, E., A Kinetic Study of Thymine 7-Hydroxylase from Neurospora Crassa. *Biochemistry* **14**, 4999-5003 (1975).
45. Dubus, A., Lloyd, M. D., Lee, H. J., Schofield, C. J., Baldwin, J. E., Frère, J. M., Probing the Penicillin Sidechain Selectivity of Recombinant Deacetoxycephalosporin C Synthase. *Cellular and Molecular Life Sciences* **58**, 835-843 (2001).
46. Welford, R. W. D., Schlemminger, I., McNeill, L. A., Hewitson, K. S., Schofield, C. J., The Selectivity and Inhibition of Alkb. *Journal of Biological Chemistry* **278**, 10157-10161 (2003).

47. Cleland, W. W., The Kinetics of Enzyme-Catalyzed Reactions with Two or More Substrates or Products: Ii. Inhibition: Nomenclature and Theory. *Biochimica et Biophysica Acta* **67**, 173-187 (1963).
48. Cleland, W. W., The Kinetics of Enzyme-Catalyzed Reactions with Two or More Substrates or Products: Iii. Prediction of Initial Velocity and Inhibition Patterns by Inspection. *Biochimica et Biophysica Acta* **67**, 188-196 (1963).
49. Thirstrup, K., Christensen, S., Moller, H. A., Ritzen, A., Bergstrom, A. L., Sager, T. N., Jensen, H. S., Endogenous 2-Oxoglutarate Levels Impact Potencies of Competitive Hif Prolyl Hydroxylase Inhibitors. *Pharmacological Research* **64**, 268-273 (2011).
50. Dang, L., White, D. W., Gross, S., Bennett, B. D., Bittinger, M. A., Driggers, E. M., Fantin, V. R., Jang, H. G., Jin, S., Keenan, M. C., Marks, K. M., Prins, R. M., Ward, P. S., Yen, K. E., Liao, L. M., Rabinowitz, J. D., Cantley, L. C., Thompson, C. B., Vander Heiden, M. G., Su, S. M., Cancer-Associated Idh1 Mutations Produce 2-Hydroxyglutarate. *Nature* **462**, 739-744. Epub . (2009).
51. Gross, S., Cairns, R. A., Minden, M. D., Driggers, E. M., Bittinger, M. A., Jang, H. G., Sasaki, M., Jin, S., Schenkein, D. P., Su, S. M., Dang, L., Fantin, V. R., Mak, T. W., Cancer-Associated Metabolite 2-Hydroxyglutarate Accumulates in Acute Myelogenous Leukemia with Isocitrate Dehydrogenase 1 and 2 Mutations. *Journal of Experimental Medicine* **207**, 339-344 (2010).
52. Xu, W., Yang, H., Liu, Y., Yang, Y., Wang, P., Kim, S. H., Ito, S., Yang, C., Xiao, M. T., Liu, L. X., Jiang, W. Q., Liu, J., Zhang, J. Y., Wang, B., Frye, S., Zhang, Y., Xu, Y. H., Lei, Q. Y., Guan, K. L., Zhao, S. M., Xiong, Y., Oncometabolite 2-Hydroxyglutarate Is a Competitive Inhibitor of Alpha-Ketoglutarate-Dependent Dioxygenases. *Cancer cell* **19**, 17-30. (2011).

Chapter 3: Survey of Simple Primary- and Secondary-Substrate Analog Inhibitors of Iron-Dependent Histone Demethylases

3.1 Introduction

Chromatin is composed of double stranded DNA wound around a histone protein core. Covalent modifications of chromatin are essential for epigenetic inheritance, regulation of transcription, and maintenance of genomic integrity.¹⁻³ The JmjC-domain containing histone demethylases (JmjC-HDMs) are mononuclear non-heme Fe(II) oxygenases that remove methyl groups from lysine residues on the tails of histones through a hydroxylation reaction. The eighteen reported JmjC-HDMs display remarkable residue and methylation-state specificities despite their high sequence homology and common active site structure.⁴⁻⁶ Much research suggests that the regulation of histone methylation becomes askew in cancer, as well as in aging and intellectual disability.⁷⁻¹⁰ JmjC-HDMs are considered attractive therapeutic targets as their expression is often increased in primary tumors.¹¹ For instance, three members of the KDM4 subfamily, KDM4A, B, and C, are found to be upregulated in breast tumors.¹²⁻¹⁴

Because JmjC-HDMs belong to the large α -ketoglutarate (α KG)-dependent oxygenase class of enzymes, selective inhibition of a subclass of JmjC-HDMs is remarkably difficult, as recent studies have shown.¹⁵⁻¹⁸ The majority of reported JmjC-HDM inhibitors are bidentate iron chelators

and thus, α KG competitors.¹⁹⁻²¹ Although some of these α KG analogs have shown degrees of subfamily and isoform selectivity, the most promising selective inhibitors compete with the primary histone substrate, such as the recently reported small molecules JIB-04 and Tripartin, a natural product (Figure 3.1).^{16, 17, 22} Although JIB-04 is a primary substrate competitor, some of its inhibitory power comes from an interaction with the enzyme active site metal center.

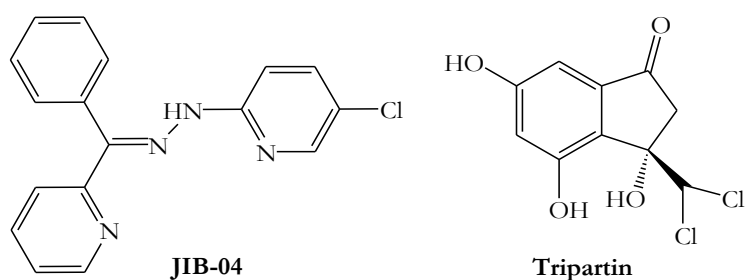


Figure 3.1. Two primary-substrate competitors of JmjC-HDMs.

The Fe(II) center in the JmjC-HDM active site is bound by a common structural motif, the His₂Asp/Glu₁ facial triad, with the three remaining positions of the octahedron taken by H₂O molecules. α KG binding displaces two waters, prompting primary substrate binding in a separate pocket and formation of a five-coordinate Fe(II). Finally, O₂ binds iron, is cleaved, and the resultant Fe(IV)-oxo reacts with the N^ε-methyl group of the lysine substrate to form an unstable hemiaminal (Figure 3.2).²³

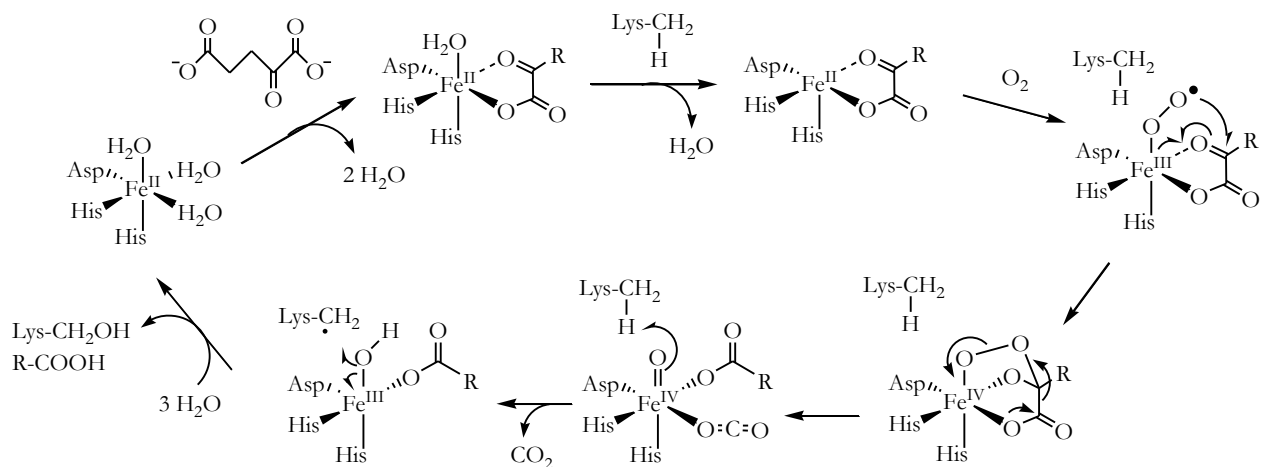
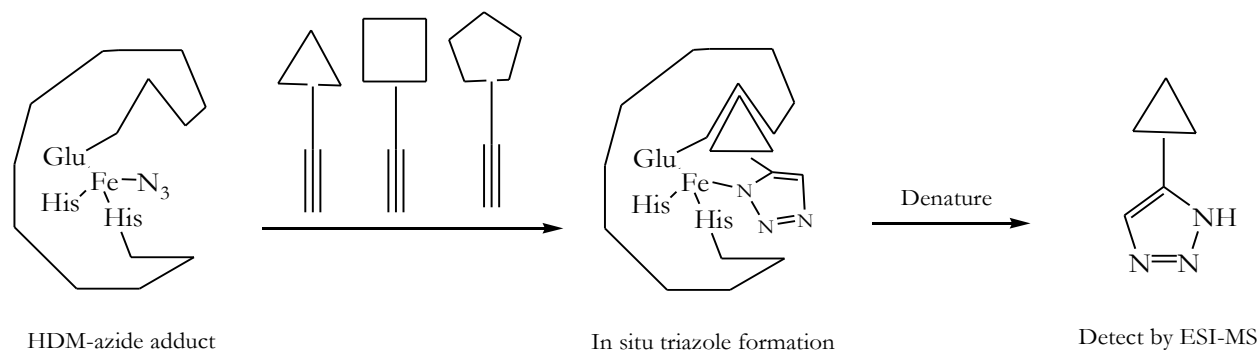


Figure 3.2. Catalytic mechanism of JmjC-HDMs.

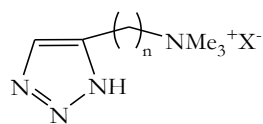
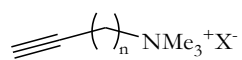
We are interested in designing inhibitors that compete for the axial O_2 -binding spot on iron in the JmjC-HDM active site. Recently, members of the KDM4 subfamily were found to display low apparent affinities for O_2 in vitro, making O_2 competitors interesting potential therapeutic targets.²⁴ An early area of interest in this work revolved around whether members of the KDM4 subfamily could act as reaction vessels in enzyme-templated Huisgen 1,3-dipolar cycloaddition reactions between enzyme – metal – azide complexes and alkyne-containing substrates (Scheme 3.1). Azide (N_3^-) has been shown to bind ferrous iron in a manner similar to dioxygen in a number of heme and non-heme iron enzymes.²⁵⁻²⁸ In this inhibitor design scheme, the HDM acts as its own specific-inhibitor synthesizer. Any formed triazole-containing compounds could be synthesized independently and tested as inhibitors of JmjC-HDMs. 1,2,3-Triazole would be expected to bind the metal center similarly as azide, albeit in a stronger manner.

Scheme 3.1. In situ HDM-templated click-chemistry



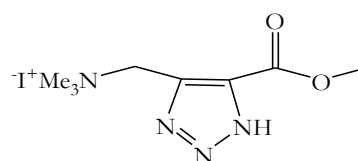
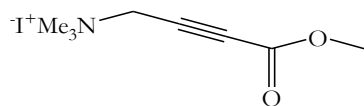
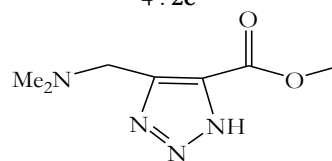
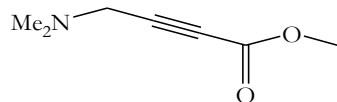
We designed simple KDM4 substrate analogs bearing carbon-carbon triple bonds or the corresponding 1,2,3-Triazole group (Figure 3.3). Primary substrate analogs were designed to mimic the di- and tri-methylammonium portion of the natural histone substrate. Secondary substrate analogs contain an α -keto group by a carboxylic acid or ester to mimic α KG and NOG. Several of the alkyne-containing compounds were tested for triazole formation in the enzyme-templated cycloaddition reaction, while some triazole-containing analogs were synthesized independently. We proposed that the analogs bearing the 1,2,3-Triazole group would be stronger inhibitors of KDM4 than those bearing the alkyne functional group, because the alkyne could not coordinate to the KDM4 metal center. Moreover, we anticipate the triazole-containing compounds to be more selective for JmjC-HDMs than other α KG-dependent oxygenases because of the JmjC-HDMs low apparent affinities for O_2 .

Primary substrate analogs:

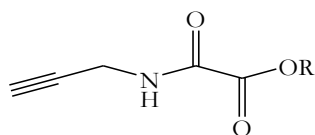


n = 1 : **1a**
2 : **1b**
4 : **1c**

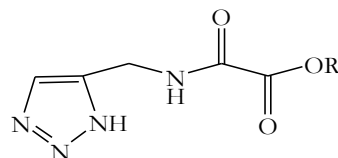
n = 1 : **2a**
2 : **2b**
4 : **2c**



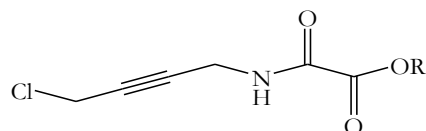
Secondary substrate analogs:



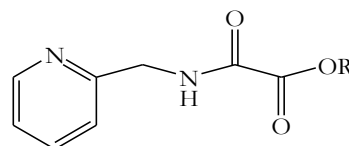
R = Et : **7a**
H : **7b**



R = Et : **8a**



R = Et : **9a**
H : **9b**



R = Et : **10a**
H : **10b**

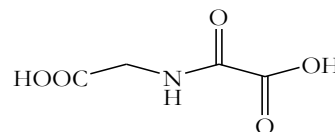
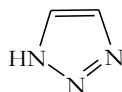
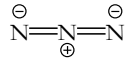


Figure 3.3. Compounds tested as inhibitors of JmjC-HDMs.

3.2 Methods

3.2.1 Synthesis of Primary Substrate Analogs

Synthesis of 1a

To a solution of 1.6 mL propargyl bromide (80% in toluene, 14.4 mmol) in 10 mL acetone was added 4.0 mL of 40% trimethylamine in H₂O (29 mmol) dropwise while stirring at room temperature. The solution was allowed to mix until no further color developed. At this time, the organic layer was removed and the aqueous layer was washed two times with acetone. Then the aqueous layer was evaporated and 50 mL cold acetone was added to the residue. Upon addition of solvent, our product of interest precipitates out of solution and is collected by vacuum filtration. White crystalline, 1.95 g, 10.95 mmol, 76% yield. **¹H NMR** (D₂O), δ: 4.78 (s, 1H), 4.24 (s, 2H), 3.21 (s, 9H). **¹³C NMR** (CD₃OD), δ: 82.71 and 72.14 (C≡C), 57.13 (CH₂), 53.48 (C₃H₉). **ESI-MS:** M⁺ of *m/z* 98.0969 (calculated), *m/z* 98.0965 (experimental).

Synthesis of 1b

To a solution of 1.0 mL 4-bromo-1-butyne (10.65 mmol) in 10 mL acetone was added 3.3 mL of 40% trimethyl amine in H₂O (24 mmol) dropwise while stirring. No color developed upon addition of trimethyl amine. The reaction was allowed to proceed at 30 °C for 3 h. The precipitate that had formed was collected by vacuum filtration and dried. White crystalline, 940 mg, 4.9 mmol, 46% yield. **¹H NMR** ((CD₃)₂SO), δ: 3.51 (t, 2H), 3.13 (t, 1H), 3.09 (s, 9H), 2.77 (t, 2H). **¹³C NMR** (CD₃OD), δ: 79.67 and 73.50 (C≡C), 65.71 (CH₂-N), 54.12(t, C₃H₉), 14.80 (CH₂-C≡C). **ESI-MS:** M⁺ of *m/z* 112.1 (calculated), *m/z* 112.1 (experimental).

Synthesis of 1c

To a solution of 1 mL of 6-chloro-1-hexyne (8.25 mmol) in 10 mL acetone was added 2.5 mL 40% trimethylamine in H₂O (18 mmol) dropwise while stirring. A yellow color developed upon addition. The reaction was allowed to progress at 30 °C for 24 h, at which time more acetone was added to the reaction flask and the solvent was evaporated. To the yellow residue remaining was added 50 mL cold acetone, resulting in the formation of crystals which were collected by vacuum filtration. White crystalline, 521 mg, 2.96 mmol, 36% yield. **¹H NMR** ((CD₃)₂SO), δ: 3.35 (m, CH₂-N), 3.07 (s, 9H), 2.88 (t, 1H), 2.24 (t, CH₂-C≡C), 1.75 (m, CH₂-CH₂-N), 1.45 (CH₂-CH₂-C≡C). **¹³C NMR** (CD₃OD), δ: 84.17 and 70.84 (C≡C), 67.32 (CH₂-NMe₃), 53.77 (t, C₃H₉), 26.40 (CH₂-CH₂-NMe₃), 23.15 (CH₂-C≡C), 18.66 (CH₂-CH₂-C≡C). **ESI-MS:** M⁺ of *m/z* 140.1 (calculated), *m/z* 140.1 (experimental).

Synthesis of 3

To a solution of 0.70 g 1-dimethylamino-2-propyne (8.42 mmol) in 15 mL dry THF at -78 °C was added n-BuLi (6.05 mL, 1.6 N, 9.68 mmol). The solution was kept under nitrogen and allowed to stir for 1 h, at which time 1.5 mL methyl chloroformate (19.41 mmol) was added dropwise. The reaction was allowed to warm to room temperature for 1 h. The reaction was quenched upon addition of 10 mL H₂O and the aqueous phase was extracted using ethyl ether (4 x 25 mL). The ethereal extracts were washed with 40 mL saturated NaCl, dried over MgSO₄, and the crude residue was purified by flash chromatography (1:1 hexane : ethyl acetate). Amber oil, 294 mg, 2.09 mmol, 25% yield. **¹H NMR** (CDCl₃), δ: 2.35 (s, 6H), 3.42 (s, 2H), 3.78 (s, 3H). **ESI-MS:** [M + H]⁺ of *m/z* 142.1 (calculated), *m/z* 142.1 (experimental)

Synthesis of 5

Compound **3** (60 mg, 0.425 mmol) was dissolved in 4.5 mL isopropanol at room temperature under nitrogen. 132 μ L iodomethane (ρ 2.28 mg/mL, 2.12 mmol) was added, and the mixture was stirred for 5 h. The product was precipitated with 10 mL dry ethyl ether, collected by vacuum filtration, washed first with ether, and finally washed with pentane. The result was a light tan powder, 82 mg, 0.29 mmol, 68% yield. **$^1\text{H NMR}$** (D_2O), δ : 3.30 (s, 9H), 3.85 (s, 3H), 4.56 (s, 2H). **ESI-MS**: $[\text{M} + \text{H}]^+$ of m/z 156.1025 (calculated), m/z 156.1019 (experimental).

General procedure for the Production of Triazoles Bearing Di- and Tri-Methylammonium Groups

One equivalent of alkyne was dissolved in D_2O or, if insoluble in water, deuterated DMSO, at a concentration of approximately 100 mg/mL. While stirring at room temperature, 5 equivalents of sodium azide were added, followed by one equivalent of ammonium chloride. The reaction proceeded under reflux at 100 $^\circ\text{C}$ and was monitored by $^1\text{H NMR}$, until complete. Once the reaction was complete, the solvent was distilled off and two consecutive cold EtOH washes were used to get rid of excess sodium azide. Once the EtOH has evaporated, the product should be stored carefully owing to the hygroscopic nature of the triazole.

Synthesis of 2a

Compound **1a** (500 mg, 2.81 mmol), 183 mg NH_4Cl (2.81 mmol), and 913 mg NaN_3 (14.05 mmol) were dissolved in 5 mL D_2O . Thirty two hours at 100 $^\circ\text{C}$ gave product at 92% completion; gold crystalline, 47% yield. **$^1\text{H NMR}$** (D_2O), δ : 8.23 (s, 1H), 4.68 (s, 2H), 3.12 (s, 9H). **$^{13}\text{C NMR}$**

(CD₃OD), δ : 135.20 (CH=C), 132.91 (CH=C), 61.23 (CH₂), 53.50 (C₃H₉). **ESI-MS**: M⁺ of m/z 141.1140 (calculated), m/z 141.1135 (experimental).

Synthesis of 2b

Compound **1b** (300 mg, 1.56 mmol), 85 mg NH₄Cl (1.56 mmol), and 510mg NaN₃ (7.85 mmol) were dissolved in 4 mL D₂O. Ten days at 100 °C gave product at 95% completion; 118 mg yellow powder, 0.50 mmol, 32% yield. **¹H NMR** ((CD₃)₂SO), δ : 7.78 (s, 1H), 3.65 (t, 2H), 3.20 (t, 2H), 3.14 (s, 9H). **ESI-MS**: M⁺ of m/z 155.1 (calculated), m/z 155.1 (experimental).

Synthesis of 2c

Compound **1c** (150 mg, 0.86 mmol), 46 mg NH₄Cl (0.86 mmol), and 280 mg NaN₃ (4.3 mmol) were dissolved in 5 mL D₂O. Eleven days at 100 °C gave product at 86% completion; 26 mg yellow powder, 0.12 mmol, 14% yield. **¹H NMR** ((CD₃)₂SO), δ : 7.64 (s, 1H), 3.29 (d, 2H), 3.05 (s, 9H), 2.59 (t, 2H), 1.74 (m, 2H), 1.60 (m, 2H). **ESI-MS**: M⁺ of m/z 183.2 (calculated), m/z 183.1 (experimental).

Synthesis of 4

Compound **3** (320 mg, 2.26 mmol), 735 mg NaN₃, (11.3 mmol), and 121.1 mg NH₄Cl (2.26 mmol) were dissolved in 4 mL (CD₃)₂SO. Five hours at 100 °C gave product at 100% completion. Purification was achieved via multiple washes with acetonitrile, as the desired product is insoluble. Medium brown powder, 368 mg, 2.0 mmol, 88% yield. **¹H NMR** (CD₃OD), δ : 3.87 (s, 2H), 3.82 (s, 3H), 2.27 (s, 6H). **ESI-MS**: [M+H]⁺ of m/z 185.1 (calculated), m/z 185.1 (experimental).

Synthesis of 6

Compound **5** (30 mg, 0.106 mmol), 62.4 mg NaN₃ (0.1 mmol), and 6 mg NH₄Cl (0.11 mmol) were dissolved in 3 mL D₂O. Three hours at 100 °C gives product at 100% completion. Tan powder, 34.4 mg, 0.1 mmol, 100% yield. **¹H NMR** (D₂O), δ: 4.77 (s, 2H), 3.90 (s, 3H), 3.10 (s, 9H). **ESI-MS**: M⁺ of *m/z* 199.1195 (calculated), *m/z* 199.1190 (experimental).

3.2.2 Synthesis of Secondary Substrate Analogs

Synthesis of 7a

To 1.0 mL propargyl amine (14.5 mmol) at 0 °C and under nitrogen was added 2 mL distilled triethylamine (14.5 mmol) and a catalytic amount (~35 mg) of dimethylaminopyridine (DMAP) in 5 mL dichloromethane. The mixture was kept on ice and stirred 5 min. Ethyl chlorooxoacetate (1.7 mL, ρ 1.227, 15.28 mmol) was added dropwise; upon completion of the addition, the reaction was allowed to progress on ice for 30 minutes, then at room temperature for 3 h. The addition of water marked the end of the reaction. The desired product was extracted by using methylene chloride, followed by a chloroform extraction. The chloroform-soluble fraction was collected, and the solvent was evaporated, resulting in a light yellow powder; 2.0 g, 13 mmol, 87% yield. **¹H NMR** (CDCl₃), δ: 7.56 (bs, 1H), 4.37 (q, 2H), 4.15 (dd, 2H), 2.30 (t, 1H), 1.39 (t, 3H). **¹³C NMR** (CDCl₃), δ: 160.08 (COO), 156.38 (CON), 78.15 and 72.33 (C≡C), 63.32 (CH₂CH₃), 29.28 (CH₂-C≡C), 13.93 (CH₃). **ESI-MS**: [M+H]⁺ of *m/z* 156.06 (calculated), *m/z* 156.22 (experimental).

Synthesis of 8a

Compound **7a** (154 mg, 1 mmol), 75 mg NaN₃ (1.15 mmol), and 54 mg NH₄Cl (1 mmol) were dissolved in 1 mL D₂O to give a 1 M solution. The triazole product decomposes under vacuum, so the synthesis was done \approx 1:1 alkyne:NaN₃ to avoid the need to evaporate solvent. Reflux at 80 °C for 72 hours gave product at 100% completion; 100% yield. **¹H NMR** (D₂O), δ : 4.03 (s, 2H), 3.68 (q, 2H), 1.20 (t, 3H). **ESI-MS**: [M+H]⁺ of m/z 199.1 (calculated), m/z 199.0 (experimental).

Synthesis of 9a

1-amino-4-chloro-2-butyne (1.015 g, 7.25 mmol) was dissolved in 10 mL dichloromethane at 0 °C and under nitrogen. Distilled triethylamine (1 mL, 7.25 mmol) and a catalytic amount (\sim 20 mg) of DMAP were added. The mixture was kept on ice and stirred 5 min. Ethyl chlorooxoacetate (0.81 mL, ρ 1.227, 7.28 mmol) was added dropwise. Upon completion of the addition, the reaction was allowed to progress on ice for 30 min, then at room temperature for 3 h. The addition of water marked the end of the reaction. The desired product was extracted by using methylene chloride, followed by a chloroform extraction. The chloroform-soluble fraction was collected and the solvent was evaporated, resulting in a pale yellow, translucent oil; 1.4 g, 6.88 mmol, 95% yield. **¹H NMR** (CDCl₃), δ : 7.51 (bs, 1H), 4.30 (q, 2H), 4.14 (m, 2H), 4.09 (t, 2H), 1.33 (t, 3H). **¹³C NMR** (CDCl₃), δ : 159.95, 156.39, 80.90, 78.43, 63.27, 30.20, 29.59, 13.86. **ESI-MS**: [M + H]⁺ of m/z 204.0 (calculated), m/z 203.9 (experimental).

Synthesis of 10a

To 0.785 g 2-picolyamine (ρ 1.049 g/mL, 7.25 mmol) at 0 °C and under nitrogen was added 1 mL distilled triethylamine (7.25 mmol) and a catalytic amount (\sim 20 mg) of DMAP in 1 mL dichloromethane. The mixture was kept on ice and stirred 5 min. Ethyl chlorooxoacetate (0.85 mL, ρ 1.227 g/mL, 7.6 mmol) in 3 mL dichloromethane was added dropwise; upon completion of the addition, the reaction was allowed to progress on ice for 30 min, then at room temperature for 3 h. The addition of water marked the end of the reaction. The product of interest was extracted by using dichloromethane. Light tan powder, 1.33 g, 6.4 mmol, 88% yield. $^1\text{H NMR}$ ($(\text{CD}_3)_2\text{SO}$), δ : 9.43 (t, NH), 8.50 (d, 1H), 7.77 (t, 1H), 7.30 (t, 2H), 4.43 (d, 2H), 4.27 (q, 2H), 1.28 (t, 3H). $^{13}\text{C NMR}$ (CDCl_3), δ : 159.80 (COO), 155.77 (NH-CO), 149.10 (N=C(-R₁-R₂)), 136.75 (N=CH-R₁), 122.40 121.93 121.65 (R₁-CH=CH=CH-R₂), 62.92 (CH₂-CH₃), 44.59 (CH₂-NH), 13.84 (CH₃). **ESI-MS**: $[\text{M} + \text{H}]^+$ m/z 209.1 (calculated), m/z 209.1 (experimental).

General procedure for the synthesis of 7b, 9b, and 10b

1 equivalent (\sim 0.5 – 1.5 mmol) of the ester-containing precursor (**7a**, **9a**, **10a**) was dissolved in 5-10 mL 1:1 MeOH:THF at room temperature. While stirring, 1.1 equivalent NaOH in H₂O was added dropwise, resulting in precipitation of product as a salt. Following removal of solvent under reduced pressure, the salt product was dissolved in a few mLs of H₂O, and HCl was added to neutralize or acidify the solution. Finally, the solvent was removed under reduced pressure, resulting in solid product.

Synthesis of 7b

Compound **7a** (66 mg, 0.43 mmol) was dissolved in 6 mL 1:1 MeOH:THF at room temperature. NaOH solution (0.45 mL of 1 M) was added dropwise. The solution was left to stir for one day. Off white crystalline, 65 mg, 0.43 mmol, 100 % yield. **¹H-NMR** (CDCl₃) of acidified product, δ : 7.22 (bs, 1H), 4.16 (dd, 2H), 2.34 (t, 1H). **ESI-MS**: [M+H]⁺ of m/z 128.0432 (calculated), m/z 128.0342 (experimental).

Synthesis of 9b

Compound **9a** (82 mg, 0.4 mmol) was dissolved in 6 mL 1:1 MeOH:THF at room temperature. NaOH solution (0.43 mL of 1 M) was added dropwise. The solution was left to stir for one day. White powder, 80 mg, 0.4 mmol, 100% yield. **¹H-NMR** ((CD₃)₂SO) of acidified product, δ : 8.78 (t, NH), 4.43 (s, 2H), 4.2 (bs, 1H), 3.91 (d, 2H). **¹³C-NMR** ((CD₃)₂SO) of acidified product, δ : 164.6, 162.7, 83.9, 76.7, 31.1, 28.3.

Synthesis of 10b

Compound **10a** (300 mg, 1.44 mmol) was dissolved in 8 mL 1:1 MeOH:THF at room temperature. NaOH solution (1.6 mL of 1 M) was added dropwise. The solution was left to stir for one day. White powder, 290 mg, 1.44 mmol, 100% yield. **¹H-NMR** ((CD₃)₂SO), δ : 9.46 (t, NH), 8.63 (d, 1H), 8.06 (t, 1H), 7.54 (m, 2H), 4.55 (s, 2H). **ESI-MS**: [M+H]⁺ of m/z 181.1 (calculated), m/z 181.0 (experimental).

3.2.3 MALDI-TOF Mass Spectrometry Inhibition Assay

Primary Substrate Analog Screening Assay

Purified KDM4E (8 μM) was incubated for 10 minutes at room temperature with 40 μM $\text{Fe}^{\text{II}}(\text{NH}_4)_2\text{SO}_4 \cdot 6\text{H}_2\text{O}$, 300 μM αKG , 500 μM sodium L-ascorbate, and 1 mM primary substrate analog. The demethylation reaction was started by the addition of $\text{H3}_{(7-14)}\text{K9me}_3$ (30 μM or 250 μM), and allowed to progress at 37 $^\circ\text{C}$ (2 or 10 min). At that time, the reaction was stopped by the addition of 2x MeOH and 0.1% TFA. The precipitated protein was removed via centrifugation, and a portion of the supernatant was mixed with 10 mg/mL α -cyano-4-hydroxycinnamic acid in 50% acetonitrile/0.1% TFA. All samples were done in duplicate. To avoid bias in the collection of MALDI spectra, all samples were analyzed using accumulated spectra of at least 1000 shots.

Percent demethylation values were determined using the relative intensities of the mono-, di-, and tri-methylated $\text{H3}_{(7-14)}\text{K9}$ peaks in the following equation (3-1):

$$\% \text{ demethylation} = \frac{(\% \text{NHme}_2 + 2 \cdot \% \text{NH}_2\text{me}_1)}{(\% \text{Nme}_3 + \% \text{NHme}_2 + 2 \cdot \% \text{NH}_2\text{me}_1)} \quad (3-1)$$

Percent demethylation values were converted to “Demethylation factors” by taking the control percent demethylation to be 100% or 1.00.

Secondary Substrate Analog Screening Assay

Purified KDM4E (8 μM) was incubated for 10 min at room temperature with 40 μM $\text{Fe}^{\text{II}}(\text{NH}_4)_2\text{SO}_4 \cdot 6\text{H}_2\text{O}$, 500 μM sodium L-ascorbate, and 1 mM secondary substrate analog. The demethylation reaction was started by the addition of αKG (75 μM or 500 μM) and $\text{H3}_{(7-14)}\text{K9me}_3$ (175 μM), and allowed to progress for 10 min at 37 $^\circ\text{C}$. At that time, the reaction was stopped by the

addition of 2x MeOH and 0.1% TFA. The precipitated protein was removed via centrifugation and a portion of the supernatant was mixed with 10 mg/mL α -cyano-4-hydroxycinnamic acid in 50% acetonitrile/0.1% TFA. All samples were done in duplicate. To avoid bias in the collection of MALDI spectra, all samples were analyzed by using accumulated spectra of at least 1000 shots. Demethylation factors were calculated in the same way as in the primary substrate analog screening assay.

3.2.4 Enzyme-Templated Cycloaddition Reaction

In a typical assay, purified HDM (150 - 250 μ M, 1 equivalent) is reconstituted with 1 equivalent metal salt (Fe^{2+} or Ni^{2+}), then incubated with three equivalents alkyne and an excess of NaN_3 (> 50 equivalents) in Tris or HEPES buffer (pH 7.5) at 4 °C for 24 hours. For primary substrate analogs, an appropriate amount of α KG was added to the solution as well. After 24 hours, a portion of the reaction solution is diluted with MeOH, the protein precipitate removed via centrifugation, and the supernatant is analyzed via ESI-MS (Thermo LCQ Deca).

3.3 Results and Discussion

Early crystallography studies of KDM4A revealed the basis for its primary and secondary substrate specificities.⁵ As shown in Figure 3.4, the interaction of *N*-oxalylglycine (NOG; an analog of the secondary substrate α -ketoglutarate) with KDM4A is due to the oxalyl portion chelating the metal center, while the other carboxylic group forms a hydrogen bond with Tyr 132. KDM4 recognition of the histone lysine substrate involves multiple interactions of the enzyme with both

histone main-chain and histone methyl lysine groups. Also shown in Figure 3.4, the histone H3 trimethylated lysine's methyl groups make multiple contacts with KDM4A residue oxygen atoms: Gly 170, Glu 190, Ser 288, and Tyr 177 (distance of 3.5 Å, omitted for clarity). All of these $R3N^+-C-H \cdots O=C$ contacts are at distances less than 3.7 Å, which makes them consistent with $CH \cdots O$ hydrogen bonding.²⁹ It is, therefore, supposed that KDM4 recognition of the histone substrate is due in part to these hydrogen bonds.

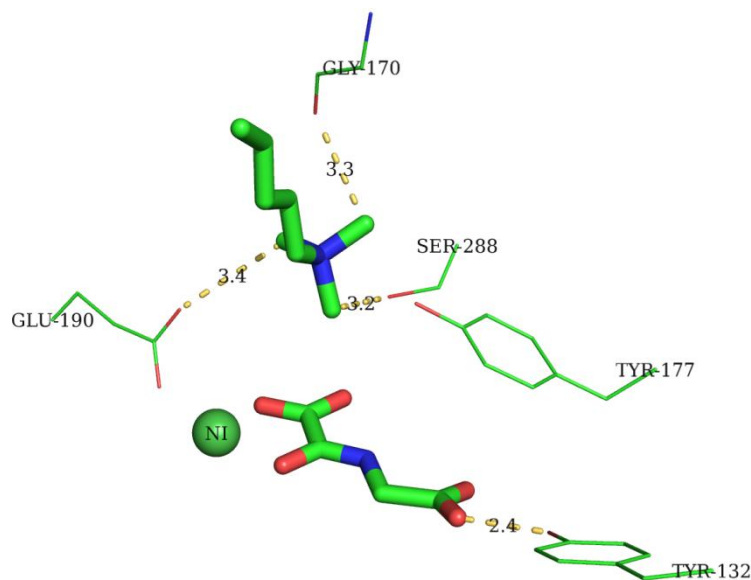


Figure 3.4. Recognition of H3K9me₃ and NOG in the KDM4A active site (PDB 2OQ6; distances in Å).⁵

At the start of this work, it was unknown whether inhibition of KDM4 isoforms could be achieved through the use of simple substrate analogs bearing dimethylamino or trimethylammonium groups to mimic the natural lysine substrate. We, therefore, synthesized a small library of primary substrate analogs that include either a carbon-carbon triple bond or the corresponding 1,2,3-triazole group (Figure 3.5) and screened the compounds for inhibition against KDM4E by using a

discontinuous MALDI-TOF MS assay. The alkynes were tested in KDM4-templated cycloaddition reactions (*vide infra*), and the corresponding triazole-containing compounds were synthesized independently to test whether they would be stronger KDM4 inhibitors than the alkyne-containing compounds. KDM4E was the enzyme chosen for the inhibition screen, as it displays the greatest *in vitro* activity of our three isoforms (which include KDM4A and KDM4C); however, it is a pseudogene-encoded HDM and is dissimilar to KDM4A and KDM4C in that it recognizes only H3K9me₃ and not H3K36me₃.

In the inhibition screen, 8 μM KDM4E was incubated with 1 mM primary substrate analog and all other reaction components except the histone peptide substrate H3₍₇₋₁₄₎K9me₃. To start the reaction, histone peptide was added at a concentration of 50 μM ($\approx K_m$) or 250 μM. Screening the inhibitors at two concentrations of peptide substrate allows us to test whether any of the analogs potentially compete with the histone peptide substrate. If inhibition of KDM4E by an analog increased at the low peptide concentration, we would have a template around which to design a library of potential JmjC-HDM specific inhibitors.

Primary substrate analogs:

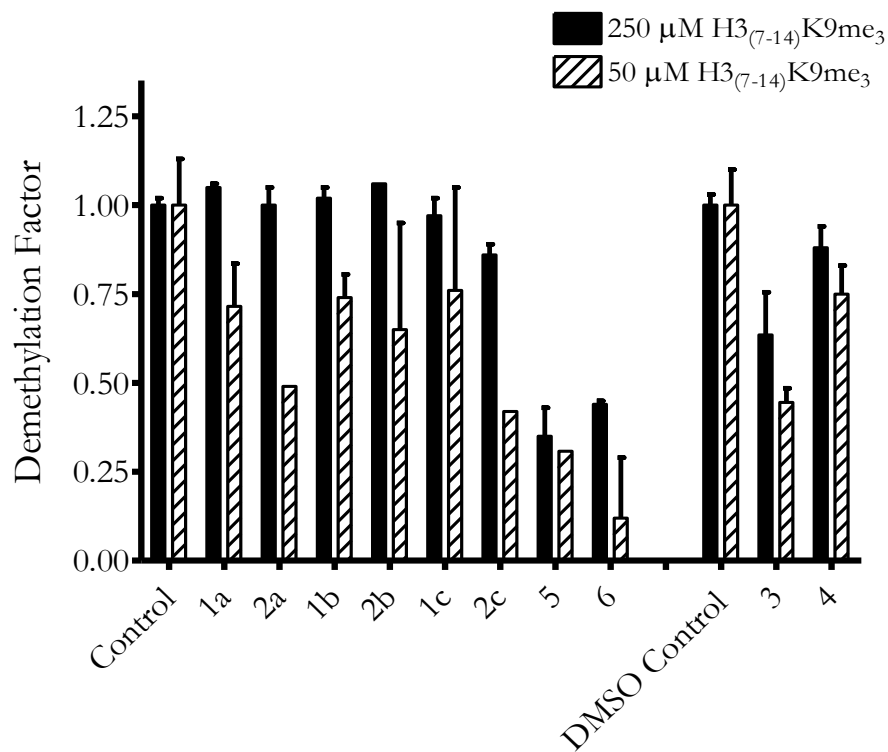
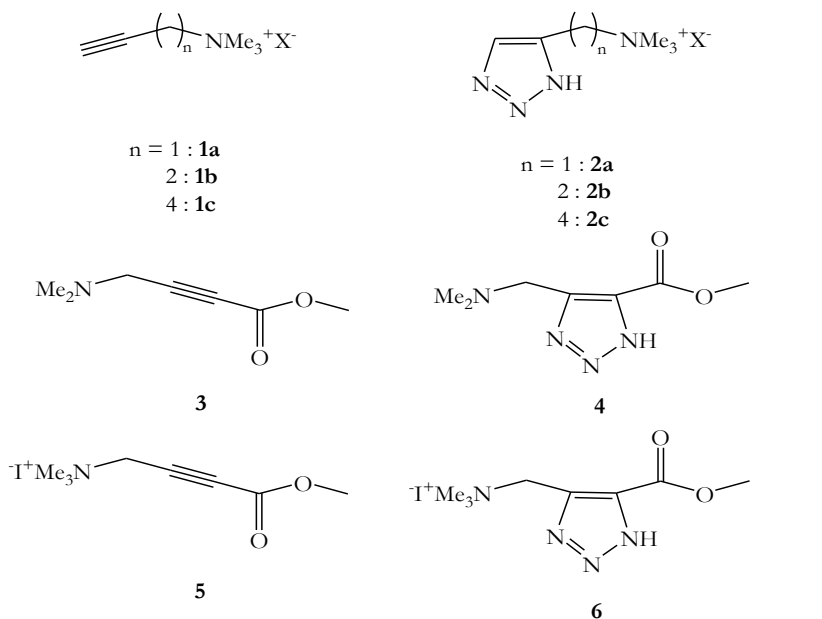


Figure 3.5. KDM4E inhibition by primary substrate analogs at two concentrations of H3₍₇₋₁₄₎K9me₃.

From Figure 3.5, we find that the most potent inhibition of KDM4E comes from analog **5** and the corresponding triazole **6**. As the dimethylamino analogs **3** and **4** inhibit KDM4E to a lesser degree, **5** and **6** may illustrate the benefit of including a trimethylammonium fragment in the design of simple JmjC-HDM inhibitors. Notably, neither **5** nor **6** show substantial increased inhibition at the lower peptide concentration, leading us to assume that these analogs bind the enzyme in a pocket other than the histone peptide binding cavity.

Our findings confirm that enzymatic recognition of the substrate involves more than just the presence of a trimethylammonium group, as demonstrated by the limited inhibition of KDM4E by analogs **1a**, **1b**, and **1c**. We see somewhat more inhibition when testing the triazole versions of these analogs, as shown by the inhibitory effects of **2a** and **2c** at lower histone peptide concentrations. In comparing **2a** and **2c**, assuming the triazole portion interacts with the metal center, the longer alkyl chain of **2c** may position the trimethylammonium in a more favorable position to form CH \cdots O hydrogen bonds, leading to slightly greater inhibition of KDM4E.

In the primary substrate analog screen, we find that the triazole compounds **2a**, **2b**, **2c**, and **6** inhibit KDM4E slightly more than the equivalent alkyne-containing compounds **1a**, **1b**, **1c**, and **5**. This trend is more apparent at the low histone peptide concentration. Interestingly, the triazole-containing **4** is a weaker KDM4E inhibitor than **3** at both histone peptide concentrations. As the only difference between **4** and **6** is an additional methyl group in **6** (and thus a positive charge on nitrogen), we can infer the importance of the trimethylammonium group in KDM4E recognition of this scaffold. Testing compound **6** in varying O₂ concentration environments with our developed O₂ consumption assay (Section 2.2.3) would allow us to assess whether this analog competes with the cosubstrate for binding to the active site metal center. Furthermore, modification of **5** and **6** could

lead to the development of potent, specific inhibitors of JmjC-HDMs, as we would not anticipate these templates to be promiscuous inhibitors of α KG- dependent oxygenases.

Since it is clear that recognition of the natural trimethyllysine substrate involves multiple main chain interactions of the peptide with the HDM, we next directed our attention to developing analogs of the secondary substrate α KG, using the same alkyne and triazole strategy as in the primary substrate analog screen. As shown in Figure 3.6, the analogs mimic the α KG amide analog NOG in that they each contain the amide oxalyl functional group.

The KDM4E inhibition screen was done in a similar manner to the primary substrate analog screening, with a pre-incubation of 8 μ M HDM and 1 mM analog, but the reaction was started by the addition of 175 μ M histone peptide and one of two α KG concentrations: 75 μ M ($\approx 3x K_m$) or 500 μ M, to test whether the analogs are α KG competitors. Unfortunately, the nature of the discontinuous MS assay does not allow for “low” (K_m) concentrations of α KG to be used, since we saw no substantial demethylation of the peptide substrate at α KG concentrations less than 75 μ M. For example, under the secondary substrate analog screening assay conditions, with no inhibitor present, use of 20 μ M α KG ($\approx K_m$) resulted in under 10% demethylated product (i.e. the relative intensities of the H3K9me₃ and H3K9me₂ peaks are 100% and 10%, respectively). Such low percentages of demethylated product make quantification of enzyme inhibition impossible. Use of 75 μ M α KG results in approximately 40% demethylated product, a high enough percentage to allow for proper inhibition analysis.

Secondary substrate analogs:

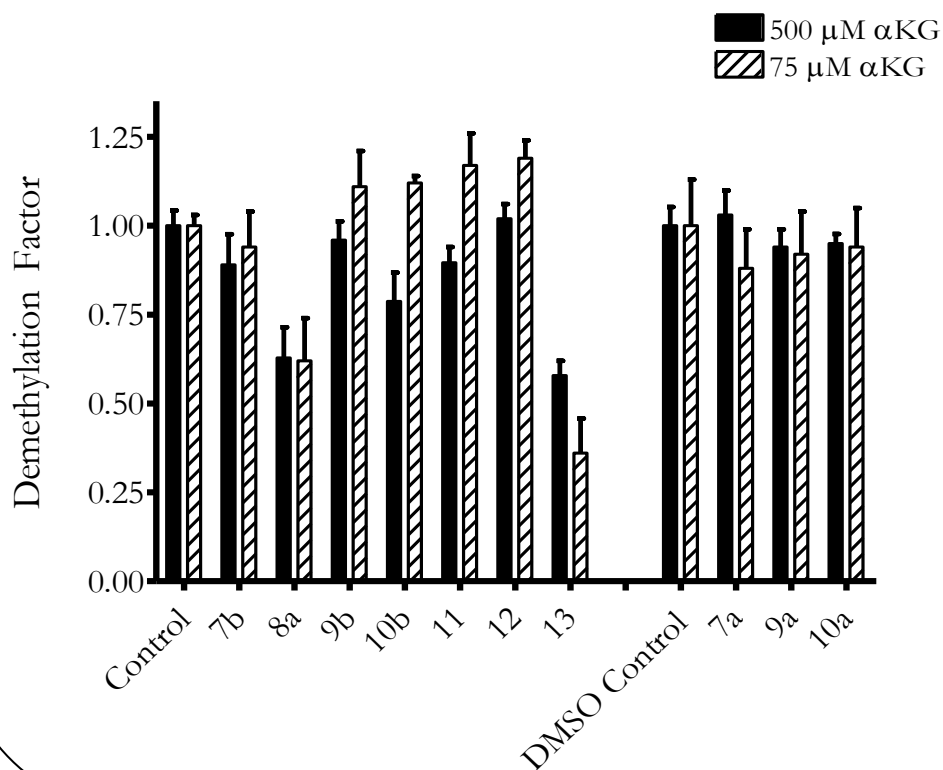
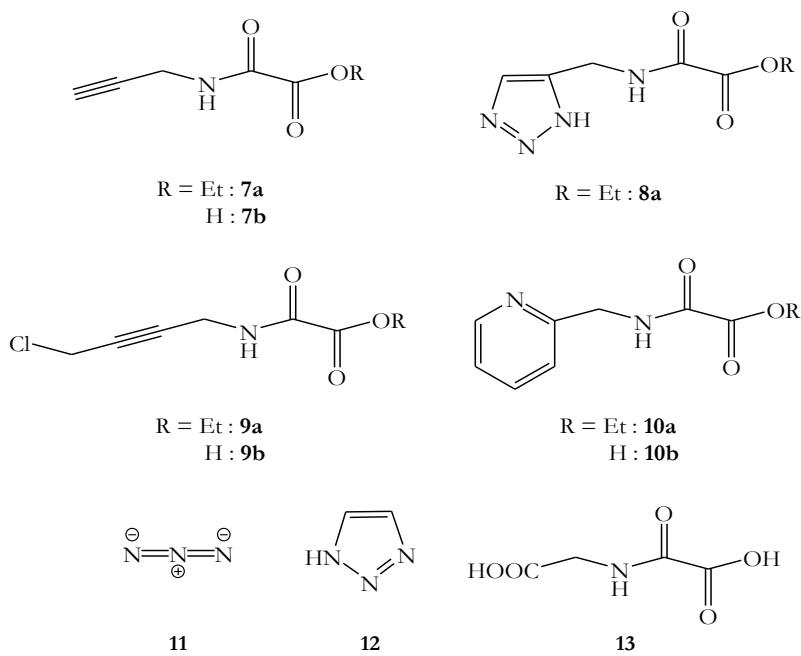


Figure 3.6. KDM4E inhibition by secondary substrate analogs at two concentrations of α KG.

Azide (**11**), 1,2,3-triazole (**12**), and NOG (**13**) were used as controls in the KDM4E inhibition screen. Compounds **11** and **12** should be competitors of O₂, and, thus, we would expect no difference in their inhibition at varying concentrations of α KG. As shown in Figure 3.6, even at the relatively high concentration of 1 mM, **11** and **12** have limited inhibitory power. Under the inhibitor screening conditions, the known JmjC-HDM inhibitor³⁰ NOG does not appear to compete with α KG, its isosteric analog, as we do not see a dramatic difference between the level of inhibition at the different concentrations of α KG. Finally, ester analogs **7a**, **9a**, and **10a** are synthetic precursors to the carboxylic acid analogs, and were used as controls in the inhibition screen. Predictably, we find no enzyme inhibition with the ester-containing analogs.

Preliminary results with **7b** suggested that the compound had limited inhibitory power, leading us to design **9b** and **10b**, as it was unclear why the oxalyl portion of **7b** was insufficient in limiting α KG binding in the KDM4E active site. The pyridine moiety in **10b** is a known metal chelator, and we find that this analog inhibits KDM4E at about the same level as **7b**, at least at the higher α KG concentration where quantification of demethylation is more reliable. This result is surprising, if we assume the oxalyl portion of each to interact with the metal center, as the pyridine in **10b** could offer more favorable interactions with KDM4E residues than the C \equiv C in **7b**. With **9b**, we were interested to see how a chlorinated compound would affect enzyme activity, as early studies with the compound JIB-04 (Figure 3.1; see Chapter 5 for further discussion) indicate that the chlorine interacts with the JmjC-HDM active site metal. We lose inhibitory power when modifying **7b** to **9b**. If the oxalyl portion of **7b** interacts with Fe in a manner similar to α KG, perhaps the chlorine of **9b** is too large to fit in the active site. As **7b**, **9b**, and **10b** are all weak inhibitors of KDM4E, our results suggest that the hydrogen bond formed between NOG and Tyr132 (Figure 3.4) is perhaps the key stabilizing interaction necessary for proper JmjC-HDM inhibition.

The only secondary substrate analog that shows inhibitory strength comparable to **13** is **8a**, the ester- and 1,2,3-triazole-containing version of **7a**. This product decomposes under reduced pressure and, thus, was synthesized from **7a** in aqueous solution. For this reason, we were unable to generate the carboxylic acid form of **8a**. Although we know from the NOG control that large differences in inhibition are unlikely under the screening conditions for α KG competitors, KDM4E inhibition by **8a** is identical at both concentrations of α KG, which could be due to it being an ester instead of an acid. Thus, **8a** is most likely not competitive with α KG, but could be competitive with O₂ owing to the inclusion of 1,2,3-triazole. As was discussed for the primary analog **6**, testing KDM4E inhibition by **8a** at varying concentrations of O₂ would allow us to judge whether this triazole is competitive with O₂.

Finally, several analogs were tested in the HDM-templated cycloaddition reaction: **1a**, **1b**, **1c**, **3**, **5**, and **7b**. No evidence of triazole formation was found in the enzyme-templated reaction for **1a**, **1b**, **1c**, or **7b**. From the KDM4E inhibition screen, we know that these compounds have limited inhibitory power and, therefore, low binding affinities. **3** and **5** were of interest as these compounds were found to be relatively good inhibitors of KDM4E. However, we found that **3** and **5** undergo cycloaddition with N₃⁻ in solution, even at 0 °C, as evidenced by ESI-MS and ¹H-NMR. The ESI-MS time study for compound **5** is given as a representative in Figure 3.7. Thus, these two compounds have C≡C bonds that are too electron deficient to be used in the enzyme-templated reaction. As **5** and the corresponding triazole **6** were found to be the strongest inhibitors of KDM4E tested, these compounds could act as templates for future development of JmjC-HDM inhibitors.

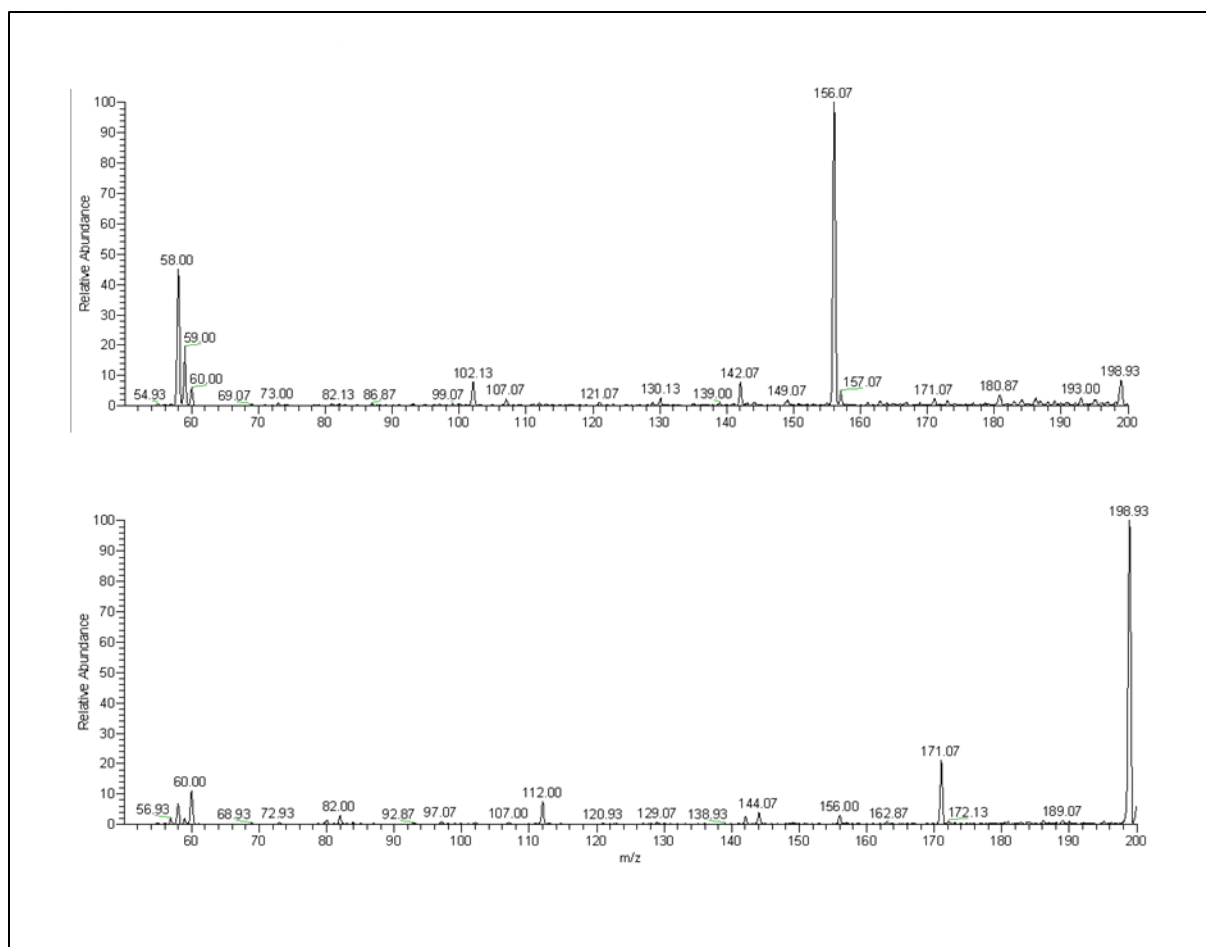


Figure 3.7. ESI-MS of **5** with excess N_3^- in water at (*top*) 0 minutes and (*bottom*) 30 minutes. The peak at m/z of 156 corresponds to the alkyne starting material **5**, m/z of 199 corresponds to the triazole product **6**.

3.4 Conclusions

In conclusion, we have synthesized a small library of molecules designed to mimic JmjC-HDM primary and secondary substrates. These small molecules include either a carbon-carbon triple bond or 1,2,3-triazole group and were tested as inhibitors of the H3K9me_{3/2} demethylase KDM4E using a discontinuous MALDI-TOF MS assay. Overall, we find that triazole-containing analogs were

more potent inhibitors than the alkyne-containing analogs, with the exception of **3** and **4**. The most promising primary substrate analogs **5** and the corresponding triazole **6** present a new scaffold for KDM4 inhibition. While none of the secondary substrate analogs were found to strongly inhibit KDM4E, the triazole **8a** may be competitive with O₂ and appears to inhibit KDM4E nearly as well as NOG. Several of the alkyne-containing analogs were tested in KDM4-templated cycloaddition reactions, and no enzyme-driven triazole formation was found. Future studies will focus on the modification of compounds **5** and **6** to increase their inhibitory power. Moreover, these compounds can be screened against other α KG-dependent oxygenases, as we anticipate them to offer JmjC-HDM-specific inhibition.

3.5 References

1. Klose, R. J., Kallin, E. M., Zhang, Y., Jmjc-Domain-Containing Proteins and Histone Demethylation. *Nature Reviews Genetics* **7**, 715-727 (2006).
2. Bhaumik, S. R., Smith, E., Shilatifard, A., Covalent Modifications of Histones During Development and Disease Pathogenesis. *Nature Structural & Molecular Biology* **14**, 1008-1016 (2007).
3. Mosammamarast, N., Shi, Y., Reversal of Histone Methylation: Biochemical and Molecular Mechanisms of Histone Demethylases. *Annual review of biochemistry* **79**, 155-179 (2010).
4. Chen, Z., Zang, J., Whetstine, J., Hong, X., Davrazou, F., Kutateladze, T. G., Simpson, M., Mao, Q., Pan, C. H., Dai, S., Hagman, J., Hansen, K., Shi, Y., Zhang, G., Structural Insights into Histone Demethylation by Jmjd2 Family Members. *Cell* **125**, 691-702. (2006).
5. Ng, S. S., Kavanagh, K. L., McDonough, M. A., Butler, D., Pilka, E. S., Lienard, B. M. R., Bray, J. E., Savitsky, P., Gileadi, O., von Delft, F., Rose, N. R., Offer, J., Scheinost, J. C., Borowski, T., Sundstrom, M., Schofield, C. J., Oppermann, U., Crystal Structures of Histone Demethylase Jmjd2a Reveal Basis for Substrate Specificity. *Nature* **448**, 87-U88 (2007).

6. Couture, J. F., Collazo, E., Ortiz-Tello, P. A., Brunzelle, J. S., Trievel, R. C., Specificity and Mechanism of Jmjd2a, a Trimethyllysine-Specific Histone Demethylase. *Nature Structural & Molecular Biology* **14**, 689-695 (2007).
7. Greer, E. L., Shi, Y., Histone Methylation: A Dynamic Mark in Health, Disease and Inheritance. *Nature Reviews Genetics* **13**, 343-357 (2012).
8. Wu, G., Broniscer, A., McEachron, T., Lu, C., Paugh, B., Becksfors, J., Qu, C., Ding, L., Huether, R., Parker, M., Zhang, J., Gajjar, A., Dyer, M., Mullighan, C., Gilbertson, R., Mardis, E., Wilson, R., Downing, J., Ellison, D. W., Zhang, J., Baker, S. J., Somatic Histone H3 Alterations in Pediatric Diffuse Intrinsic Pontine Gliomas and Non-Brainstem Glioblastomas. *Nature genetics* **44**, 251-253 (2012).
9. Baylin, S. B., Jones, P. A., A Decade of Exploring the Cancer Epigenome—Biological and Translational Implications. *Nature reviews cancer* **11**, 726-734 (2011).
10. Schwartzenuber, J., Korshunov, A., Liu, X.-Y., Jones, D. T., Pfaff, E., Jacob, K., Sturm, D., Fontebasso, A. M., Quang, D.-A. K., Tönjes, M., Driver Mutations in Histone H3. 3 and Chromatin Remodelling Genes in Paediatric Glioblastoma. *Nature* **482**, 226-231 (2012).
11. HÅ, jfeldt, J. W., Agger, K., Helin, K., Histone Lysine Demethylases as Targets for Anticancer Therapy. *Nature Reviews Drug Discovery* **12**, 917-930 (2013).
12. Liu, G., Bollig-Fischer, A., Kreike, B., van de Vijver, M. J., Abrams, J., Ethier, S. P., Yang, Z. Q., Genomic Amplification and Oncogenic Properties of the Gasc1 Histone Demethylase Gene in Breast Cancer. *Oncogene*, (2009).
13. Kawazu, M., Saso, K., Tong, K. I., McQuire, T., Goto, K., Son, D.-O., Wakeham, A., Miyagishi, M., Mak, T. W., Okada, H., Histone Demethylase Jmjd2b Functions as a Co-Factor of Estrogen Receptor in Breast Cancer Proliferation and Mammary Gland Development. *PLoS One* **6**, e17830 (2011).
14. Berdel, B., Nieminen, K., Soini, Y., Tengström, M., Malinen, M., Kosma, V.-M., Palvimo, J. J., Mannermaa, A., Histone Demethylase Gasc1-a Potential Prognostic and Predictive Marker in Invasive Breast Cancer. *BMC cancer* **12**, 516 (2012).
15. Lohse, B., Nielsen, A. L., Kristensen, J. B. L., Helgstrand, C., Cloos, P. A. C., Olsen, L., Gajhede, M., Clausen, R. P., Kristensen, J. L., Targeting Histone Lysine Demethylases by

- Truncating the Histone 3 Tail to Obtain Selective Substrate-Based Inhibitors. *Angewandte Chemie, International Edition in English* **123**, 9266-9269 (2011).
16. Woon, E. C. Y., Tumber, A., Kawamura, A., Hillringhaus, L., Ge, W., Rose, N. R., Ma, J. H. Y., Chan, M. C., Walport, L. J., Che, K. H., Ng, S. S., Marsden, B. D., Oppermann, U., McDonough, M. A., Schofield, C. J., Linking of 2-Oxoglutarate and Substrate Binding Sites Enables Potent and Highly Selective Inhibition of Jmjc Histone Demethylases. *Angewandte Chemie International Edition* **51**, 1631-1634 (2012).
 17. Wang, L., Chang, J., Varghese, D., Dellinger, M., Kumar, S., Best, A. M., Ruiz, J., Bruick, R., Peña-Llopis, S., Xu, J., A Small Molecule Modulates Jumonji Histone Demethylase Activity and Selectively Inhibits Cancer Growth. *Nature communications* **4**, (2013).
 18. Thinnes, C. C., England, K. S., Kawamura, A., Chowdhury, R., Schofield, C. J., Hopkinson, R. J., Targeting Histone Lysine Demethylases—Progress, Challenges, and the Future. *Biochimica et Biophysica Acta (BBA)-Gene Regulatory Mechanisms* **1839**, 1416-1432 (2014).
 19. Rose, N. R., McDonough, M. A., King, O. N. F., Kawamura, A., Schofield, C. J., Inhibition of 2-Oxoglutarate Dependent Oxygenases. *Chemical Society Reviews* **40**, 4364-4397 (2011).
 20. Chang, K.-H., King, O. N. F., Tumber, A., Woon, E. C. Y., Heightman, T. D., McDonough, M. A., Schofield, C. J., Rose, N. R., Inhibition of Histone Demethylases by 4-Carboxy-2,2'-Bipyridyl Compounds. *ChemMedChem* **6**, 759-764 (2011).
 21. King, O. N., Li, X. S., Sakurai, M., Kawamura, A., Rose, N. R., Ng, S. S., Quinn, A. M., Rai, G., Mott, B. T., Beswick, P., Quantitative High-Throughput Screening Identifies 8-Hydroxyquinolines as Cell-Active Histone Demethylase Inhibitors. *PLoS One* **5**, e15535 (2010).
 22. Kim, S.-H., Kwon, S. H., Park, S.-H., Lee, J. K., Bang, H.-S., Nam, S.-J., Kwon, H. C., Shin, J., Oh, D.-C., Tripartin, a Histone Demethylase Inhibitor from a Bacterium Associated with a Dung Beetle Larva. *Organic Letters* **15**, 1834-1837 (2013).
 23. Walport, L. J., Hopkinson, R. J., Schofield, C. J., Mechanisms of Human Histone and Nucleic Acid Demethylases. *Current Opinion in Chemical Biology* **16**, 525-534 (2012).
 24. Cascella, B., Mirica, L. M., Kinetic Analysis of Iron-Dependent Histone Demethylases: A-Ketoglutarate Substrate Inhibition and Potential Relevance to the Regulation of Histone Demethylation in Cancer Cells. *Biochemistry* **51**, 8699-8701 (2012).

25. Sugishima, M., Sakamoto, H., Higashimoto, Y., Omata, Y., Hayashi, S., Noguchi, M., Fukuyama, K., Crystal Structure of Rat Heme Oxygenase-1 in Complex with Heme Bound to Azide - Implication for Regiospecific Hydroxylation of Heme at the Alpha-Meso Carbon. *Journal of Biological Chemistry* **277**, 45086-45090 (2002).
26. Andersson, M. E., Hogbom, M., Rinaldo-Matthis, A., Andersson, K. K., Sjoberg, B. M., Nordlund, P., The Crystal Structure of an Azide Complex of the Diferrous R2 Subunit of Ribonucleotide Reductase Displays a Novel Carboxylate Shift with Important Mechanistic Implications for Diiron-Catalyzed Oxygen Activation. *Journal of the American Chemical Society* **121**, 2346-2352 (1999).
27. Shearer, J., Fitch, S. B., Kaminsky, W., Benedict, J., Scarrow, R. C., Kovacs, J. A., How Does Cyanide Inhibit Superoxide Reductase? Insight from Synthetic (Fen4s)-N-III Model Complexes. *Proceedings of the National Academy of Sciences of the United States of America* **100**, 3671-3676 (2003).
28. Kemsley, J. N., Zaleski, K. L., Chow, M. S., Decker, A., Shishova, E. Y., Wasinger, E. C., Hedman, B., Hodgson, K. O., Solomon, E. I., Spectroscopic Studies of the Interaction of Ferrous Bleomycin with DNA. *Journal of the American Chemical Society* **125**, 10810-10821 (2003).
29. Cannizzaro, C. E., Houk, K., Magnitudes and Chemical Consequences of R3n+-Ch---Oc Hydrogen Bonding. *Journal of the American Chemical Society* **124**, 7163-7169 (2002).
30. Hamada, S., Kim, T. D., Suzuki, T., Itoh, Y., Tsumoto, H., Nakagawa, H., Janknecht, R., Miyata, N., Synthesis and Activity of N-Oxalylglycine and Its Derivatives as Jumonji C-Domain-Containing Histone Lysine Demethylase Inhibitors. *Bioorganic & Medicinal Chemistry Letters* **19**, 2852-2855 (2009).

Chapter 4: Inhibition of JmjC-Histone Demethylases with a Modified Histone H3 Peptide

4.1 Introduction

Several reports have elucidated reasons behind the KDM4 subfamily substrate specificities.¹⁻⁵ Although KDM4D is active toward H3K9me₃ only, other members of the subfamily (KDM4A, B, C) show activity towards both H3K9me₃ and H3K36me₃, despite low sequence homology of the two histone sites.⁶ The KDM4 subfamily members have very similar active-site topologies, and the residues lining the methylammonium-binding pocket are highly conserved.⁵ Overall, KDM4 subfamily substrate selectivities come from the amino acid residues surrounding the di- or tri-methylated lysine. Recognition of the histone substrate is due primarily to contacts with main-chain atoms of the substrate, rather than the side-chain atoms. One notable exception is the side chain of arginine at the -1 position in H3K9, which hydrogen bonds with the carboxylate of Glu169 in KDM4A. Other peptide residues important for recognition are the alanine at -2 and serine at +1.³ For KDM4A, the Gly-Gly motif (at +3 and +4 in H3K9) is reported to be essential for enzymatic activity.⁴

With this knowledge, several recently designed KDM4-specific inhibitors include a short peptide fragment to enhance HDM recognition of the substrate analog.^{7,8} KDM4C is capable of recognizing the truncated peptide fragment H3₍₇₋₁₀₎K9me₃, while the shortest peptide KDM4A recognizes is H3₍₇₋₁₄₎K9me₃. Interestingly, deletion of even one methylene group from the K9me_n (n = 2, 3) side chain results in no demethylation by KDM4A or KDM4C. One report details an

effort to make an inhibitor with isoform specificity: a five amino acid-long peptide H3₇₋₁₁K9 was synthesized with an iron chelator (a uracil) at the N^ε position of K9 (Figure 4.1). The 5-mer was chosen because it would be selective for KDM4C over KDM4A; using the modified peptide, the authors report a K_i of 27 μ M for KDM4C and a K_i of 118 μ M for KDM4A, while finding no inhibition of the related H3K9me_{2/1} demethylase PHF8.⁷

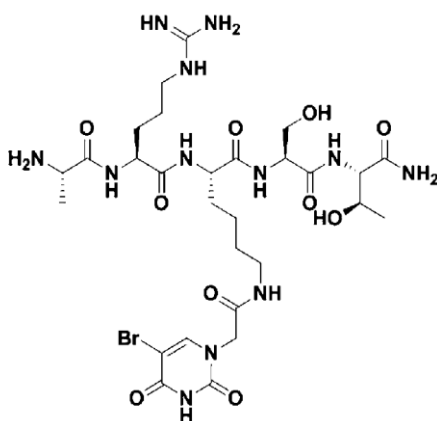


Figure 4.1. A substrate-based inhibitor, selective for KDM4C over PHF8.⁷

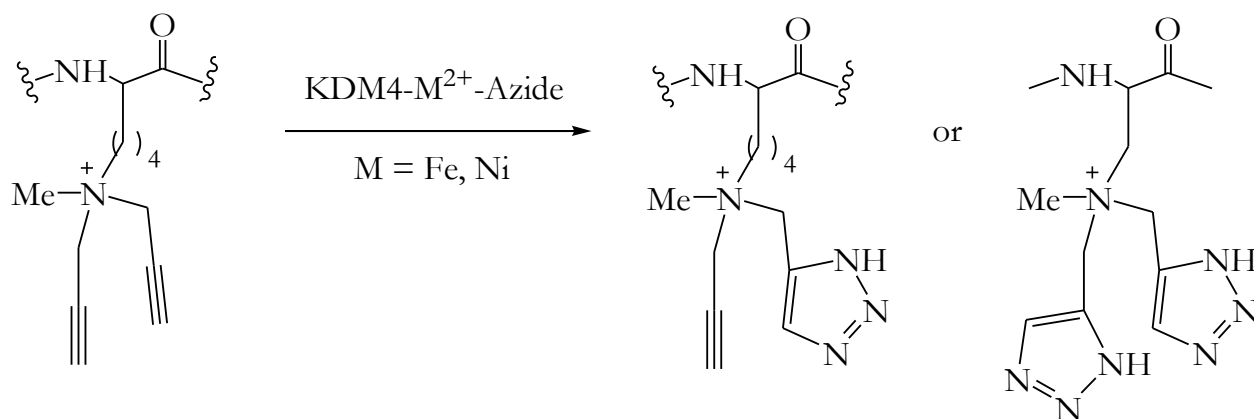
A more recent report used the 8-mer H3₍₇₋₁₄₎K9me₃ with an iron chelator (*N*-oxalyl-D-cysteine) connected to the peptide at the threonine (+2) position. This modified peptide inhibits KDM4A and KDM4E selectively over α KG oxygenases FIH, PHD2, and JMJD1E.⁸ We see from these reports that the development of *specific* inhibitors of the KDM4 subfamily members may require the inclusion of a peptide fragment.

In this study, we developed a modified histone H3 peptide with the intention of selectively inhibiting KDM4C over KDM4A. The 5-mer H3₍₇₋₁₁₎K9(*N*^ε-bis(propargyl)) incorporates two propargyl groups conjugated to lysine's N^ε in place of the natural trimethyl ammonium group. Moreover, a methylated 5-mer H3₍₇₋₁₁₎K9⁺(*N*^ε-methyl (bis-propargyl)) was produced to test whether a charged K9 would enhance recognition of the peptide by the KDM4 subfamily, thus enhancing

inhibition of this group of enzymes. Surprisingly, we found that KDM4A can indeed recognize the methylated 5-mer, challenging earlier studies of the enzyme with the more natural H3₍₇₋₁₁₎K9me₃ peptide.⁷

An ongoing interest in our study of the KDM4 subfamily revolves around whether these enzymes are suited to act as “vessels” in enzyme-templated Huisgen 1, 3-dipolar cycloaddition reactions between enzyme-azide adducts and small molecules bearing carbon-carbon triple bonds. As earlier studies of KDM4-templated cycloaddition of simple alkynes bearing trimethylammonium groups with the enzyme-azide adduct failed to show triazole formation (Chapter 3), the 5-mers in this study were designed to project the propargyl groups toward the metal center in the KDM4C active site (Scheme 4.1).

Scheme 4.1. Huisgen 1, 3-dipolar cycloaddition of ARK⁺(N^ε- methyl bis(propargyl))ST with a KDM4-M²⁺-azide adduct.



4.2 Methods

4.2.1 Synthesis of a Modified Histone H3 Peptide

Synthesis of Boc-Lys(*N*^ε-bis-(propargyl))-OMe ⁹

Boc-Lys-OMe·HCl (4 g, 13.48 mmol) was dried under vacuum at 35 °C for two hours, then 62.5 mL tetrahydrofuran (THF) was added under nitrogen and the temperature was raised to 50 °C. Next, 4.5 mL pyridine (54 mmol) and 5.8 mL propargyl bromide (80% in toluene, 54 mmol) were added slowly. Following the addition of propargyl bromide, the solution turned from clear and colorless to cloudy and orange. The reaction was followed by TLC; after 4 days at 50 °C, the reaction solution was vacuum filtered, and the filtrate was concentrated. Pure product was extracted from the dark brown, oily crude through warm 1:2 ethyl acetate:hexane washes; yellow oil, 1.5 g, 4.46 mmol, 33% yield. ¹H NMR (CDCl₃), δ: 5.0 (d, 1H), 4.30 (m, 1H), 3.74 (s, 3H), 3.41 (d, 4H), 2.51 (t, 2H), 2.22 (t, 1H), 1.80 (m, 2H), 1.65 (m, 2H), 1.50 (m, 1H), 1.44 (s, 9H), 1.25 (s, 2H). ¹³C NMR (CDCl₃), δ: 173.24, 155.29, 79.54, 78.61, 73.04, 53.49, 53.23, 52.27, 41.91, 32.22, 28.21, 26.73, 22.96. See Appendix B for NMR spectra. **ESI-MS** [M + H]⁺ *m/z* 337.2 (calculated), *m/z* 337.2 (experimental).

Synthesis of ARK(*N*^ε-bis(propargyl))ST

Boc-Lys(*N*^ε-bis-(propargyl))-OMe (1 g) was sent to AnaSpec Inc. for synthesis of the desired peptide; 25 mg of mostly pure product was generated with impurities that include incomplete peptides RK(*N*^ε-bis(propargyl))ST and K(*N*^ε-bis(propargyl))ST. **ESI-MS** and **MALDI-TOF MS**: [M + H]⁺ *m/z* 638.3 (calculated), *m/z* 638.3 (experimental). While we find no evidence of

the mono-propargyl species in the ESI-MS, we do find an $[M + H - 38]^+$ peak in the MALDI-TOF mass spectrum (Appendix B).

Synthesis of $\text{ARK}^+(\text{N}^\text{F}$ -methyl bis(propargyl))ST

ARK(N^F -bis(propargyl))ST (3.9 mg, 6.1 μmol) was dissolved in 20 μL DMSO. Methyl iodide (10 μL , ρ 2.28 g/mL, 161 μmol) was dissolved in 10 μL DMSO, and the methyl iodide solution was added directly to the peptide solution at room temperature. The reaction solution was mixed for 2 h at room temperature, and at this time ESI-MS showed no remaining starting material. To quench excess methyl iodide, water was added to create a 30 mM stock solution. **ESI-MS and MALDI-TOF MS:** M^+ of m/z 652.4 (calculated), m/z 652.4 (experimental). While few find no evidence of the mono-propargyl species in the ESI-MS, we did find an $[M-38]^+$ peak in the MALDI-TOF mass spectrum (Appendix B). **ESI-CID-MS/MS:** Following ion selection at 326.8 (M^{2+}), fragments at 425.3 ($(K^+_{\text{me}}\text{ST})^{1+}$) and 232.7 ($(\text{ARK}^+_{\text{me}})^{2+}$) confirm that lysine is the methylated residue of the 5-mer. Absent from the spectrum is any peak that could correspond to arginine being the methylated residue. See Appendix B for relevant spectra.

4.2.2 MALDI-TOF Mass Spectrometry Assays

KDM4A and KDM4C Inhibition by $\text{ARK}(\text{N}^\text{F}$ bis(propargyl))ST and $\text{ARK}^+(\text{N}^\text{F}$ methyl bis(propargyl))ST

Purified HDM (6 μM) was incubated for 10 minutes at room temperature with 30 μM $\text{Fe}^{\text{II}}(\text{NH}_4)_2\text{SO}_4 \cdot 6\text{H}_2\text{O}$, 300 μM α -ketoglutarate (pH 7.5), 500 μM sodium L-ascorbate, 50 mM HEPES pH 7.5, and varying $\text{ARK}(\text{N}^\text{F}$ -bis(propargyl))ST (0 – 1000 μM) or

ARK⁺(N^ε-methyl bis(propargyl))ST (0 – 1000 μM). The reaction is started by the addition of 60 μM H3₍₇₋₁₄₎K9me₃ and allowed to progress for 20 min at 37 °C. To stop the reaction, the solution was diluted two times with methanol and centrifuged, and the supernatant was collected. Supernatant was mixed 1:1 with 10 mg/mL α-cyano-4-hydroxycinnamic acid in 50% ACN/0.1% TFA, and the mixture was spotted directly onto the MALDI plate. For analysis, an ABI DE-STR MALDI TOF instrument was used.

As a control for the ARK⁺(N^ε-methyl bis(propargyl))ST inhibition study, the inhibition of KDM4A and KDM4C by a solution of CH₃I in H₂O/DMSO was tested. The solution was made by dissolving 10 μL methyl iodide in 30 μL DMSO, then by diluting this five times with H₂O. Using this as the “30 mM” stock solution, enzyme inhibition was tested as above, in concentrations varying from “0 – 1000 μM” CH₃I solution.

Demethylation of ARK⁺(N^ε-methyl bis(propargyl))ST by KDM4A, KDM4C, and KDM4E

Purified HDM (8 μM) was incubated with 50 mM HEPES pH 7.5, 40 μM Fe^{II}(NH₄)₂SO₄·6H₂O, 300 μM αKG, 500 μM sodium L-ascorbate, and 400 μM ARK⁺(N^ε-methyl bis(propargyl))ST at room temperature for varying amounts of time (0, 5, 20, and 60 min). At each time point, the solution was diluted two times with methanol and centrifuged, and the supernatant was collected. Supernatant was mixed 1:1 with 10 mg/mL α-cyano-4-hydroxycinnamic acid in 50% ACN/0.1% TFA, and the mixture was spotted directly onto the MALDI plate.

In situ click chemistry studies with ARK(*N*^ε-bis(propargyl))ST and ARK⁺(*N*^ε-methyl bis(propargyl))ST

Purified HDM (250 μM) was incubated with 250 μM NiCl₂·6H₂O or Fe^{II}(NH₄)₂SO₄·6H₂O, followed by the addition of 2 mM αKG pH 7.5, 1 mM NaCl, 750 μM ARK(*N*^ε bis(propargyl))ST or ARK⁺(*N*^ε methyl bis(propargyl))ST, 200 mM NaN₃, and HEPES pH 7.5. The incubation was done at varying temperatures (4, 20, and 37 °C) and for varying amounts of time (4 – 24 h). “Metal-only” controls (i.e. 250 μM NiCl₂·6H₂O or Fe^{II}(NH₄)₂SO₄·6H₂O without HDM) were done for each experimental setup. For analysis, a portion of each sample was diluted two times with 50 mM EDTA (pH 8.0), then diluted ten times with MeOH:H₂O. Each solution is centrifuged, and the supernatant was collected and desalted using ZipTip (C₁₈) or ZipTip (SCX) and spotted onto the MALDI plate, either directly or after eluting with matrix solution. Matrix solution containing 10 μM standard (H₃₍₇₋₁₄₎K9me₃) was layered on top of each spot for calibration purposes.

4.2.3 Docking studies of ARK(*N*^ε- bis(propargyl))S with KDM4A

Low energy conformers of ARK(*N*^ε bis(propargyl))S were generated using OMEGA following minimization by SZYBKI (both OpenEye). The conformers were modeled into the KDM4A active site (PDB 2Q8C) with OpenEye’s HYBRID ligand-guided docking program using the Poisson-Boltzmann solvation method at 310 K, taking into account cavity solvation energies. All renderings were generated using PyMol.

4.3 Results and Discussion

As members of the KDM4 subfamily of JmjC-HDMs are candidate oncogenes, inhibition of these enzymes is an active area of study. However, selective inhibition is of the utmost importance, as other JmjC-HDM subfamilies may have members that act as tumor suppressors. Achieving subfamily or isoform selectivity within the JmjC-HDMs is proving difficult for several reasons. First, many JmjC-HDMs have similar active-site structures owing to high sequence homologies. Secondly, inhibitors designed to bind the ferrous iron in place of α KG in the active site can be promiscuous in nature, and may interfere with other histone-modifying metalloenzymes.^{10, 11} Lastly, primary substrate recognition involves both catalytic (JmjC, JmjN) and non-catalytic (PHD, Tudor-Tudor) domains, complicating substrate-based inhibitor design efforts.^{1, 4, 5, 12-14}

Using a peptidomimetic approach, we designed a modified H3K9 peptide in an effort to selectively inhibit KDM4C over the closely related enzyme KDM4A, as the two are thought to contribute to different cancers through varying mechanisms.¹⁵⁻²⁰ In this study, the inhibitor is a 5-mer H3₍₇₋₁₁₎K9 (ARKST) containing a lysine residue with two propargyl groups attached to the epsilon nitrogen. Shown in Figure 4.2 is the methylated version of the peptide, ARK⁺(N^ε-methyl bis(propargyl))ST, designed to test whether inhibition of KDM4C would be increased with a charged lysine as in the natural trimethylammonium substrate.

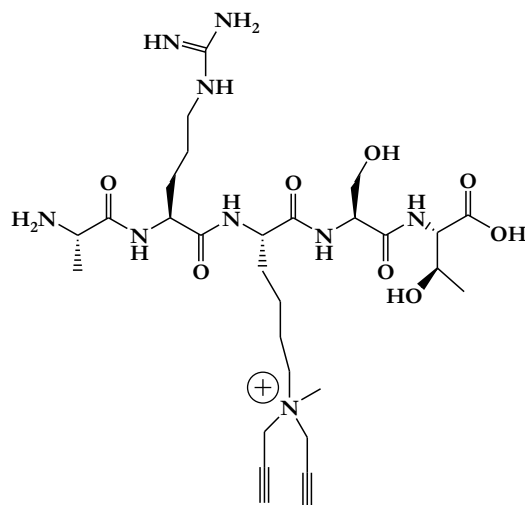


Figure 4.2. The novel histone H3 peptide, ARK⁺(N⁷-methyl bis(propargyl))ST, designed to selectively inhibit KDM4C over KDM4A.

Both peptides were devised to have the N⁷ propargyl groups project toward the Fe(II) metal center in the KDM4C active site. Such positioning of the propargyl groups would be desirable for two reasons. First, we could test whether either of the enzymes could hydroxylate this non-natural alkyl substrate, as another study had shown KDM4E to have activity toward H3K9(N⁷-ethyl) substrates.²¹ Second, positioning the propargyl groups to project toward the metal center could serve to facilitate triazole formation between the alkyne(s) and an HDM-metal-azide complex. This in situ click chemistry has been a topic of interest in our studies and has been explored for various alkyne-containing substrates, with no concrete evidence of enzyme-driven triazole formation. Thus, a peptide that should be recognized by KDM4C containing propargyl groups aimed at the metal center provides a good opportunity to test whether KDM4C is capable of acting as the reaction “vessel” for triazole formation.

Since no crystal structure of KDM4C in ternary complex with an H3K9 peptide has been solved, docking studies of our novel peptide ARK(N^{E} -bis(propargyl))ST were done with the catalytic core of KDM4A (Figure 4.3). We find that the most favorable conformation has the termini of the two propargyl groups at distances of 4.0 and 5.2 Å from the metal center. An approximate distance of 5 Å should provide sufficient room for reaction between an Fe^{IV} -oxo species and alkyl substrate.²²

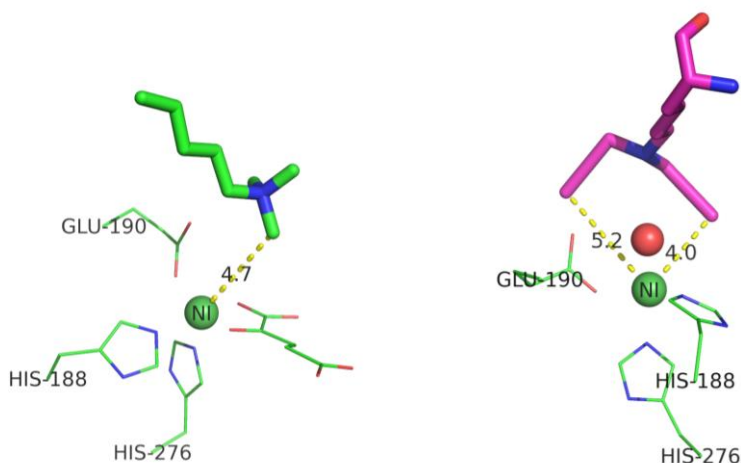


Figure 4.3. (*left*) $\text{H3}_{(7-14)}\text{K9me}_3$ crystallized in the KDM4A active site; (*right*) $\text{H3}_{(7-14)}\text{K9}(\text{bis}(\text{propargyl}))$ docked into the KDM4A active site.

We first tested for selective inhibition of KDM4C over KDM4A with the non-methylated peptide ARK(N^{E} - bis(propargyl))ST using a discontinuous MALDI-TOF MS assay. Briefly, all reaction components aside from the natural primary substrate (ARKme₃STGGK) were incubated with the holoenzyme for several minutes, a method common for substrate-based inhibitors.⁸ After addition of the primary substrate, the demethylation reaction was allowed to progress, and then stopped by precipitation of the protein. Analysis of samples ranging in concentration of ARK(N^{E} - bis(propargyl))ST from 0 – 1000 μM reveal that this peptide does indeed selectively inhibit

KDM4C over KDM4A (Figure 4.4). Although we find no inhibition of KDM4A, the inhibition of KDM4C is quite mild, with an IC_{50} greater than 1 mM.

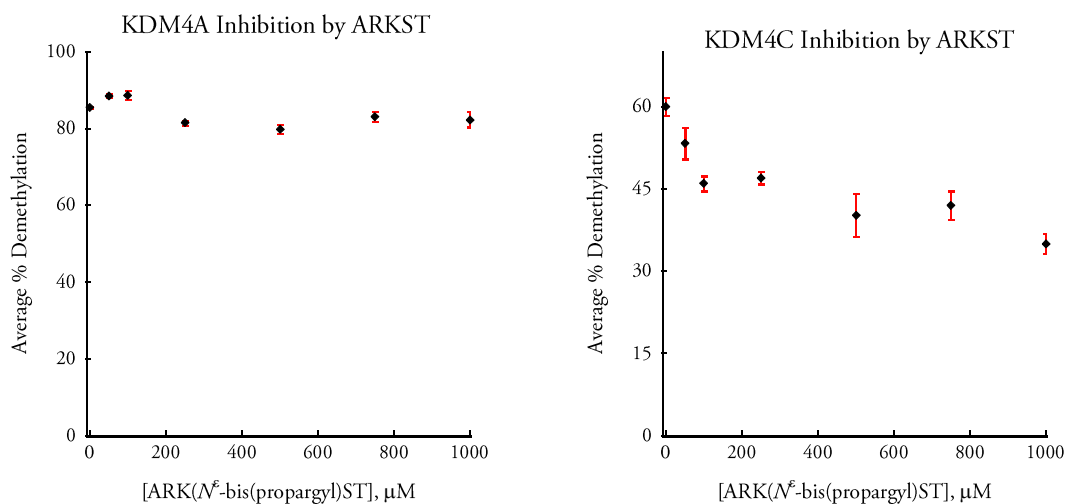


Figure 4.4. Selective inhibition of KDM4C over KDM4A using ARK(N^{ϵ} -bis(propargyl))ST.

Next, ARK(N^{ϵ} -bis(propargyl))ST was methylated to ARK⁺(N^{ϵ} -methyl bis(propargyl))ST using methyl iodide. Confirmation that lysine was the methylated residue came from ESI-CID-MS/MS analysis (Appendix B). As the natural KDM4C substrate, H3K9me_{3/2}, features a positively charged lysine, we posited that the methylated peptide would lead to increased inhibition of KDM4C. Using the same MALDI-TOF MS assay, we obtain surprising results. Not only do we see increased inhibition of KDM4C with the methylated peptide ($\log IC_{50} = -3.355 \pm 0.120$; $IC_{50} \approx 440 \mu\text{M}$), we see a similar level of inhibition of KDM4A ($\log IC_{50} = -3.269 \pm 0.048$; $IC_{50} \approx 540 \mu\text{M}$) (Figure 4.5 and Table 4.1). This inhibition of KDM4A was unexpected as an earlier study had found KDM4A to be incapable of recognizing a peptide shorter than H3₍₇₋₁₄₎K9.⁷

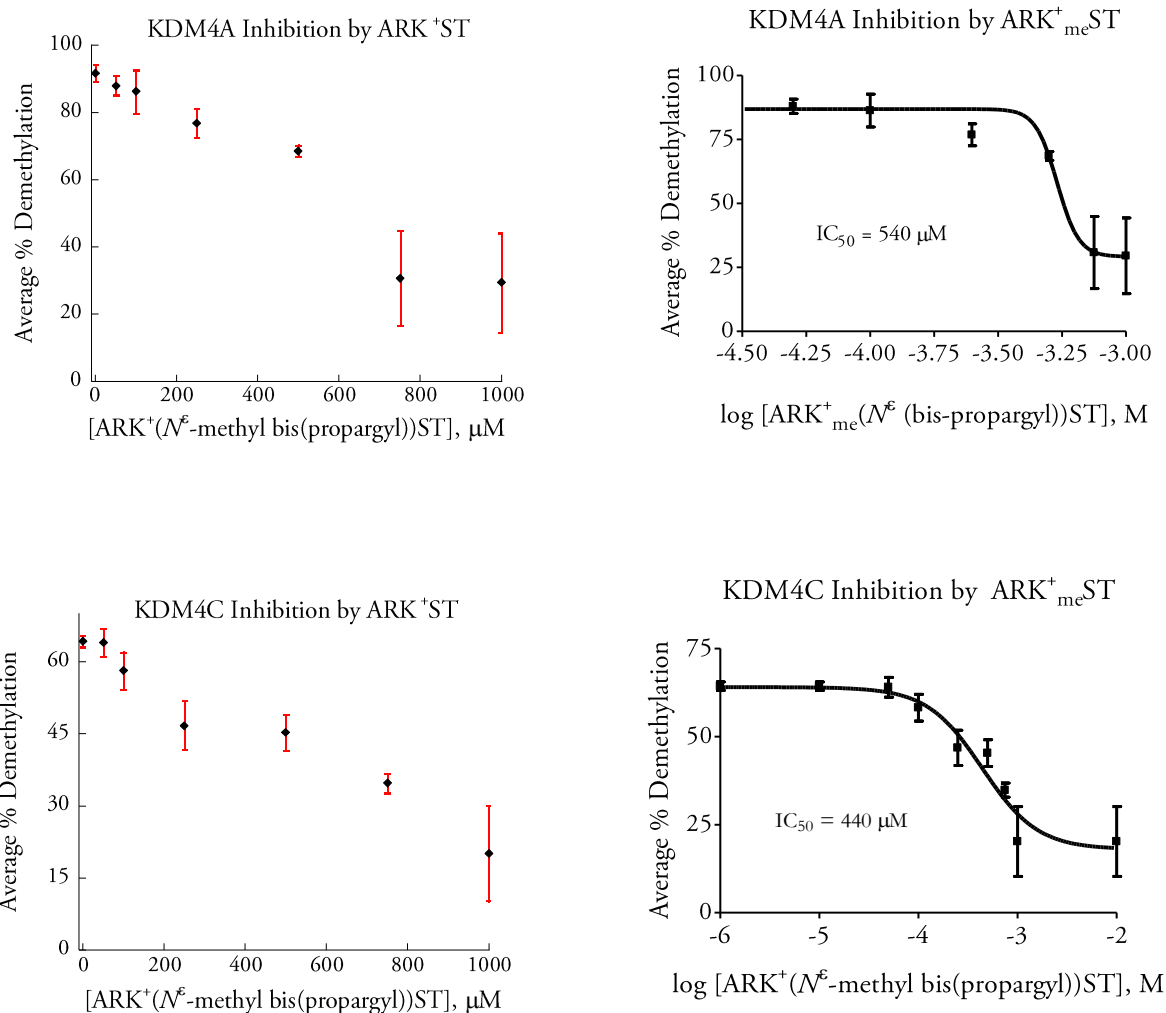


Figure 4.5. Inhibition of KDM4A (*top*) and KDM4C (*bottom*) by ARK⁺(N^E-methyl bis(propargyl))ST.

Conversion of the IC₅₀ values obtained above to apparent K_i binding affinities can be done using the Cheng-Prusoff equation (4-1).²³ Using the H3₍₇₋₁₄₎K9me₃ K_m values obtained in Chapter 2 of this work, we find that the K_i^{app} for KDM4A is approximately 184 μM; for KDM4C, K_i^{app} is 153 μM. While neither of these binding affinities is remarkably high, it is worth noting that these small molecules are inhibiting KDM4A and KDM4C without chelating the metal center in the active

site. Thus, to our knowledge, this is the first peptide-based inhibitor of KDM4 isoforms that does not include an α KG analog to enhance inhibitory effectiveness.^{7,8}

$$K_i = \frac{IC_{50}}{1 + \frac{[S]}{K_m}} \quad (4-1)$$

Table 4.1. Inhibition data for KDM4A and KDM4C with modified H3K9 peptides.^a

	ARK(N^{ϵ} - bis(propargyl))ST		ARK ⁺ (N^{ϵ} - methyl bis(propargyl))ST	
	IC ₅₀	K _i ^{app}	IC ₅₀	K _i ^{app}
KDM4A	N.D.	N.D.	540 μ M	184 μ M
KDM4C	> 1 mM	> 340 μ M	440 μ M	153 μ M

^a See section 4.2.2 for experimental conditions.

Previous studies found KDM4A to demethylate H3K9me₃ three-fold more efficiently than H3K9me₂, with KDM4C behaving similarly.^{1,5} In this study, we found a near 3-fold increase in KDM4C inhibition when modifying our H3K9 peptide from a Lys- N^{ϵ} tertiary amine to a quaternary amine. While we anticipated an increase in inhibition of KDM4C when moving from ARK(N^{ϵ} - bis(propargyl))ST to ARK⁺(N^{ϵ} - methyl bis(propargyl))ST, it was surprising to see such inhibition of KDM4A when using the methylated peptide. As KDM4A does not appear to have demethylase or hydroxylase activity towards the modified peptide (vide infra), the positive charge on K9 may provide enough favorable electrostatic interaction in or near the KDM4A active site to weaken the enzyme's ability to bind the more natural ARKme₃STGGK substrate.

To ensure that ARK⁺(N^{ϵ} - methyl bis(propargyl))ST is the species responsible for the observed inhibition, a solution of methyl iodide in H₂O/DMSO was tested against KDM4A and

KDM4C, as the $\text{ARK}^+(\text{N}^\text{E}-\text{methyl bis(propargyl)})\text{ST}$ reaction solution contained excess methyl iodide quenched with H_2O . As seen in Figure 4.6, there is minimal inhibition of KDM4C using the methyl iodide solution, and virtually no inhibition observed for KDM4A.

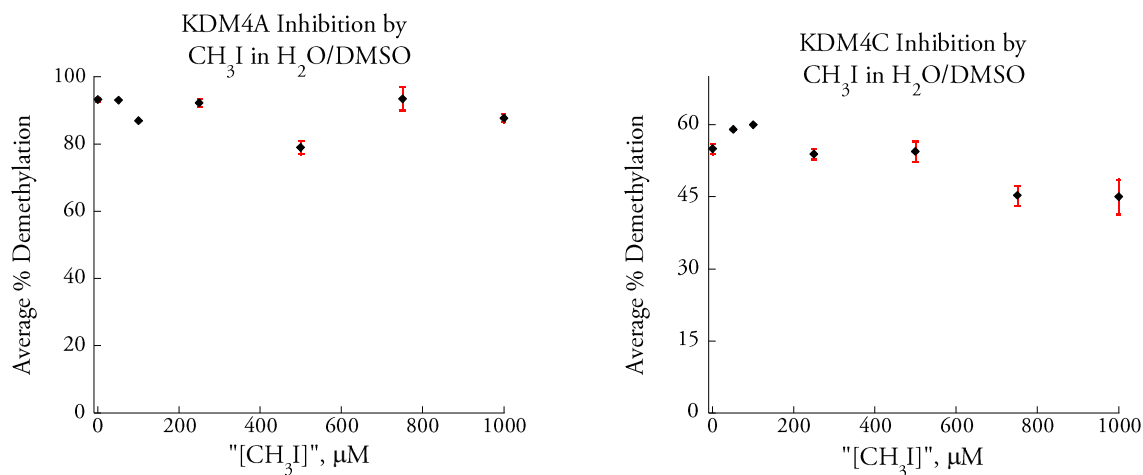


Figure 4.6. Minimal inhibition of KDM4A (*left*) and KDM4C (*right*) using a methyl iodide solution.

We next tested to find if any of our three JmjC-HDMs (KDM4A/C/E) display hydroxylase or demethylase activity toward $\text{ARK}^+(\text{N}^\text{E}-\text{methyl bis(propargyl)})\text{ST}$. Briefly, the holoenzyme was incubated with necessary reaction components (buffer, αKG , ascorbic acid) and 400 μM peptide for up to one hour at room temperature. For all three enzymes, the $t = 0$ min spectra are nearly identical to the $t = 60$ min spectra (Appendix B). Dominant peaks in each spectrum correspond to the starting material and its sodium adduct, as well as $\text{ARK}^+(\text{N}^\text{E}-\text{methyl mono(propargyl)})\text{ST}$ at $[\text{M} - 38]^+$. The KDM4C $t = 0$ min and $t = 60$ min spectra are given as representatives in Figure 4.7. The mono-propargyl peak does not grow with time, and we find no peaks corresponding to demethylation $[\text{M} - 14]^+$ or hydroxylation $[\text{M} + 17]^+$.

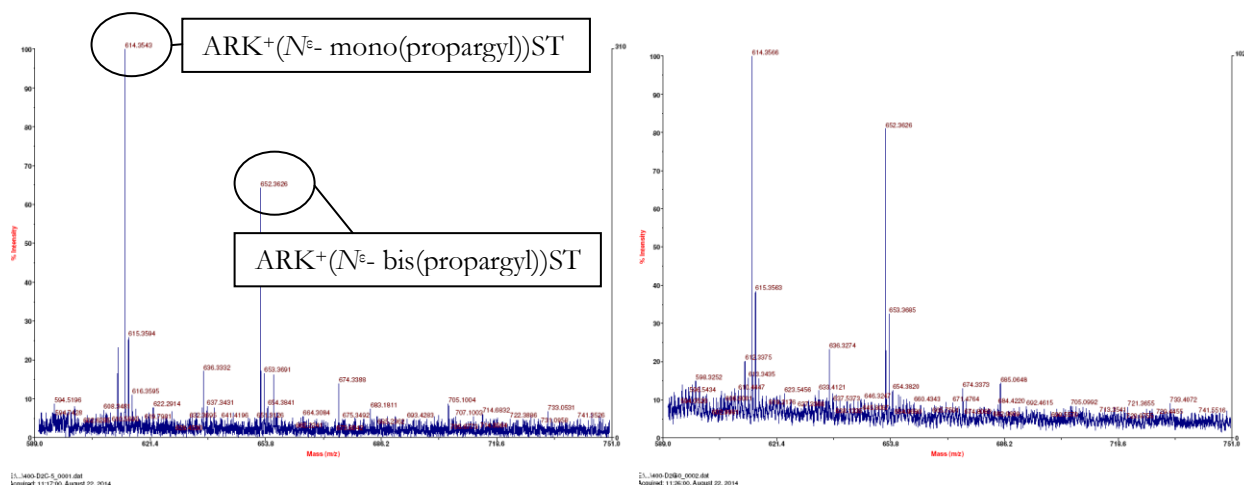


Figure 4.7. MALDI-TOF spectra obtained from KDM4C incubation with ARK⁺ST for (*left*) 0 minutes and (*right*) 60 minutes.

It is unclear as to why not one of our HDMs, and KDM4C in particular, displays demethylase or hydroxylase activity toward ARK⁺(N^ε-methyl bis(propargyl))ST. We know from the literature that KDM4 enzymes show no detectable activity toward the H3K9 substrate ARK⁺me₁STGGK, most likely due to orientation of the lone methyl group away from the Fe(IV)-oxo active species.⁴ The bulkiness of the propargyl groups in our inhibitor may prevent proper orientation of the ARK⁺(N^ε-methyl bis(propargyl))ST methyl group needed for demethylation to take place. Moreover, hydroxylation at the propargyl methylene groups may not occur owing to these carbons being too far from or too close to the Fe(IV)-oxo species. Modification of ARK⁺(N^ε-methyl bis(propargyl))ST could lead to effective specific inhibitors of JmjC-HDMs, because this peptide does not act as a substrate and will not be consumed in the reaction, thereby retaining its inhibitory effectiveness.

Finally, both ARK(N^ε-bis(propargyl))ST and the methylated peptide were used to test in situ Huisgen 1, 3- dipolar cycloaddition with KDM4A and KDM4C iron- and nickel-azide complexes.

Briefly, 250 μM HDM was incubated with 1 equivalent metal salt (Fe(II) or Ni(II)), αKG , NaCl, 3 equivalents modified ARKST peptide, and 200 mM sodium azide. The high concentration of azide is necessary owing to apparent low affinity of N_3^- for our HDM/Fe complexes. As shown in Figure 4.8, azide is a very weak inhibitor of KDM4A and KDM4C, with IC_{50} values greater than 10 mM.

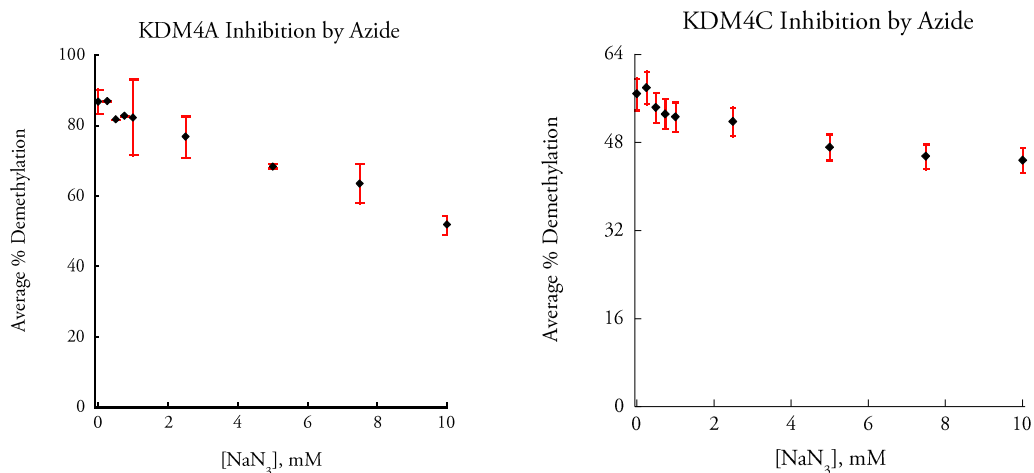


Figure 4.8. N_3^- is a weak inhibitor of KDM4A and KDM4C, as shown by MALDI-TOF MS.

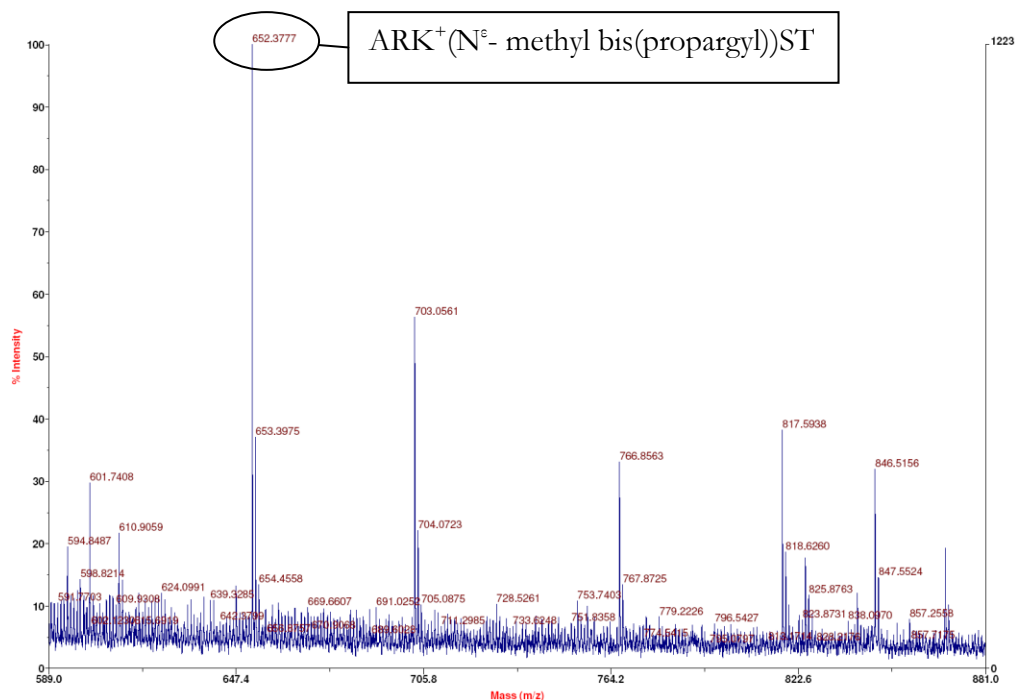
Varying conditions were used to test for triazole formation: 1) varying temperature (4, 20, and 37 $^{\circ}\text{C}$), 2) varying amounts of time (4 – 24 h), and 3) varying metal salt (Fe and Ni) for holoenzyme generation. From earlier model studies in our group, we know that nickel and cobalt are more effective at click chemistry than iron; unfortunately, our purified HDMs precipitate upon reconstitution with cobalt salts.²⁴

ESI-MS and MALDI-TOF MS analyses reveal no evidence of triazole formation by using either $\text{ARK}(\text{N}^{\text{E}}\text{-bis}(\text{propargyl}))\text{ST}$ or the methylated peptide with KDM4A or KDM4C. MALDI analysis of KDM4C samples with Fe or Ni and $\text{ARK}^+(\text{N}^{\text{E}}\text{-methyl bis}(\text{propargyl}))\text{ST}$ are given as

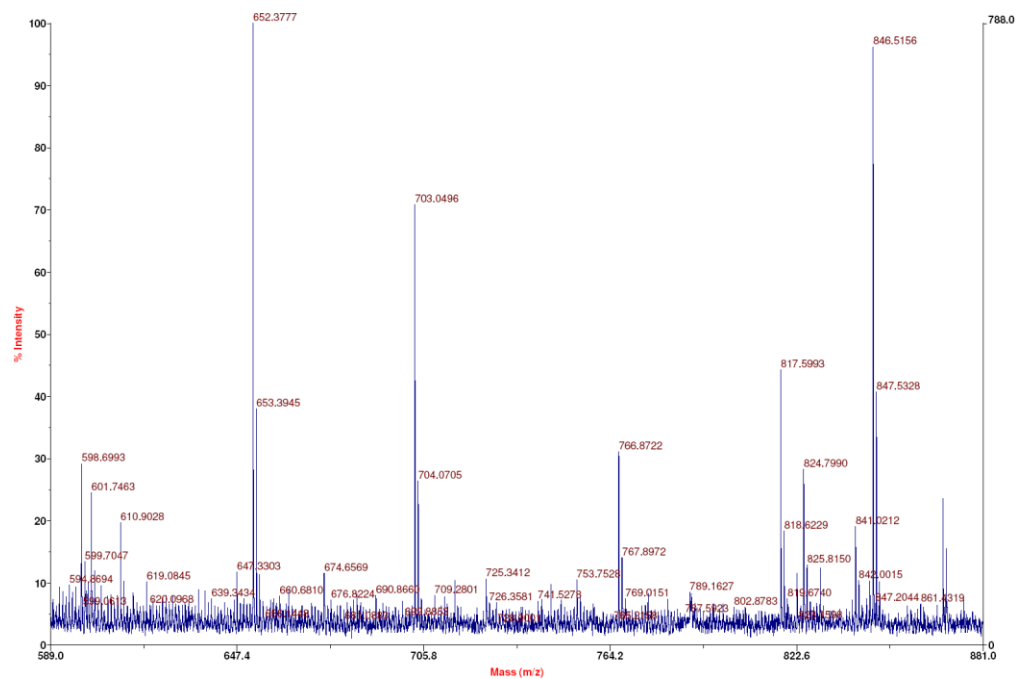
representatives in Figure 4.9. The m/z values corresponding to potential peaks of interest are given in Table 4.2. Note that following spotting of samples purified by C₁₈ or SCX Zip Tip on the MALDI plate, an overlay of ARKme₃STGGK (m/z 846) in matrix was used for calibration purposes.

Table 4.2. ARK⁺(N^ε-methyl bis(propargyl))ST peaks of interest in the enzyme-templated cycloaddition experiment.

Species	m/z of Interest
Starting material	M ¹⁺ = 652.4
Demethylated	M ¹⁺ = 638.4
Mono-triazole	M ¹⁺ = 695.4
Di-triazole	M ¹⁺ = 738.4



E:_D2C Fe ARK+ST w Overlay_0008.dat
Acquired: 07:37:00, August 25, 2014



E:_D2C Ni ARK+ST super w Overlay_0004.dat
Acquired: 07:29:00, August 25, 2014

Figure 4.9. MALDI-TOF MS results for (*top*) KDM4C-Fe-azide and (*bottom*) KDM4C-Ni-azide incubations with ARK⁺(N^ε- methyl bis(propargyl))ST.

Since we have evidence of KDM4A and KDM4C inhibition by our modified H3K9 peptides, potential explanations as to why we find no enzyme-driven triazole formation in any of our experimental setups are varied. One reason may be due to weak enzyme-metal-azide adduct formation, a variable over which we have no control. A second reason could be due to poor orientation of the propargyl groups within the active site that leads to improper interaction with the metal center. For instance, the azide-iron bond length, which a previous study found to be 2.3 Å in a diferrous protein,²⁵ may not be appropriate for any triazole formation to take place, with the propargyl C≡C predicted to be at between 4 – 5 Å from the metal center. There may not be enough room in the KDM4 active site to accommodate the Lys- N^{ϵ} alkyl groups in addition to the metal-azide adduct, if it does indeed form. Keeping the Lys propargyl groups, but shortening the Lys side chain by one or two methylene groups could offer a potential remedy if the issue is crowding within the KDM4C active site.

4.4 Conclusions

In conclusion, we have developed two novel histone H3 peptides in an effort to selectively inhibit the H3K9/H3K36 HDM KDM4C over the closely related KDM4A. The two 5-mers come from residues 7-11 on histone 3, ARKST, with the Lys residues modified to incorporate two propargyl groups on the terminal nitrogen, with one of the peptides having an additional methyl group on the terminal nitrogen to make it quaternary. We find selective, albeit weak, inhibition of KDM4C over KDM4A using the unmethylated peptide ARK(N^{ϵ} -bis(propargyl))ST. Using the methylated peptide ARK⁺(N^{ϵ} -methyl bis(propargyl))ST, we find a near 3-fold increase in the inhibition of KDM4C, and unexpectedly, a similar level of inhibition of KDM4A. The obtained K_i^{app} values reflect the difficulty in achieving potent inhibition of JmjC-HDMs by small molecules that do

not chelate the active site metal center. We find that none of our three KDM4 enzymes display hydroxylase or demethylase activity toward either modified H3 peptide, suggesting that these peptides could offer a starting point in the design of effective specific inhibitors of JmjdC-HDMs. Furthermore, we find no evidence of triazole formation in KDM4-driven cycloaddition studies with either of our modified peptides, suggesting once more that these enzymes may not be well suited for enzyme-templated Huisgen 1, 3- dipolar cycloaddition reactions.

4.5 References

1. Couture, J. F., Collazo, E., Ortiz-Tello, P. A., Brunzelle, J. S., Trievel, R. C., Specificity and Mechanism of Jmjd2a, a Trimethyllysine-Specific Histone Demethylase. *Nature Structural & Molecular Biology* **14**, 689-695 (2007).
2. Chen, Z., Zang, J., Whetstine, J., Hong, X., Davrazou, F., Kutateladze, T. G., Simpson, M., Mao, Q., Pan, C. H., Dai, S., Hagman, J., Hansen, K., Shi, Y., Zhang, G., Structural Insights into Histone Demethylation by Jmjd2 Family Members. *Cell* **125**, 691-702. (2006).
3. Ponnaluri, V. K. C., Vavilala, D. T., Mukherji, M., Studies on Substrate Specificity of Jmjd2a-C Histone Demethylases. *Biochemical and Biophysical Research Communications* **405**, 588-592 (2011).
4. Ng, S. S., Kavanagh, K. L., McDonough, M. A., Butler, D., Pilka, E. S., Lienard, B. M. R., Bray, J. E., Savitsky, P., Gileadi, O., von Delft, F., Rose, N. R., Offer, J., Scheinost, J. C., Borowski, T., Sundstrom, M., Schofield, C. J., Oppermann, U., Crystal Structures of Histone Demethylase Jmjd2a Reveal Basis for Substrate Specificity. *Nature* **448**, 87-U88 (2007).
5. Hillringhaus, L., Yue, W. W., Rose, N. R., Ng, S. S., Gileadi, C., Loenarz, C., Bello, S. H., Bray, J. E., Schofield, C. J., Oppermann, U., Structural and Evolutionary Basis for the Dual Substrate Selectivity of Human Kdm4 Histone Demethylase Family. *Journal of Biological Chemistry* **286**, 41616-41625 (2011).

6. Whetstine, J. R., Nottke, A., Lan, F., Huarte, M., Smolikov, S., Chen, Z., Spooner, E., Li, E., Zhang, G., Colaiacovo, M., Reversal of Histone Lysine Trimethylation by the Jmjd2 Family of Histone Demethylases. *Cell* **125**, 467-481 (2006).
7. Lohse, B., Nielsen, A. L., Kristensen, J. B. L., Helgstrand, C., Cloos, P. A. C., Olsen, L., Gajhede, M., Clausen, R. P., Kristensen, J. L., Targeting Histone Lysine Demethylases by Truncating the Histone 3 Tail to Obtain Selective Substrate-Based Inhibitors. *Angewandte Chemie, International Edition in English* **123**, 9266-9269 (2011).
8. Woon, E. C. Y., Tumber, A., Kawamura, A., Hillringhaus, L., Ge, W., Rose, N. R., Ma, J. H. Y., Chan, M. C., Walport, L. J., Che, K. H., Ng, S. S., Marsden, B. D., Oppermann, U., McDonough, M. A., Schofield, C. J., Linking of 2-Oxoglutarate and Substrate Binding Sites Enables Potent and Highly Selective Inhibition of Jmjc Histone Demethylases. *Angewandte Chemie International Edition* **51**, 1631-1634 (2012).
9. Mindt, T. L., Schweinsberg, C., Brans, L., Hagenbach, A., Abram, U., Tourwen, D., Garcia-Garayoa, E., Schibli, R., A Click Approach to Structurally Diverse Conjugates Containing a Central Di-1, 2, 3-Triazole Metal Chelate. *ChemMedChem* **4**, 529-539 (2009).
10. Lohse, B., Kristensen, J. L., Kristensen, L. H., Agger, K., Helin, K., Gajhede, M., Clausen, R. P., Inhibitors of Histone Demethylases. *Bioorganic & Medicinal Chemistry* **19**, 3625-3636 (2011).
11. Johnstone, R. W., Histone-Deacetylase Inhibitors: Novel Drugs for the Treatment of Cancer. *Nature Reviews Drug Discovery* **1**, 287-299 (2002).
12. Chen, Z., Zang, J., Kappler, J., Hong, X., Crawford, F., Wang, Q., Lan, F., Jiang, C., Whetstine, J., Dai, S., Structural Basis of the Recognition of a Methylated Histone Tail by Jmjd2a. *Proceedings of the National Academy of Sciences* **104**, 10818-10823 (2007).
13. Horton, J. R., Upadhyay, A. K., Qi, H. H., Zhang, X., Shi, Y., Cheng, X., Enzymatic and Structural Insights for Substrate Specificity of a Family of Jumonji Histone Lysine Demethylases. *Nature Structural & Molecular Biology* **17**, 38-43 (2010).
14. Loenarz, C., Ge, W., Coleman, M. L., Rose, N. R., Cooper, C. D., Klose, R. J., Ratcliffe, P. J., Schofield, C. J., Phf8, a Gene Associated with Cleft Lip/Palate and Mental Retardation, Encodes for an Ne-Dimethyl Lysine Demethylase. *Human molecular genetics* **19**, 217-222 (2010).

15. Cloos, P. A. C., Christensen, J., Agger, K., Maiolica, A., Rappsilber, J., Antal, T., Hansen, K. H., Helin, K., The Putative Oncogene Gasc1 Demethylates Tri- and Dimethylated Lysine 9 on Histone H3. *Nature* **442**, 307-311 (2006).
16. Luo, W., Chang, R., Zhong, J., Pandey, A., Semenza, G. L., Histone Demethylase Jmjd2c Is a Coactivator for Hypoxia-Inducible Factor 1 That Is Required for Breast Cancer Progression. *Proceedings of the National Academy of Sciences* **109**, E3367-E3376 (2012).
17. Kim, T.-D., Fuchs, J. R., Schwartz, E., Abdelhamid, D., Etter, J., Berry, W. L., Li, C., Ihnat, M. A., Li, P.-K., Janknecht, R., Pro-Growth Role of the Jmjd2c Histone Demethylase in Hct-116 Colon Cancer Cells and Identification of Curcuminoids as Jmjd2 Inhibitors. *American Journal of Translational Research* **6**, 236-247 (2014).
18. Berry, W. L., Shin, S., Lightfoot, S. A., Janknecht, R., Oncogenic Features of the Jmjd2a Histone Demethylase in Breast Cancer. *International Journal of Oncology* **41**, 1701-1706 (2012).
19. Mallette, F. A., Richard, S., Jmjd2a Promotes Cellular Transformation by Blocking Cellular Senescence through Transcriptional Repression of the Tumor Suppressor Chd5. *Cell reports* **2**, 1233-1243 (2012).
20. Black, J. C., Manning, A. L., Van Rechem, C., Kim, J., Ladd, B., Cho, J., Pineda, C. M., Murphy, N., Daniels, D. L., Montagna, C., Kdm4a Lysine Demethylase Induces Site-Specific Copy Gain and Rereplication of Regions Amplified in Tumors. *Cell* **154**, 541-555 (2013).
21. Hopkinson, R. J., Walport, L. J., Münzel, M., Rose, N. R., Smart, T. J., Kawamura, A., Claridge, T. D., Schofield, C. J., Is Jmjc Oxygenase Catalysis Limited to Demethylation? *Angewandte Chemie* **125**, 7863-7867 (2013).
22. Costas, M., Mehn, M. P., Jensen, M. P., Que, L., Jr., Dioxygen Activation at Mononuclear Nonheme Iron Active Sites: Enzymes, Models, and Intermediates. *Chemical Reviews* **104**, 939-986 (2004).
23. Yung-Chi, C., Prusoff, W. H., Relationship between the Inhibition Constant K_i and the Concentration of Inhibitor Which Causes 50 Per Cent Inhibition ($I_{c_{50}}$) of an Enzymatic Reaction. *Biochemical Pharmacology* **22**, 3099-3108 (1973).
24. Evangelio, E., Rath, N. P., Mirica, L. M., Cycloaddition Reactivity Studies of First-Row Transition Metal-Azide Complexes and Alkynes: An Inorganic Click Reaction for Metalloenzyme Inhibitor Synthesis. *Dalton Transactions* **41**, 8010-8021 (2012).

25. Andersson, M. E., Hogbom, M., Rinaldo-Matthis, A., Andersson, K. K., Sjoberg, B. M., Nordlund, P., The Crystal Structure of an Azide Complex of the Diferrous R2 Subunit of Ribonucleotide Reductase Displays a Novel Carboxylate Shift with Important Mechanistic Implications for Diiron-Catalyzed Oxygen Activation. *Journal of the American Chemical Society* **121**, 2346-2352 (1999).

Chapter 5: Inhibition and Crystallography

Studies of KDM4A with the Small Molecule

JIB-04

5.1 Introduction

The small molecule JIB-04 is the first reported specific pan-selective inhibitor of JmjC-domain containing histone demethylases (JmjC-HDMs). From a cell-based assay screening of 2,080 compounds, the pyridine hydrazone was identified as an epigenetic modulator.¹ JIB-04 has two forms, the E- and Z- isomers, as shown in Figure 5.1. The study found only the E- isomer to be active in cell-based assays, with the Z- isomer up to 100-fold less potent. To test the inhibition of histone-modifying enzymes, the authors used three in vitro methods when appropriate: a ¹H-NMR assay, utilizing the signal intensity of the trimethyl H3K9me₃ peak; a formaldehyde dehydrogenase (FDH) coupled assay, wherein the oxidation of the demethylation reaction side product formaldehyde is coupled with the reduction of NAD⁺ to the fluorescent NADH; and lastly, direct western analyses of a full-length histone H3 substrate. Furthermore, the anticancer potential of JIB-04 was tested, as the activities of JmjC-HDMs become deregulated in various cancers. The inhibitor consistently displayed specificity of action in cancerous cells over patient-matched healthy cells.

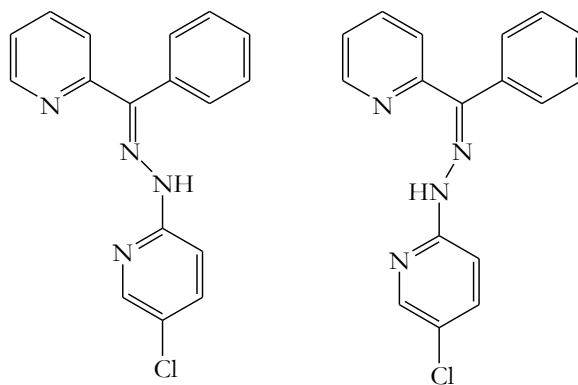


Figure 5.1. JIB-04 (*left*) E- and (*right*) Z- isomers.

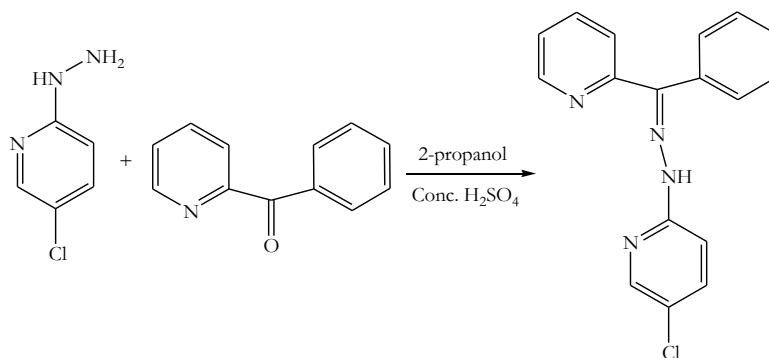
The published study finds JIB-04 to slow the activities of a broad range of JmjC-HDMs, with the E- isomer displaying its most potent inhibition on the pure H3K4me₃ (KDM5A) and H3K9me₃ demethylases (KDM4D-E), with lesser action against the H3K27 (KDM6B) and mixed H3K9/H3K36 demethylases (KDM4A-C). Reported IC₅₀ values range from 200 nM to 1.1 μM, which scale to what we find in the present study using alternative enzyme and substrate concentrations (*vide infra*). Importantly, JIB-04 does not show action against the related αKG-dependent prolyl hydroxylases (PHDs) and TET enzymes or other chromatin-modifying enzymes such as histone deacetylases (HDACs).

With the exception of a natural product named Tripartin, JIB-04 is the first specific inhibitor of JmjC-HDMs that is not a competitor of α-ketoglutarate.² While the authors find JIB-04 to be competitive with the primary histone substrate instead, the exact mode of inhibition was unclear. No crystal structure of a JmjC-HDM in complex with JIB-04 had been solved, nor were there any experiments done that might elucidate if JIB-04 is competitive with O₂ in addition to the histone substrate.

The present study examines the inhibition of the mixed H3K9/H3K36 demethylase KDM4A with respect to the cosubstrate O₂ by determining IC₅₀ values at three concentrations of O₂ using a real-time dioxygen consumption assay. Molecular modeling studies of the JIB-04 E- and Z- isomers in the KDM4A active site reveal the potential basis for the isomer-specific inhibition. Finally, a binary complex of the catalytic core of KDM4A with JIB-04 was resolved, revealing only a portion of the inhibitor in the KDM4A active site.

5.2 Methods

5.2.1 Synthesis of JIB-04¹



5-chloro-2-hydrazinopyridine (50 mg, 0.35 mmol, 1 equiv.) and 63.8 mg 2-benzoylpyridine (0.35 mmol, 1 equiv.) were dissolved in 2.1 mL 2-propanol and set to stir at room temperature. Hydrochloric acid (1.75 mmol, 5 equiv.) was added dropwise, and the solution was heated to 50 °C in an oil bath. The reaction was monitored by TLC in ethyl acetate; once complete, the solution was cooled to room temperature and neutralized using saturated sodium bicarbonate solution. The resulting precipitate was vacuum dried at 60 °C for 12 hours; monohydrate pale golden powder, 30:1 E- : Z- isomer, 78.6 mg, 0.24 mmol, 68% yield. ¹H NMR ((CD₃)₂SO), δ: 8.83 (d, 1H), 8.44 (s, 1H),

8.20 (m, 1H), 8.13 (s, 1H), 7.84 (m, 2H), 7.55 (m, 4H), 7.35 (s, 3H). **¹³C NMR** (CDCl₃), δ: 155.93, 154.68, 149.30, 146.94, 146.19, 138.07, 136.21, 131.72, 129.75, 129.02, 123.15, 122.92, 121.23, 108.73. See Appendix C for NMR spectra. **ESI-MS** *m/z* 309.1 (calculated), *m/z* 309.1 (experimental).

5.2.2 Inhibition of KDM4A by JIB-04

JIB-04 has limited solubility in aqueous solution, so inhibitor stock solutions were made in DMSO. The overall volume of DMSO in any given reaction solution was kept at 0.1%, as DMSO inhibits KDM4A at higher concentrations. In addition, when testing concentrations of JIB-04 greater than 20 μM, it was necessary to include 0.01% Tween-20 in order to keep JIB from precipitating out of the buffered reaction solutions.

MALDI-TOF Mass Spectrometry Inhibition Assays

KDM4A was tested for inhibition by the small molecule JIB-04 using the discontinuous MALDI-TOF MS assay. Purified KDM4A (8 μM) was incubated with 8 μM Fe^{II}(NH₄)₂SO₄·6H₂O and, if a pre-incubation trial, 0-500 μM JIB-04 in DMSO. Pre-incubation trials allowed for five minutes of pre-incubation on ice before the reaction was started by the addition of a solution containing 80 μM H₃(⁷⁻¹⁴)K9me₃ in 50 mM HEPES (pH 7.5), 500 μM sodium L-ascorbate, and 300 μM αKG. The reaction was allowed to proceed at 37 °C for 20 minutes. The enzymatic demethylation was stopped by addition of MeOH and TFA, the precipitated protein is removed via centrifugation, and the resulting supernatant is collected. An aliquot of the reaction solution was

added to 10 mg/mL α -cyano-4-hydroxycinnamic acid MALDI matrix in 50% acetonitrile/0.1% TFA and spotted directly onto the MALDI plate. For analysis, an ABI DE-STR MALDI TOF instrument was used.

Percent demethylation values were determined using the relative intensities of the mono-, di-, and tri-methylated H3₍₇₋₁₄₎K9 peaks in the following equation (5-1):

$$\% \text{ demethylation} = \frac{(\% \text{ NHme}_2 + 2 \cdot \% \text{ NH}_2\text{me}_1)}{(\% \text{ Nme}_3 + \% \text{ NHme}_2 + 2 \cdot \% \text{ NH}_2\text{me}_1)} \quad (5-1)$$

O₂ Consumption Inhibition Assays

KDM4A was tested for inhibition by the small molecule JIB-04 using the O₂ consumption assay. The reaction solution containing 50 mM HEPES (pH 7.5), 300 μ M α KG (pH 7.5), 500 μ M sodium L-ascorbate, 100 μ M H3₇₋₁₄K9me₃, and \pm JIB-04 (in DMSO) was equilibrated 2 – 5 min under an atmosphere of varying O₂ concentration. Following equilibration, the electrode was lowered into the reaction solution, and a 4 min background O₂ consumption reading was allowed. Separately, purified KDM4A (2 μ M) was reconstituted with Fe^{II}(NH₄)₂SO₄·6H₂O (2 μ M) and, if a pre-incubation trial, to the holoenzyme was added JIB-04 in DMSO (0 – 20 μ M) for a pre-incubation time of approximately 1 min. In pre-incubation trials, the volume of DMSO added to the KDM4A/Fe aliquot was 1 μ L (less than 20% of the HDM/Fe aliquot volume, and 0.1% of the reaction volume). The reaction was started by the addition of KDM4A/Fe/ \pm JIB-04 to the O₂ electrode chamber. All final rates were calculated by subtracting background oxygen consumption due to ascorbate and the holoenzyme in the absence of peptide substrate.

IC₅₀ values were determined by fitting the inhibition data to the sigmoidal dose-response (variable slope) equation (5-2) using the program GraphPad Prism, where “top” and “bottom” are the y-values at the top and bottom plateaus:

$$y = \text{Bottom} + \frac{(\text{Top}-\text{Bottom})}{1+10^{(\log IC_{50}-x) \cdot \text{Hillslope}}} \quad (5-2)$$

5.2.3 Docking Studies of KDM4A with JIB-04 Isomers

Low energy conformers of JIB-04 E- and Z- isomers were generated using OMEGA following minimization by SZYBKI (both OpenEye). The conformers were modeled into the KDM4A active site (PDB 2Q8C) with OpenEye’s FRED fast exhaustive docking program using the Poisson-Boltzmann solvation method at 310 K, taking into account cavity solvation energies. All renderings were generated using PyMol.

5.2.4 Crystallography

Protein crystals were grown by the hanging drop vapor diffusion method at 4 °C. Crystals of KDM4A (12 mg/mL) in complex with JIB-04 (750 μM) formed in drops of a 1:1 mixture of protein and crystallization buffer (0.1 M citrate pH 6.0, 17.5% PEG-3500, 4 mM NiCl₂ or Fe^{II}(NH₄)₂SO₄·6H₂O). Crystals were harvested from the mother liquor with a nylon loop, mounted on a goniometer, and directly frozen in a liquid N₂ vapor stream at 100 K. Data were collected by Dr. Soon Goo Lee using 19ID beamline at Argonne National Laboratory Advanced Photon Source with a CCD detector at a distance of 327.18 mm from the crystal. Images (180 frames) were collected at 0.979 Å in 1.0° oscillations (a 180° hemisphere), indexed (P 2 21 21), and scaled using HKL 3000.³ This resulted in 14,068 reflections in the 50 - 3.2 Å resolution range. Unit cell parameters and data reduction statistics are summarized in Table C.1 in Appendix C.

Detector	CCD
Type	ADSC QUANTUM 315r
Details	Rosenbaum-Rock high-resolution double-crystal monochromator

The structure of KDM4A was phased by using the molecular replacement method with Phaser and a model of the crystal structure of KDM4A complexed with inhibitor (PDB: 3RVH) structure.⁴ Based on the Matthew's coefficient, two protein monomers were expected in the asymmetric unit. The solution from Phaser had a top TFZ of 17.6. Manual fitting was initiated using COOT.⁵ Refinement was performed using Phenix with 10% of the data excluded from refinement for the R_{free} calculation.^{6, 7} The structure models were analyzed at TLS Motion Determination Server and refined with eight TLS groups, yielding a model with an R_{cryst} of 21.8% and R_{free} of 29.1%.⁸ The final model was analyzed using the CCP4 programs SFCHECK and PROCHECK.^{9, 10, 11} Refinement statistics are listed in Table C.1 in Appendix C.

5.2.5 Stability of JIB-04 in Aqueous Solution

The stability of JIB-04 in aqueous solution was tested at pH 6.0 (50 mM Citrate) and pH 7.5 (50 mM HEPES), as pH 6.0 citrate buffer was used for protein crystallization, and pH 7.5 HEPES was the buffer used in the MALDI-TOF MS and O₂ consumption assays. ESI-MS scan range of m/z 100 – 500 shows JIB-04 $[M + H]^+$ and $[M + Na]^+$ peaks. When the same samples were tested three days later, the only peaks seen are $[M + H]^+$ and $[M + Na]^+$. Thus, JIB-04 appears to be stable in aqueous solution.

Next, the stability of JIB-04 was tested in the presence of KDM4A. *Testing conditions:* 60 μM KDM4A, 60 μM $\text{Fe}^{\text{II}}(\text{NH}_4)_2\text{SO}_4 \cdot 6\text{H}_2\text{O}$, 300 μM JIB-04, 0.01% Tween-20, 50 mM HEPES pH 7.5 or Citrate pH 6.0. Small portions of each sample were removed at various times and diluted 2x with 5 mM EDTA in HEPES buffer. Then, the protein was precipitated with MeOH and the supernatant was analyzed by ESI-MS. After five days at 4 $^\circ\text{C}$, JIB appeared to be stable in the presence of KDM4A.

5.3 Results and Discussion

The small molecule JIB-04 is made up of several pyridine moieties and a hydrazone group that together selectively inhibit multiple JmjC-HDMs in an isomer-specific fashion. As JIB-04 shows remarkable action in promoting cell death in cancerous cells over patient-matched healthy cells, and does not alter the activities of related enzymes such as the αKG -dependent PHDs and TET enzymes, understanding the inhibitor's mode of action is an active area of interest.

Initially, we were interested to see how JIB-04 affected the activity of the H3K9/H3K36 HDM KDM4A as shown through two of our in vitro assays. KDM4A was first tested for inhibition by JIB-04 without pre-incubation of the holoenzyme and inhibitor using the O_2 consumption assay. Briefly, KDM4A (2 μM) was reconstituted with $\text{Fe}(\text{II})$ (2 μM) prior to injection into the reaction chamber containing αKG (300 μM), ascorbic acid (500 μM), $\text{H3}_{(7-14)}\text{K9me}_3$ (100 μM), HEPES (pH 7.5, 50 mM), Tween-20 (0.1%), and JIB-04 in DMSO (0 – 500 μM). The obtained plot shown in Figure 5.2 displays a modest decrease in enzymatic activity when JIB-04 is present in the reaction solution. The inhibitory effect seems to level off at >100 μM JIB-04, which is likely due to the

insolubility of JIB-04 in aqueous solution at high concentrations, even with the addition of the solubilizing agent Tween-20.

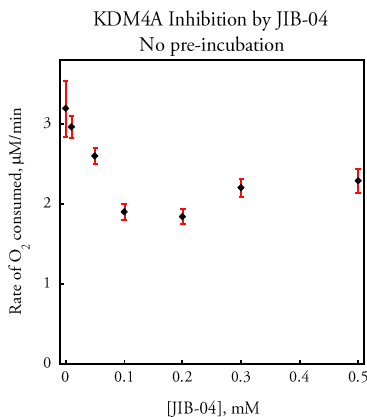


Figure 5.2. Mild inhibition of KDM4A by JIB-04 as shown by the O₂ consumption assay.

It is worth noting that the initial report of JIB-04 was vague concerning the in vitro inhibition assay conditions.¹ The authors report an IC₅₀ of 445 nM when using a KDM4A concentration of 206 nM. However, the authors do not specify the concentration of H3K9me₃ peptide used, nor do they specify the length of peptide used, and both of these variables would affect IC₅₀ values. Assuming that the common octapeptide H3₍₇₋₁₄₎K9me₃ was used, a 1:6.5 ratio of KDM4A:H3K9me₃ is calculated (400 ng KDM4A ≈ 9.1e-9 mmol, 50 ng H3₍₇₋₁₄₎K9me₃ ≈ 5.9e-8 mmol). In our preliminary O₂ consumption study, a 1:50 ratio of KDM4A:H3₍₇₋₁₄₎K9me₃ was used, from which we obtain Figure 5.2. Since JIB-04 is a putative histone peptide substrate competitor, we can reasonably expect a lower level of inhibition than that found in the published study. The low level of inhibition found when JIB-04 is added to the reaction solution, as opposed to the holoenzyme directly for pre-incubation, was further confirmed by a discontinuous MALDI-TOF

MS assay (Figure C.1 in Appendix C). Moreover, we find the same level of inhibition when using 1:1 KDM4A:Fe(II) or an excess of Fe(II) to produce the holoenzyme, indicating that the low level of inhibition is not due to JIB-04 interacting with excess iron in solution.

Next, the inhibition of KDM4A was tested using the MALDI-TOF MS assay, allowing for pre-incubation of the holoenzyme with JIB-04 (Figure 5.3). Briefly, KDM4A (8 μM) was reconstituted with one equivalent Fe(II) salt, then JIB-04 (0-500 μM) was added, and the mixture was allowed to incubate for several minutes. Then the reaction is started by the addition of αKG , $\text{H3}_{(7-14)}\text{K9me}_3$ and ascorbic acid. Using this method, we find substantial inhibition of the enzyme, with an IC_{50} of approximately 20 μM ($\log\text{IC}_{50} = -4.67 \pm 0.01$). This level of inhibition is in line with that found for KDM4A in the published study, as scaling from the 206 nM KDM4A used in the study to the 8 μM KDM4A used in this research, it is reasonable to expect an IC_{50} near 20 μM .

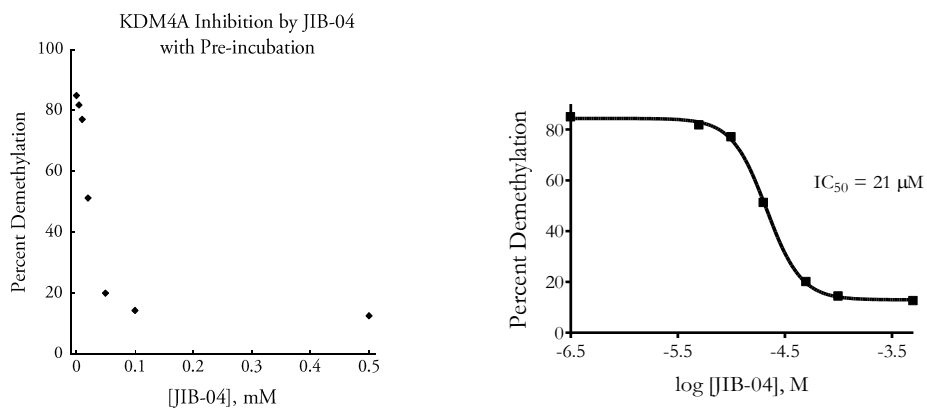


Figure 5.3. Inhibition of KDM4A by JIB-04 following pre-incubation with holoenzyme, as found by MALDI-TOF MS.

Having confirmed that pre-incubation of the holoenzyme with JIB-04 was necessary for substantial inhibition of KDM4A, the inhibition was screened at three different concentrations of O₂ using the dioxygen consumption assay. The inhibition screen was done in an effort to see whether the inhibition by JIB-04 is O₂-dependent. A stronger inhibitory effect at low concentrations of O₂ could signify that JIB-04 interacts with the KDM4A active site metal center in a similar manner as O₂. Briefly, reaction components (buffer, αKG, H3₍₇₋₁₄₎K9me₃, reducing agent) are equilibrated under varying atmospheres of O₂, while outside the reaction vessel, the holoenzyme is incubated with JIB-04 (0 - 20 μM). Injection of the HDM/Fe/JIB-04 complex into the reaction solution marks the start of the reaction. The concentrations of O₂ chosen are as follows: 258 μM (the concentration of O₂ in air-saturated water), 1200 μM (O₂-saturated water), and 60 μM (≈ K_m(O₂) for KDM4A). The KDM4A activities and corresponding IC₅₀ plots at the three concentrations of O₂ are given in Figure 5.4.

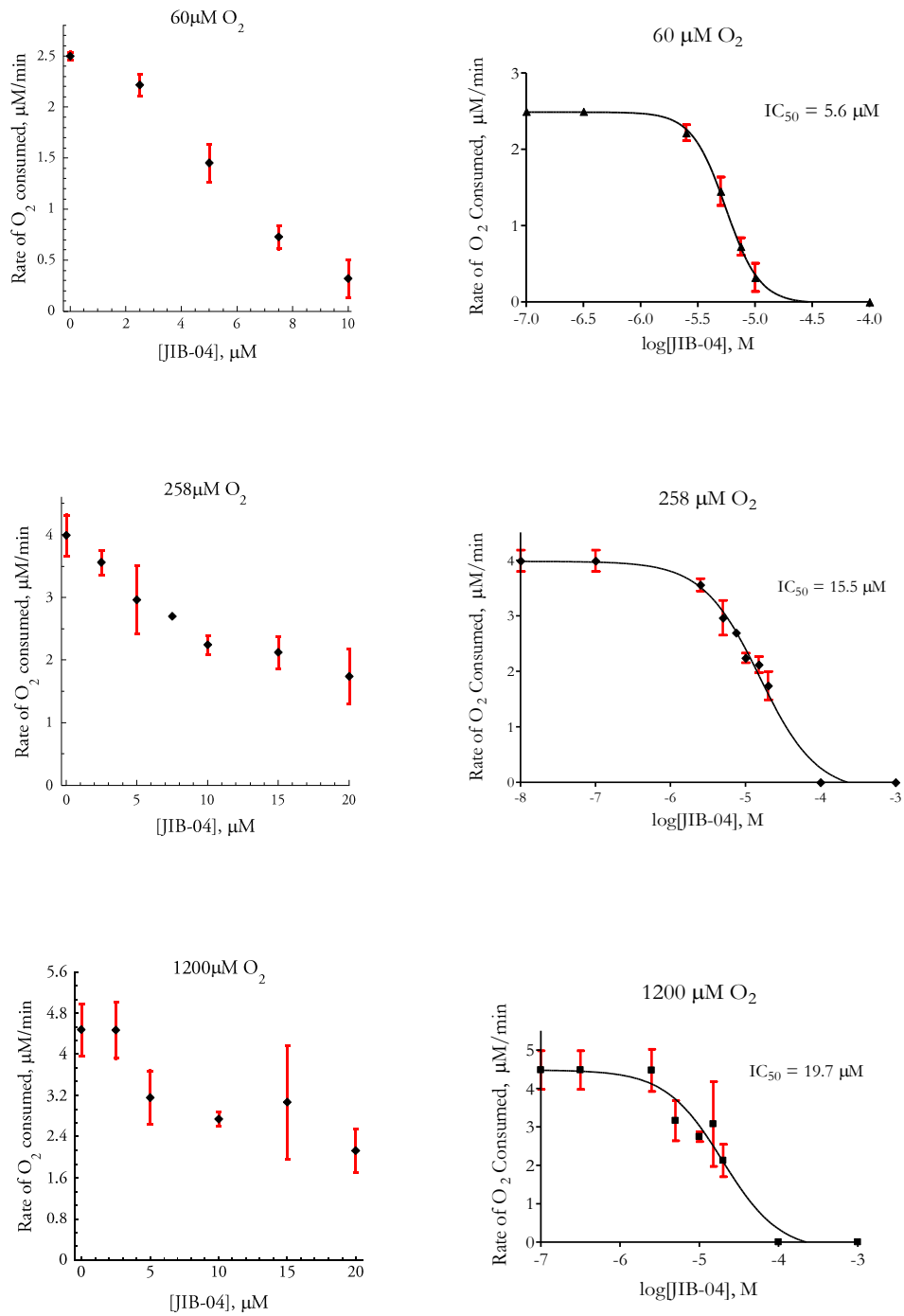


Figure 5.4. Inhibition of KDM4A by JIB-04 as tested at three concentrations of O₂.

Interestingly, with decreasing O₂ concentration we find decreasing IC₅₀ values, and thus increasing potency of JIB-04 inhibition (60 μM O₂: logIC₅₀ = -5.256 ± 0.009; 258 μM O₂: logIC₅₀ = -4.81 ± 0.06; 1200 μM O₂: logIC₅₀ = -4.7 ± 0.1). We find a nearly 3-fold increase in inhibition when going from 258 to 60 μM O₂. Unfortunately, experimental limitations prohibit the testing of the inhibition at truly low concentrations of O₂, as KDM4A exhibits little enzymatic activity at concentrations less than 60 μM. The discrepancy between the IC₅₀'s found in air-saturated water (258 μM O₂) for the MALDI-TOF assay (Figure 5.3, IC₅₀ ≈ 20 μM) and the O₂ consumption assay (IC₅₀ of 15.5 μM) is likely due to varying experimental conditions, with the O₂ consumption assay giving a more accurate representation of enzymatic activity and inhibition. The IC₅₀ values at 258 μM and 1200 μM are similar within experimental error, as would be expected since both of these O₂ concentrations are significantly higher than the K_m(O₂) for KDM4A. While a true measure of the inhibitor's competition with O₂ could be found by obtaining O₂ K_m plots at varying concentrations of JIB-04, the varying IC₅₀ values obtained at the three O₂ concentrations provide evidence that JIB-04 potentially disrupts O₂ binding in the KDM4A active site.

Molecular modeling studies of the JIB-04 E- and Z-isomers provide further support as to the mode of inhibition of KDM4A (Figure 5.5). Importantly, both JIB-04 isomers were docked into the KDM4A active site without ligand-guided assistance. Ligand-guided docking uses the electron density of and chemical complementarity to known bound ligands to aid in the virtual screening of molecular poses.¹² Thus, the shape of the histone peptide substrate was not used to guide the modeling of either JIB-04 isomer. As seen in Figure 5.5, the aromatic moieties of only the E-isomer orient themselves in such a way as to mimic the projection of the natural H3K9me₃ substrate into the KDM4A active site. Therefore, the predicted energetically favorable fit for the JIB-04 E-isomer

is in place of the histone substrate, which helps to explain the isomer-specific inhibition of JmjC-HDMs by this compound.

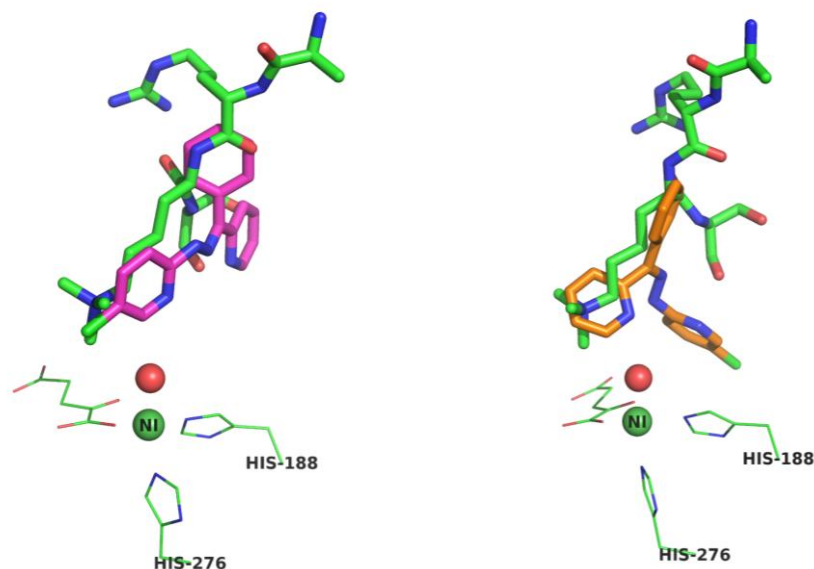


Figure 5.5. (*left*) JIB-04 E-isomer (pink sticks) competes with the histone peptide substrate (green sticks) in the KDM4A active site, with H₂O shown as red sphere (PDB 2Q8C); (*right*) JIB-04 Z-isomer is a weak inhibitor of KDM4 enzymes, as it does not compete with the peptide substrate.

A closer look at the binding of the E-isomer is depicted in Figure 5.6. We find that the chlorine of this isomer points toward the metal center in a manner similar to the NMe₃⁺ group, which would make it the most likely portion of the inhibitor to affect O₂ binding. The Ni(II) – Cl distance (4.8 Å) as modeled is substantially longer than that found in the obtained crystal structure (vide infra). Both pyridine nitrogens and the hydrazone group are predicted to form hydrogen bonds with Lys 241 at 3.1 Å and 2.7 Å, respectively, while the hydrazone group could form an additional hydrogen bond with Asp 191, at 2.9 Å. We find no evidence of π - π stacking interactions to stabilize JIB-04 binding, as the nearest aromatic residue, Tyr 175, is slightly displaced and over 5 Å away.

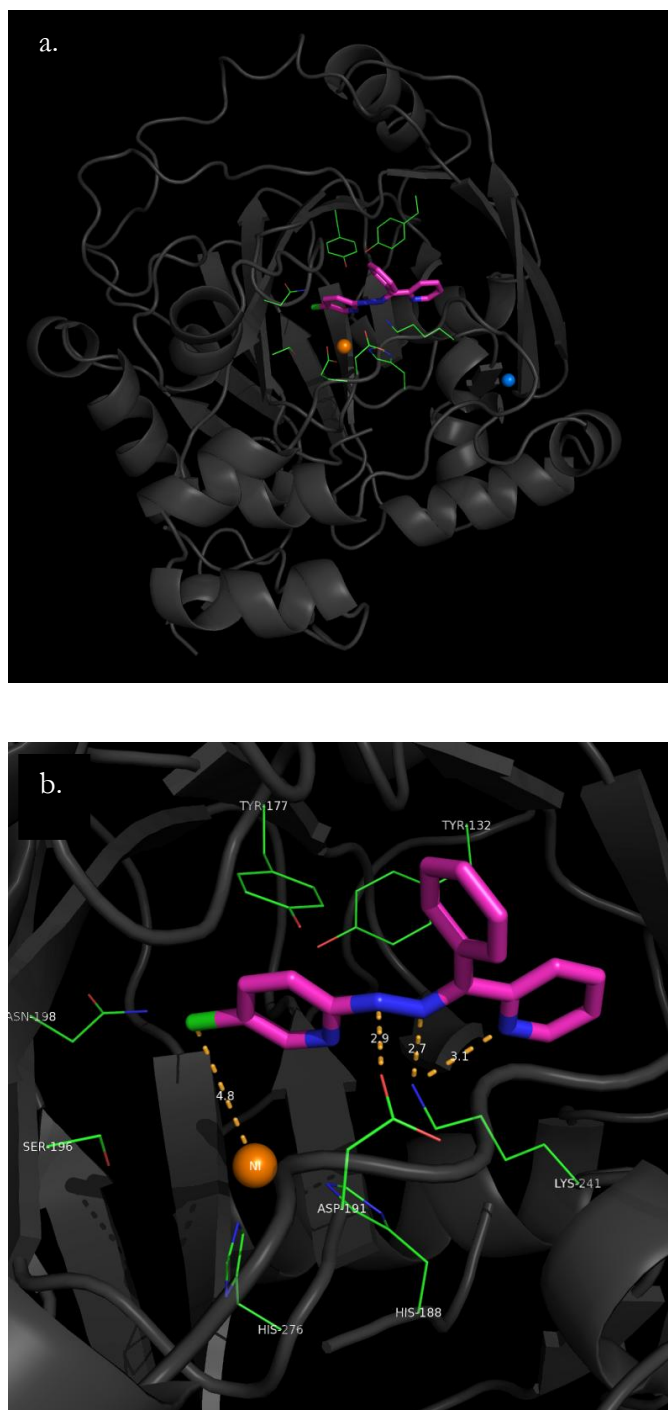


Figure 5.6. (a) View of JIB-04 E-isomer as modeled in the KDM4A active site. KDM4A shown as transparent ribbons and green sticks; JIB-04 shown as pink sticks, with the chlorine colored green. Ni(II) (orange sphere) replaces Fe(II) in the active site, and structural Zn(II) is shown as a blue sphere. (b) Close-up view of JIB-04 modeled in the KDM4A active site, showing predicted polar contacts with Asp 191 and Lys 241.

Crystallization of JIB-04 with KDM4A was attempted, and a crystal structure of a JIB-04 fragment in complex with the catalytic core of KDM4A (residues 1-349) was obtained to 3.1 Å resolution (Figure 5.7 and Table C.1 in Appendix C). No α KG or α KG analog was added to the crystallization solution to ensure that there was no bias in JIB-04 binding, and therefore the complex is binary. Refinement of the obtained structure made clear that JIB-04 was not present in its whole form. Rather, the ligand electron density is a bit ambiguous, and could be accounted for by only a portion of the inhibitor, predicted to be 2-amino-5-chloropyridine, as shown in Figure 5.7.

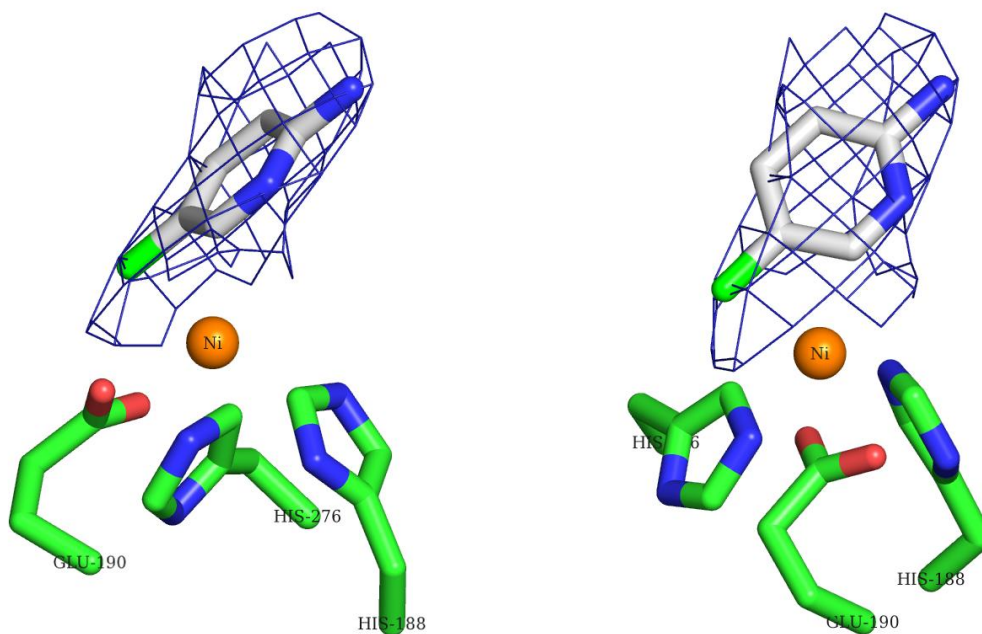


Figure 5.7. The experimental $2F_o - F_c$ electron density, displayed as blue mesh, is shown for the ligand fragment in two alternate views.

As only a fragment of JIB-04 was determined to be in complex with KDM4A in the crystal structure, JIB-04's susceptibility to hydrolysis or decomposition was tested in two ways. Briefly, JIB-04 was tested for stability in citrate pH 6.0 and HEPES pH 7.5 buffers up to two weeks at 4 °C,

with no evidence of decomposition via analysis by ESI-MS. Next, JIB-04 was tested for stability in the presence of KDM4A/Fe(II) and citrate pH 6.0 or HEPES pH 7.5 buffers at 4 °C for up to five days, with no evidence of decomposition. As the stability of JIB-04 was not tested in the presence of KDM4A/Ni(II), it is possible that the nickel-containing HDM catalyzed the hydrolysis of JIB-04 and cleavage of the hydrazone N-N bond during the crystallization.

While a higher resolution structure would help to confirm 2-amino-5-chloropyridine as the portion of JIB-04 that can be accounted for in the crystal structure, we can go forward and compare the crystallography results with those of the docking study. We find that the inhibitor fragment chelates to the metal center through its chlorine, as shown in Figure 5.8. Notably, the Cl – Ni(II) distance found in the crystal structure (2.4 Å) is substantially smaller than that predicted from the docking study (4.8 Å). Moreover, the orientation of the JIB-04 fragment is quite different in the crystal structure when compared to the docking results. Instead of the pyridine nitrogen and 2-amino group forming predicted polar contacts with Asp 191 and Lys 241, we find a single, weak hydrogen bond (3.5 Å) between the 2-amino group and Tyr 132, plus a potential weak aromatic interaction with Phe 185 (4.4 Å).

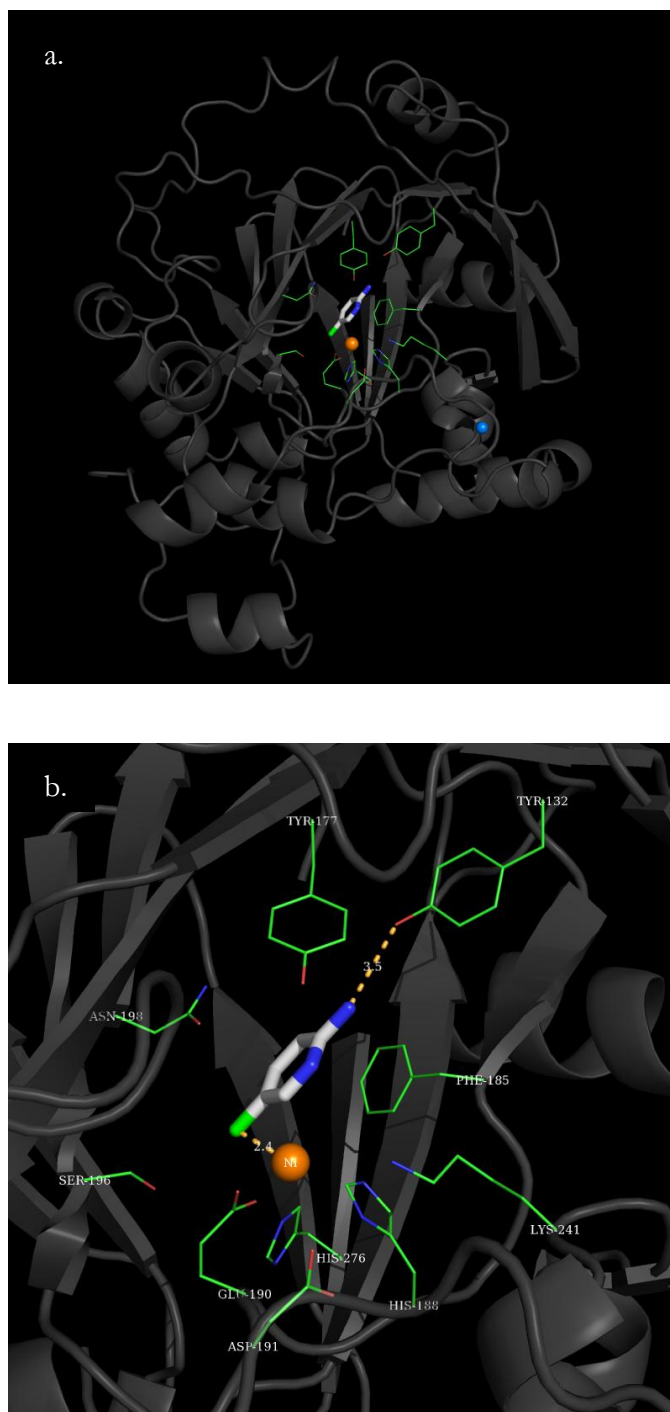


Figure 5.8. (a) View of the KDM4A:JIB-04 fragment crystal structure. KDM4A shown as transparent ribbons and green sticks; the JIB-04 fragment shown as gray sticks, with the chlorine colored green. Ni(II) (orange sphere) replaces Fe(II) in the active site, and structural Zn(II) is shown as a blue sphere. (b) Close-up view of the JIB-04 fragment in the KDM4A active site, showing hydrogen bonding to Tyr 132 and chelation to Ni(II).

It is difficult to know if the information obtained from the structural experiment is in agreement with what happens with the inhibitor in situ. However, if JIB-04 does indeed hydrolyze in the presence of KDM4A, as seen in the crystal structure, the short Ni(II) – Cl distance could lead to altered O₂ binding in the active site, as suggested by our O₂ competition study (Figure 5.4). The orientation of the JIB-04 fragment in the crystal structure does not appear to be competitive with the histone H3 substrate, in disagreement with what the published study concluded and our docking studies predicted. It is important to note that the protein crystals were formed in the absence of the cosubstrate α KG or the amide analog *N*-oxalylglycine (NOG), while the molecular modeling study was done with a KDM4A/Ni(II)/ α KG/H3K9me₃ complex. Obtaining another crystal structure in the presence of α KG or NOG could help resolve some of the discrepancies encountered in the present study.

5.4 Conclusions

In conclusion, we have examined the inhibition of KDM4A by the small molecule JIB-04 with respect to the cosubstrate O₂. We find that the inhibition by JIB-04 increases with decreasing O₂ concentration. Varying IC₅₀ values at different O₂ concentrations suggest that JIB-04 may inhibit KDM4A in part by disrupting the binding of O₂. The E- and Z- isomers of JIB-04 were modeled into the KDM4A active site, revealing that the aromatic moieties of the E- isomer are predicted to orient themselves in a way that mimics the natural projection of the histone H3 substrate into the enzyme active site. Lastly, a 3.1 Å crystal structure of the catalytic core of KDM4A in complex with JIB-04 was solved, and the ligand electron density is accounted for by only a portion of the inhibitor. Future studies might focus on obtaining higher resolution crystal structures of KDM4A in complex with JIB-04, both with and without α KG or the amide analog NOG.

5.5 References

1. Wang, L., Chang, J., Varghese, D., Dellinger, M., Kumar, S., Best, A. M., Ruiz, J., Bruick, R., Peña-Llopis, S., Xu, J., A Small Molecule Modulates Jumonji Histone Demethylase Activity and Selectively Inhibits Cancer Growth. *Nature communications* **4**, (2013).
2. Kim, S.-H., Kwon, S. H., Park, S.-H., Lee, J. K., Bang, H.-S., Nam, S.-J., Kwon, H. C., Shin, J., Oh, D.-C., Tripartin, a Histone Demethylase Inhibitor from a Bacterium Associated with a Dung Beetle Larva. *Organic Letters* **15**, 1834-1837 (2013).
3. Minor, W., Cymborowski, M., Otwinowski, Z., Chruszcz, M., Hkl-3000: The Integration of Data Reduction and Structure Solution-from Diffraction Images to an Initial Model in Minutes. *Acta Crystallographica Section D: Biological Crystallography* **62**, 859-866 (2006).
4. McCoy, A. J., Grosse-Kunstleve, R. W., Adams, P. D., Winn, M. D., Storoni, L. C., Read, R. J., Phaser Crystallographic Software. *Journal of Applied Crystallography* **40**, 658-674 (2007).
5. Emsley, P., Cowtan, K., Coot: Model-Building Tools for Molecular Graphics. *Acta Crystallographica Section D: Biological Crystallography* **60**, 2126-2132 (2004).
6. Adams, P. D., Afonine, P. V., Bunkóczi, G., Chen, V. B., Davis, I. W., Echols, N., Headd, J. J., Hung, L.-W., Kapral, G. J., Grosse-Kunstleve, R. W., Phenix: A Comprehensive Python-Based System for Macromolecular Structure Solution. *Acta Crystallographica Section D: Biological Crystallography* **66**, 213-221 (2010).
7. Brunger, A. T., Adams, P. D., Clore, G. M., DeLano, W. L., Gros, P., Grosse-Kunstleve, R. W., Jiang, J. S., Kuszewski, J., Nilges, M., Pannu, N. S., Read, R. J., Rice, L. M., Simonson, T., Warren, G. L., Crystallography & Nmr System: A New Software Suite for Macromolecular Structure Determination. *Acta Crystallographica* **D54**, 905-921. (1998).
8. Painter, J., Merritt, E. A., Optimal Description of a Protein Structure in Terms of Multiple Groups Undergoing Tls Motion. *Acta Crystallographica Section D: Biological Crystallography* **62**, 439-450 (2006).
9. Collaborative Computational Project, N., The Ccp4 Suite: Programs for Protein Crystallography. *Acta Crystallographica* **D50**, 760-763 (1994).

10. Vaguine, A. A., Richelle, J., Wodak, S. J., Sfccheck: A Unified Set of Procedures for Evaluating the Quality of Macromolecular Structure-Factor Data and Their Agreement with the Atomic Model. *Acta Crystallographica* **D55 (Pt 1)**, 191-205 (1999).
11. Laskowsky, R. A., W., M. M., Moss, D. S., Thornton, J. M., Procheck: A Program to Check Stereochemical Quality of Protein Structure Coordinates. *J Applied Crystallography* **26**, 283-291 (1993).
12. McGaughey, G. B., Sheridan, R. P., Bayly, C. I., Culberson, J. C., Kretsoulas, C., Lindsley, S., Maiorov, V., Truchon, J.-F., Cornell, W. D., Comparison of Topological, Shape, and Docking Methods in Virtual Screening. *Journal of Chemical Information and Modeling* **47**, 1504-1519 (2007).

Chapter 6: Conclusions and Future Directions

The JmjC domain-containing HDMs are α KG-dependent, O_2 -activating, non-heme iron enzymes. At the start of this dissertation work, little was known of the enzymology of the KDM4 subfamily of HDMs. This work focused on three members of the KDM4 subfamily: the mixed H3K9/H3K36 demethylases KDM4A and KDM4C and the pure H3K9 demethylase KDM4E. KDM4A and KDM4C were of particular interest, as these enzymes have been implicated in numerous cancers, while KDM4E was studied for its similarity to KDM4D, an enzyme responsible for the regulation of the tumor suppressor p53.¹⁻⁴ The major goals of this dissertation work were to develop an understanding of the *in vitro* kinetics and inhibition of our three JmjC-HDMs, as well as to develop a continuous, real-time enzymatic assay to monitor the activity of our HDMs.

Initially, we achieved a detailed kinetic analysis of our HDMs using three enzyme activity assays, including a novel continuous O_2 consumption assay. From our studies, we propose that members of the KDM4 subfamily may act as O_2 sensors *in vivo* due to their low apparent affinities for O_2 . Also from this initial study, we found that the co-substrate α KG inhibits KDM4C, with KDM4C displaying its optimal activity *in vitro* at α KG concentrations found in cancer cells. Future studies of the KDM4 subfamily should focus on the *in vivo* implications of the observed α KG substrate inhibition. As a complement to this study, crystallization of the catalytic core of KDM4C with a large excess of α KG should be attempted, to see if two molecules of α KG bind in the KDM4C active site.

Early in this work, a small library of simple molecules was synthesized in an effort to identify potential scaffolds for JmjC-HDM inhibition. The molecules were designed to mimic the primary or secondary substrates, by the inclusion of dimethylamino or trimethylammonium groups or amide or oxalyl groups, respectively. Furthermore, the molecules included carbon-carbon triple bonds or the corresponding 1,2,3-triazole group, as we proposed that the triazole-containing compounds would be more potent inhibitors, due to the KDM4 low apparent affinities for O₂. From this study, we learned that the inhibition of JmjC-HDMs is a difficult task, as recognition of the primary substrate is due to multiple histone H3 main-chain contacts with the enzyme. Also from this study, we found no evidence of KDM4-driven triazole formation using any of our alkyne-containing small molecules. Future studies can focus on the modification of our most promising analogs, the trimethylammonium- and ester- containing **5** and **6** (Figure 6.1), toward the development of specific inhibitors of JmjC-HDMs. These compounds should be screened against other α KG-dependent oxygenases, such as to confirm their specificity. An additional study could test whether the triazole-containing **6** is competitive with O₂, using our developed O₂ consumption assay.

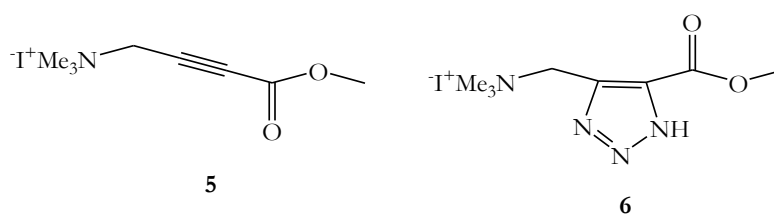


Figure 6.1. Two inhibitors of KDM4E, as described in Chapter 3.

A peptidomimetic approach was taken in a second study of JmjC-HDM inhibition. Two histone H3₍₇₋₁₁₎ peptides were synthesized, with modified Lys residues. We find

ARK(N^{ϵ} -bis(propargyl))ST to be selective for KDM4C over KDM4A, as predicted. Stronger, but less selective, inhibition came with the positively charged ARK⁺(N^{ϵ} -methyl bis(propargyl))ST. Our three JmjC-HDMs showed no hydroxylase activity toward either peptide. One possible direction in the modification of ARK⁺(N^{ϵ} -methyl bis(propargyl))ST to make it a stronger KDM4C inhibitor might be in the shortening of the Lys side chain by one or two methylene groups, to account for the length of the propargyl groups. Future studies should test ARK⁺(N^{ϵ} -methyl bis(propargyl))ST and all modified peptides for specificity against other JmjC-HDMs, such as PHF8.

Testing of the KDM4 subfamily members with a multitude of alkyne-containing substrates in enzyme-templated Huisgen 1,3-dipolar cycloaddition reactions has given no evidence of enzyme-driven 1,2,3-triazole formation. From these studies, we conclude that JmjC-HDMs are not suitable “vessels” for in situ cycloaddition reactions, likely due to the low affinity of azide for the HDM metal center.

Our final study of KDM4 inhibition was with the pan-selective JmjC-HDM inhibitor JIB-04. We found that the inhibition of KDM4A by JIB-04 increased with decreasing O₂ concentration, suggesting that JIB-04 may work in part by altering the binding of O₂ to the Fe(II) metal center. A published study found the JIB-04 E-isomer to be competitive with the H3K9 substrate, and our docking studies agreed. A 3.1 Å crystal structure of KDM4A in complex with Ni(II) and JIB-04 revealed only a portion of the inhibitor, predicted to be 2-amino-5-chloropyridine, to be bound in the enzyme active site. This surprising result should be confirmed by additional crystallography studies. Future studies should focus on obtaining a higher resolution structure of JIB-04 in complex with KDM4A, both with and without α KG or NOG.

References

1. Berry, W. L., Janknecht, R., Kdm4/Jmjd2 Histone Demethylases: Epigenetic Regulators in Cancer Cells. *Cancer Research* **73**, 2936-2942 (2013).
2. Cloos, P. A. C., Christensen, J., Agger, K., Maiolica, A., Rappsilber, J., Antal, T., Hansen, K. H., Helin, K., The Putative Oncogene Gasc1 Demethylates Tri- and Dimethylated Lysine 9 on Histone H3. *Nature* **442**, 307-311 (2006).
3. Kim, T.-D., Oh, S., Shin, S., Janknecht, R., Regulation of Tumor Suppressor P53 and Hct116 Cell Physiology by Histone Demethylase Jmjd2d/Kdm4d. *PLoS One* **7**, e34618 (2012).
4. Berry, W. L., Shin, S., Lightfoot, S. A., Janknecht, R., Oncogenic Features of the Jmjd2a Histone Demethylase in Breast Cancer. *International Journal of Oncology* **41**, 1701-1706 (2012).

Appendix A: Supplementary Information for
Chapter 2

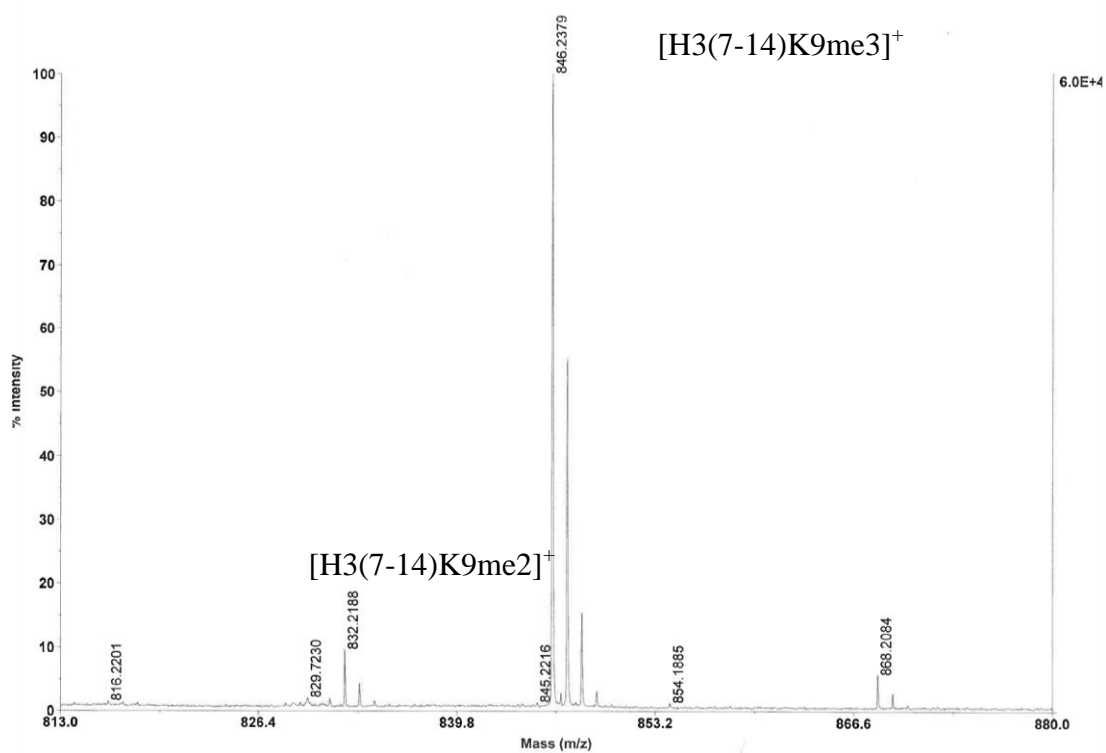
Table A.1. Data collection and refinement statistics for KDM4A/Ni²⁺/αKG.^a

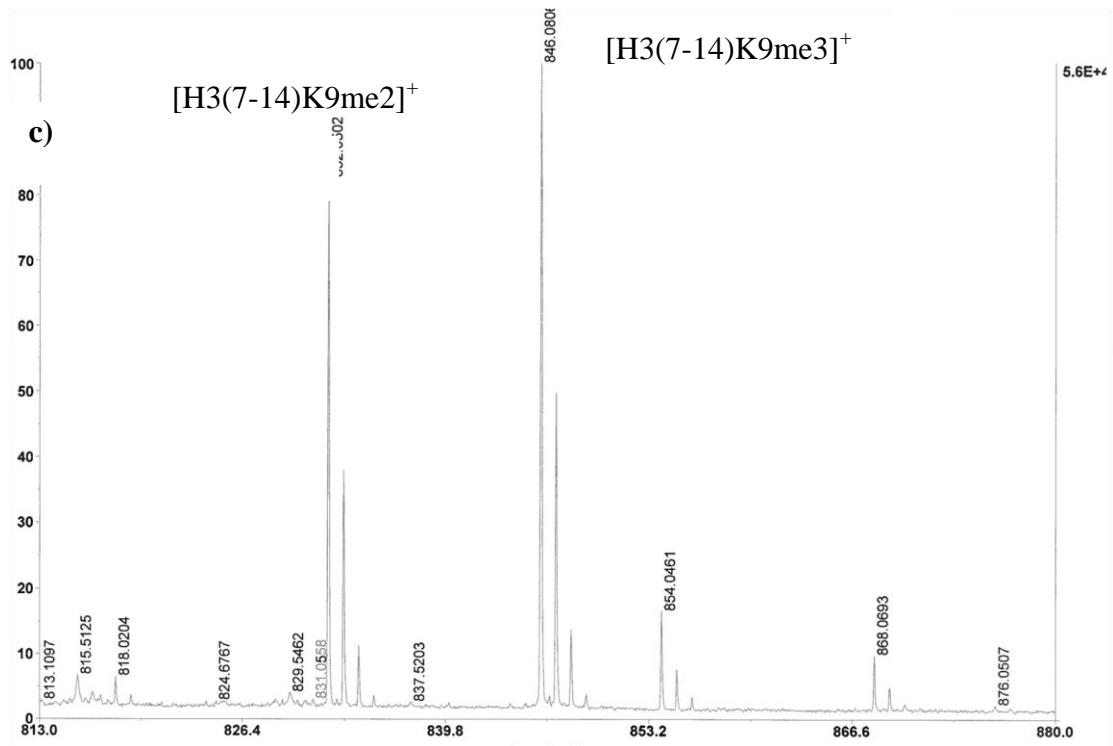
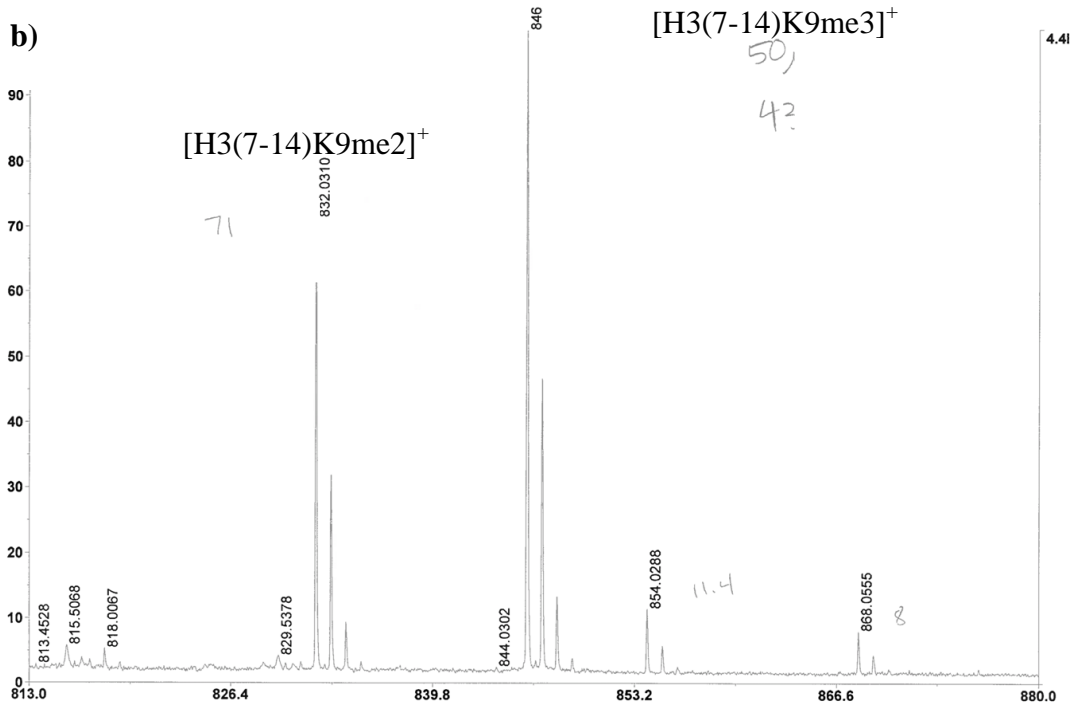
Resolution range (Å...)	35.15 - 2.093 (2.168 - 2.093)
Space group	P 2 21 21
Unit cell	57.143 101.122 149.028 90 90 90
Unique reflections	50379 (4412)
Completeness (%)	97.34 (86.85)
Mean I/sigma(I)	15.20 (4.11)
Wilson B-factor	23.48
R-work	0.1812 (0.2122)
R-free	0.2236 (0.2598)
Number of non-hydrogen atoms	6125
macromolecules	5735
ligands	24
water	366
Protein residues	699
RMS(bonds)	0.005
RMS(angles)	0.93
Ramachandran favored (%)	98
Ramachandran outliers (%)	0
Clashscore	6.07
Average B-factor	35.00
Macromolecules	34.70
Ligands	31.50
Solvent	39.20

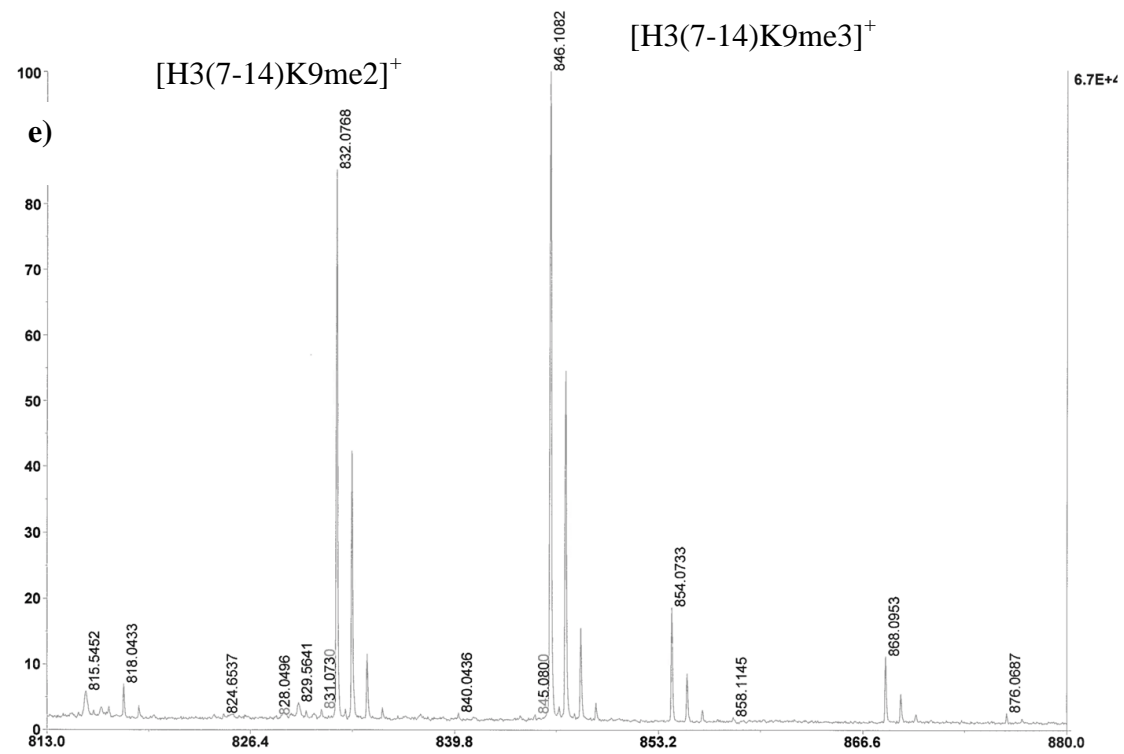
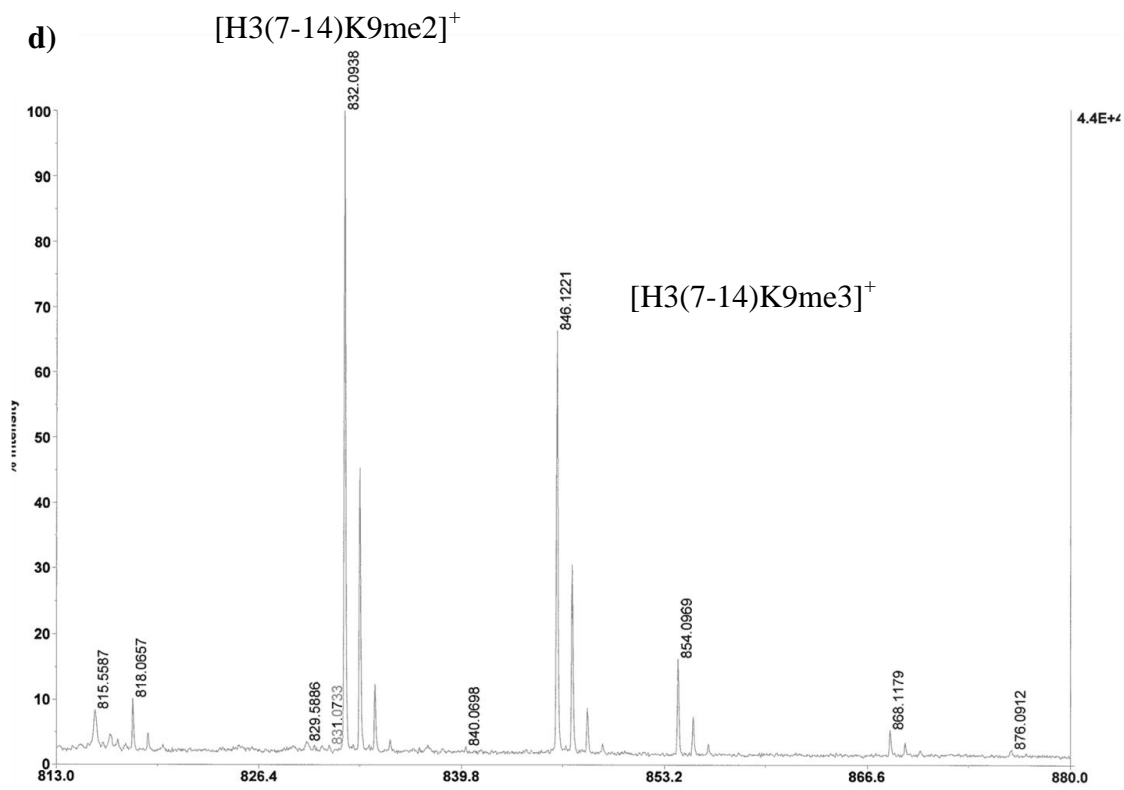
^a Statistics for the highest-resolution shell are shown in parentheses.

A.1. MALDI-TOF MS Assay

a)







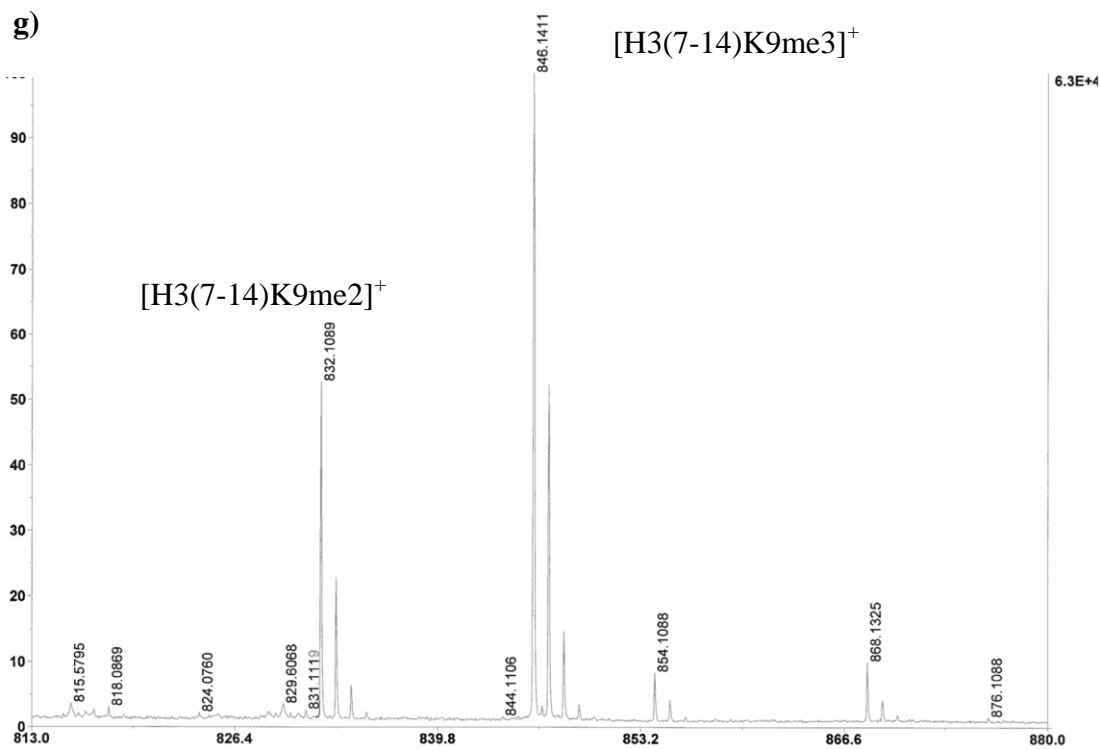
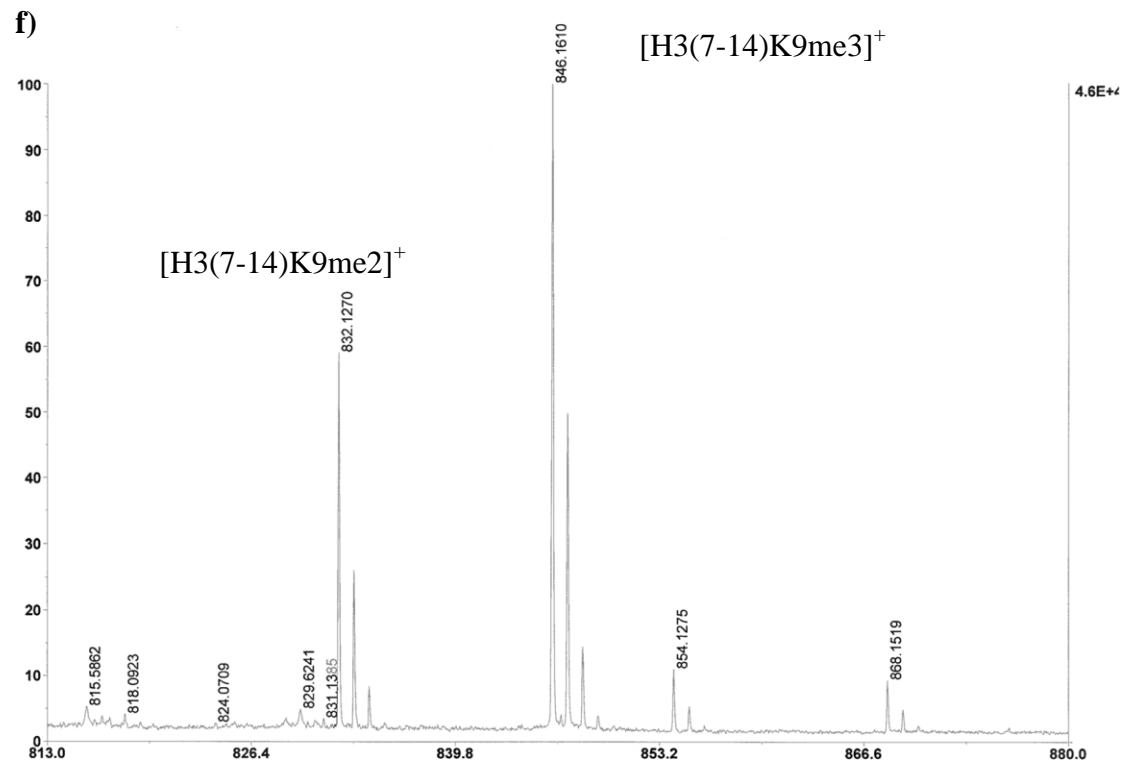
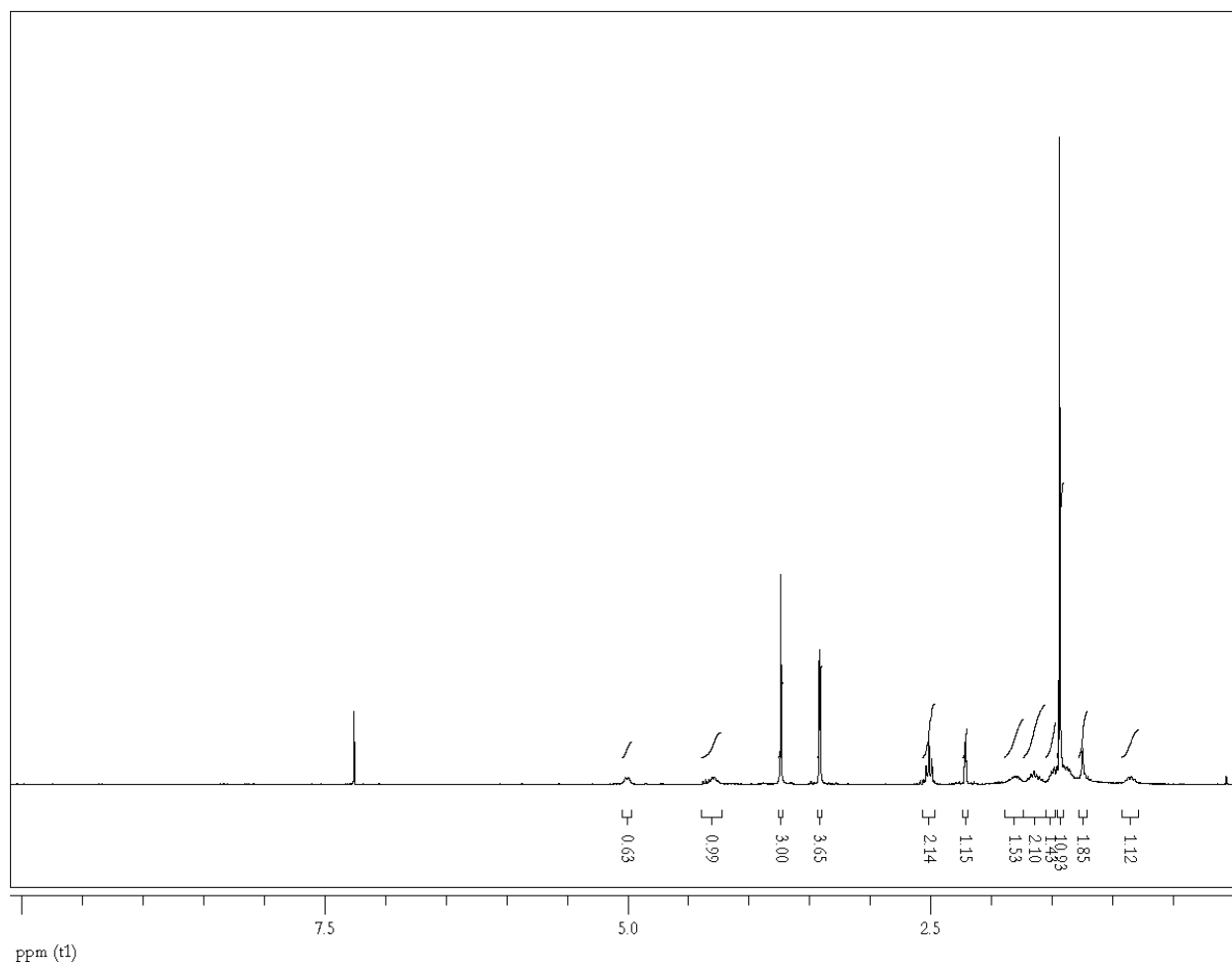


Figure A.1. KDM4C demethylase activity and substrate inhibition by α KG, as monitored by MALDI-TOF MS: **a)** ~0 minute reaction time, **b)** 10 minute reaction time with 50 μ M α KG, **c)** 10

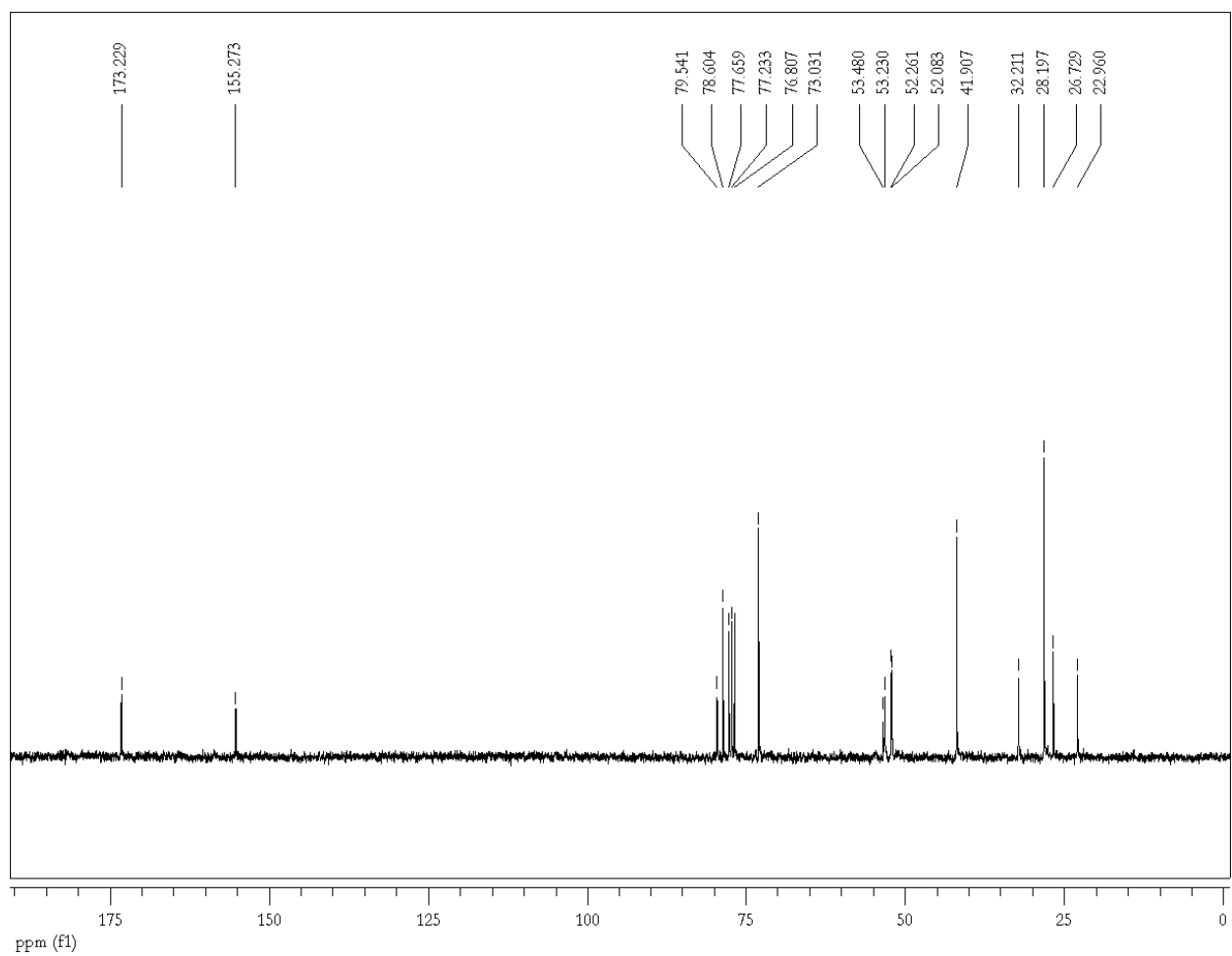
minute reaction time with 100 μM αKG , **d)** 10 minute reaction time with 300 μM αKG , **e)** 10 minute reaction time with 1 mM αKG , **f)** 10 minute reaction time with 3 mM αKG , **g)** 10 minute reaction time with 5 mM αKG .

Appendix B: Supplementary Information for Chapter 4

¹H-NMR of Boc-Lys(*N*^ε- bis(propargyl))-OMe in CDCl₃:



^{13}C -NMR of Boc-Lys(N^{ϵ} - bis(propargyl)-OMe in CDCl_3 :



ESI-MS of ARK(N^{\ominus} - bis(propargyl))ST: $[M+H]^+ = 638.3$; $[M-H+2Na]^+ = 682.3$

121313_131213105709

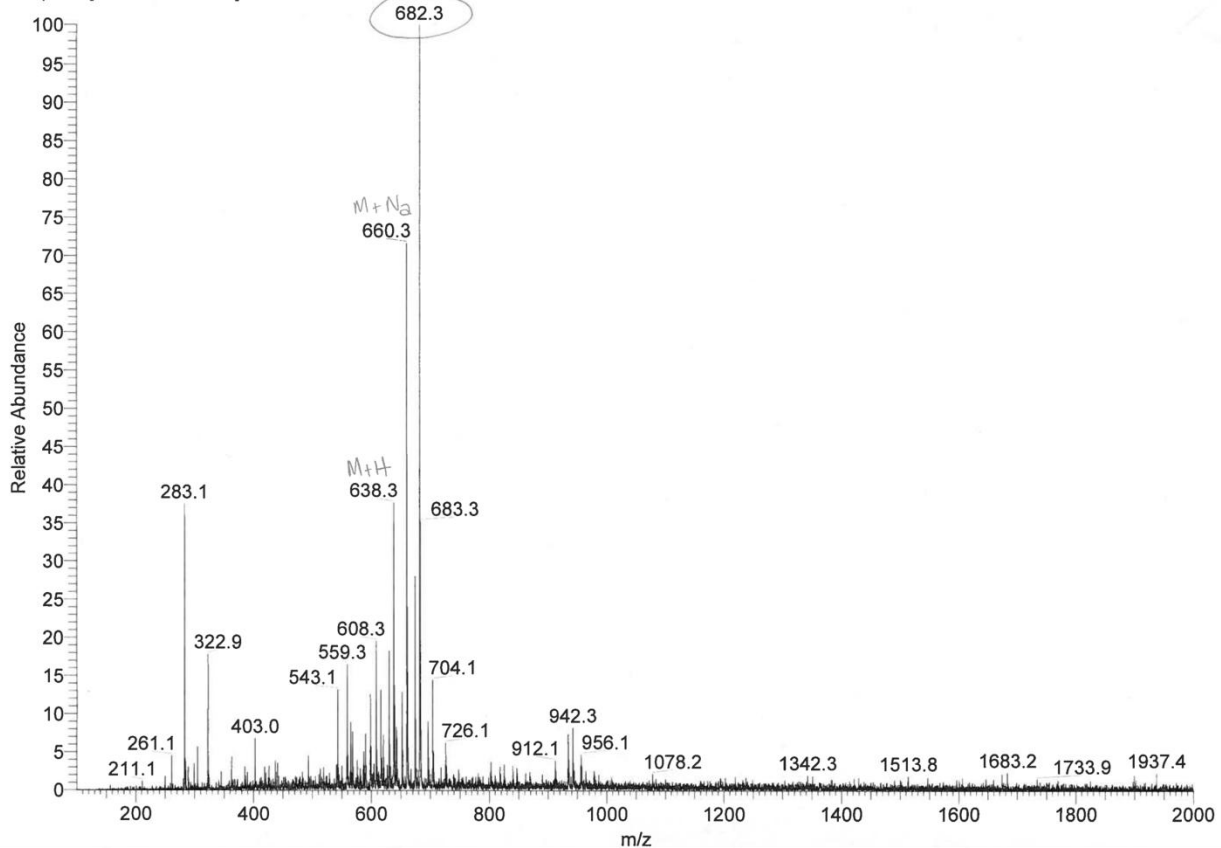
12/13/2013 10:57:09 AM

ARK(bis-propargyl)ST

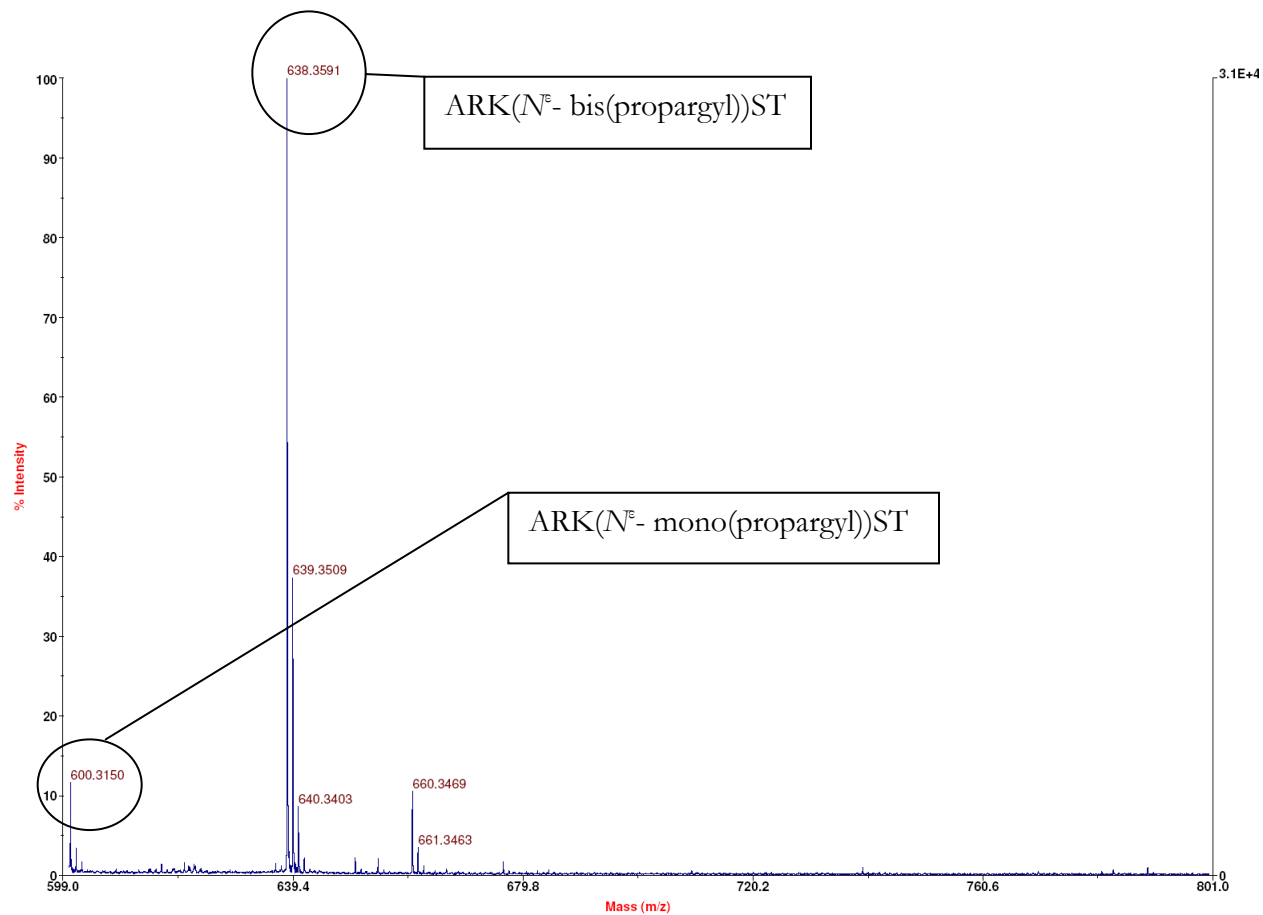
1:1 MeOH:H₂O

121313_131213105709 #202-273 RT: 4.50-5.97 AV: 72 NL: 1.34E6

T: + p ms [100.00-2000.00]

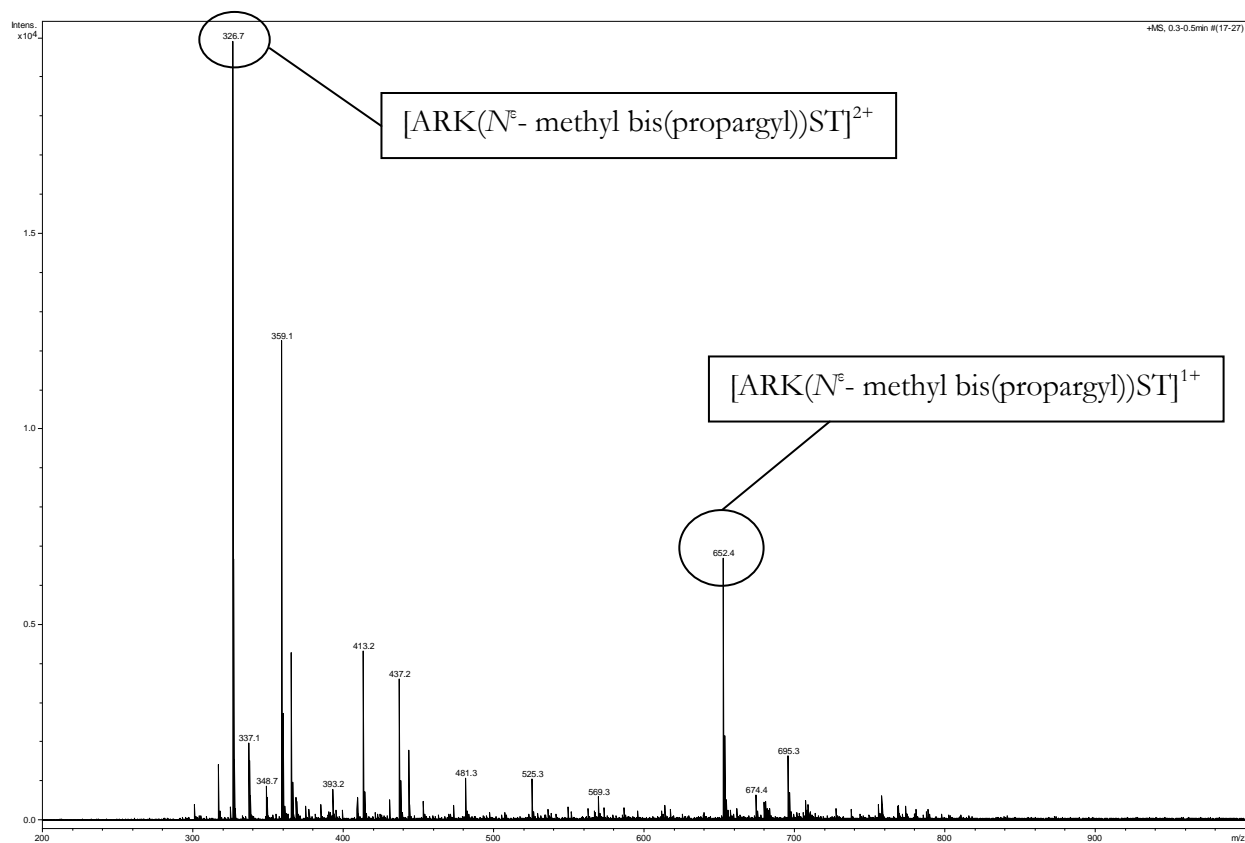


MALDI-TOF MS of ARK(N^{ϵ} - bis(propargyl))ST:



E:\...4hr RT ARKST Control ZiptipSCX_0003.dat
Acquired: 12:39:00, March 31, 2014

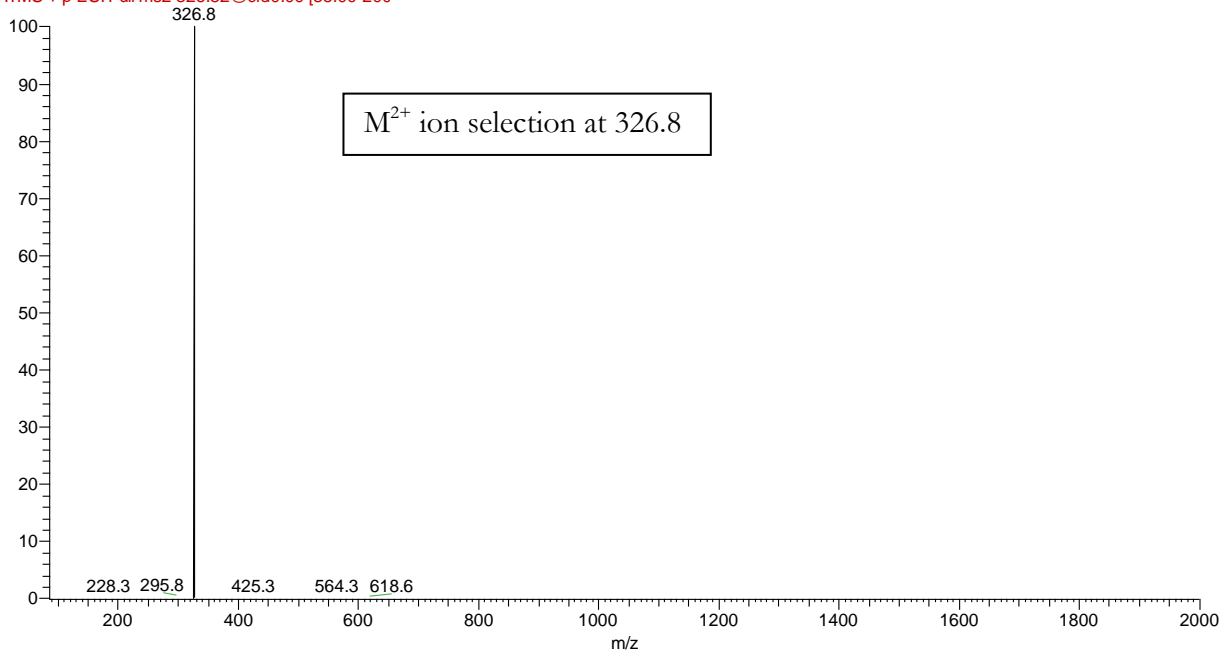
ESI-MS of methylated ARK⁺(N^E-methyl bis(propargyl))ST:



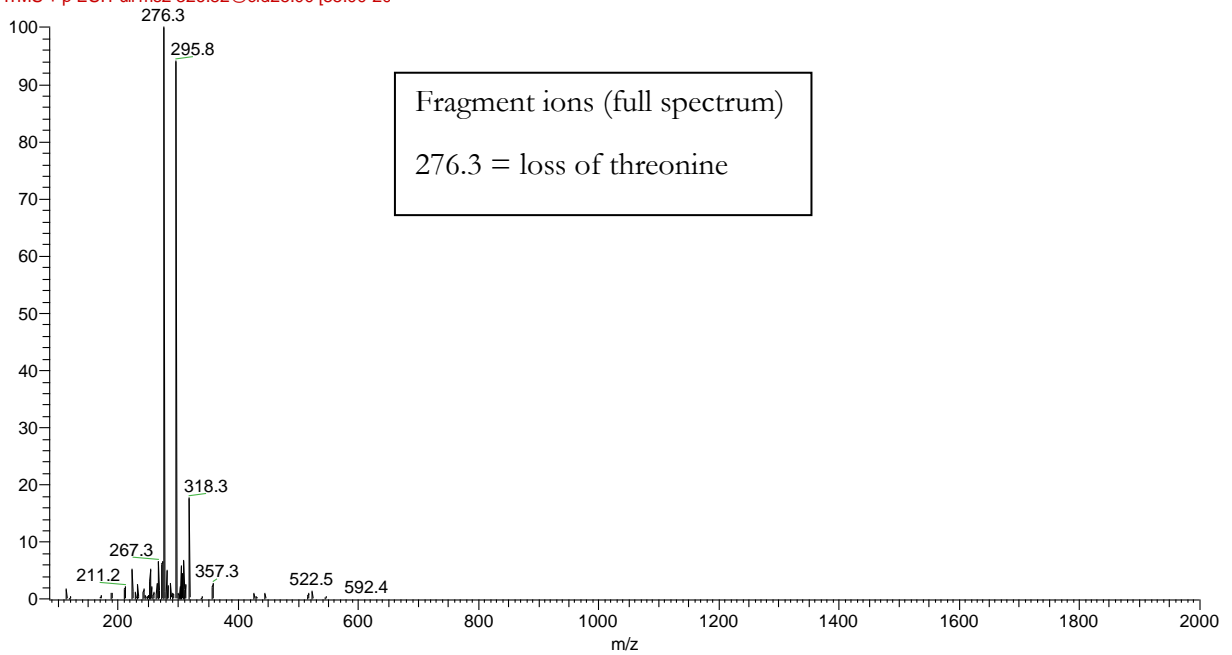
ESI-CID-MS/MS:

Note: absent from the spectrum is a peak at 260, which would correspond to AR(methylated)

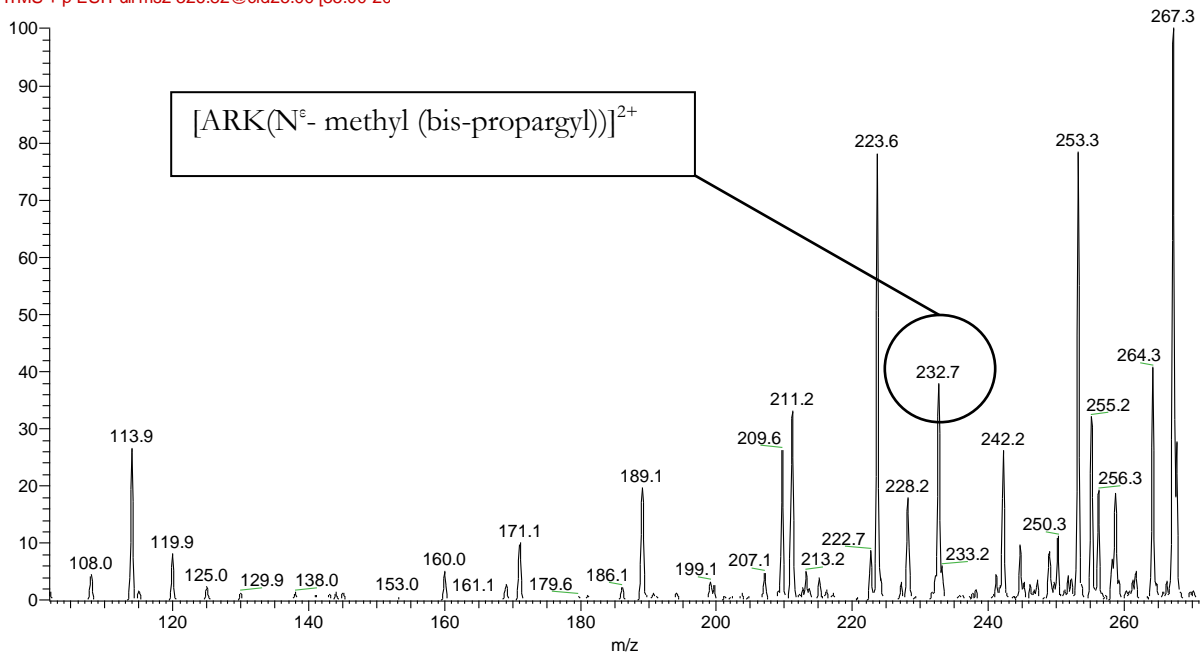
06262014-Barrie-peptide-MS2 #502-525 RT: 1.95-2.25 AV: 24 NL: 1.04E6
F: ITMS + p ESI Full ms2 326.82@cid0.00 [85.00-200]



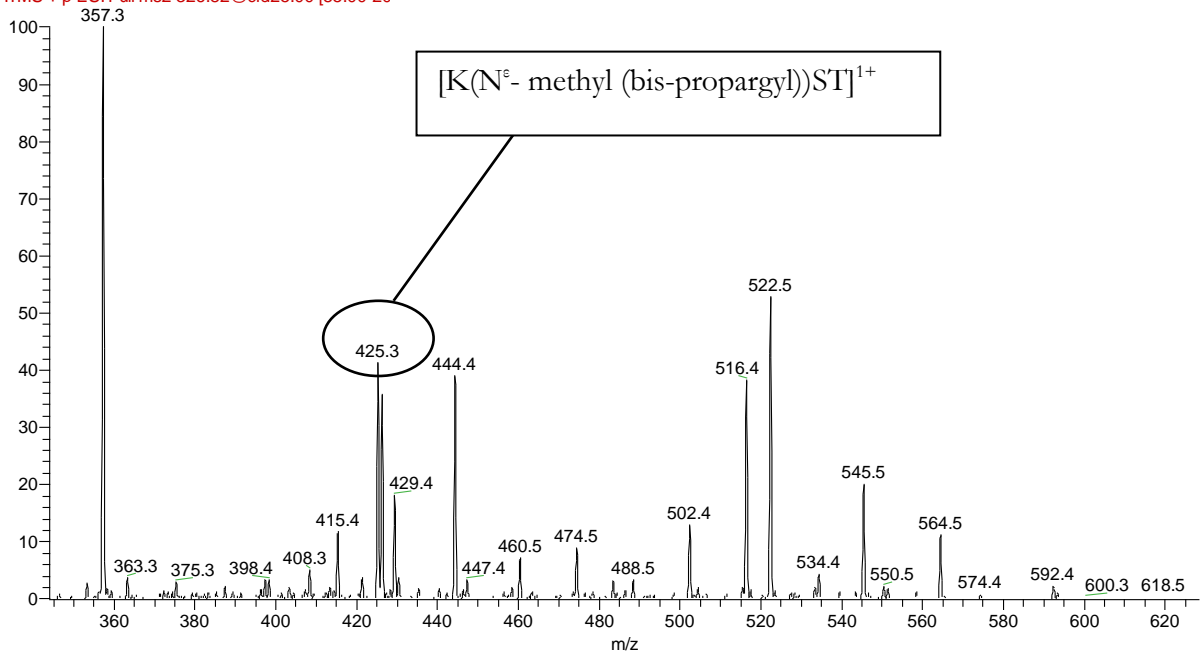
06262014-Barrie-peptide-MS2 #630-650 RT: 3.65-3.88 AV: 19 NL: 7.09E5
F: ITMS + p ESI Full ms2 326.82@cid25.00 [85.00-200]



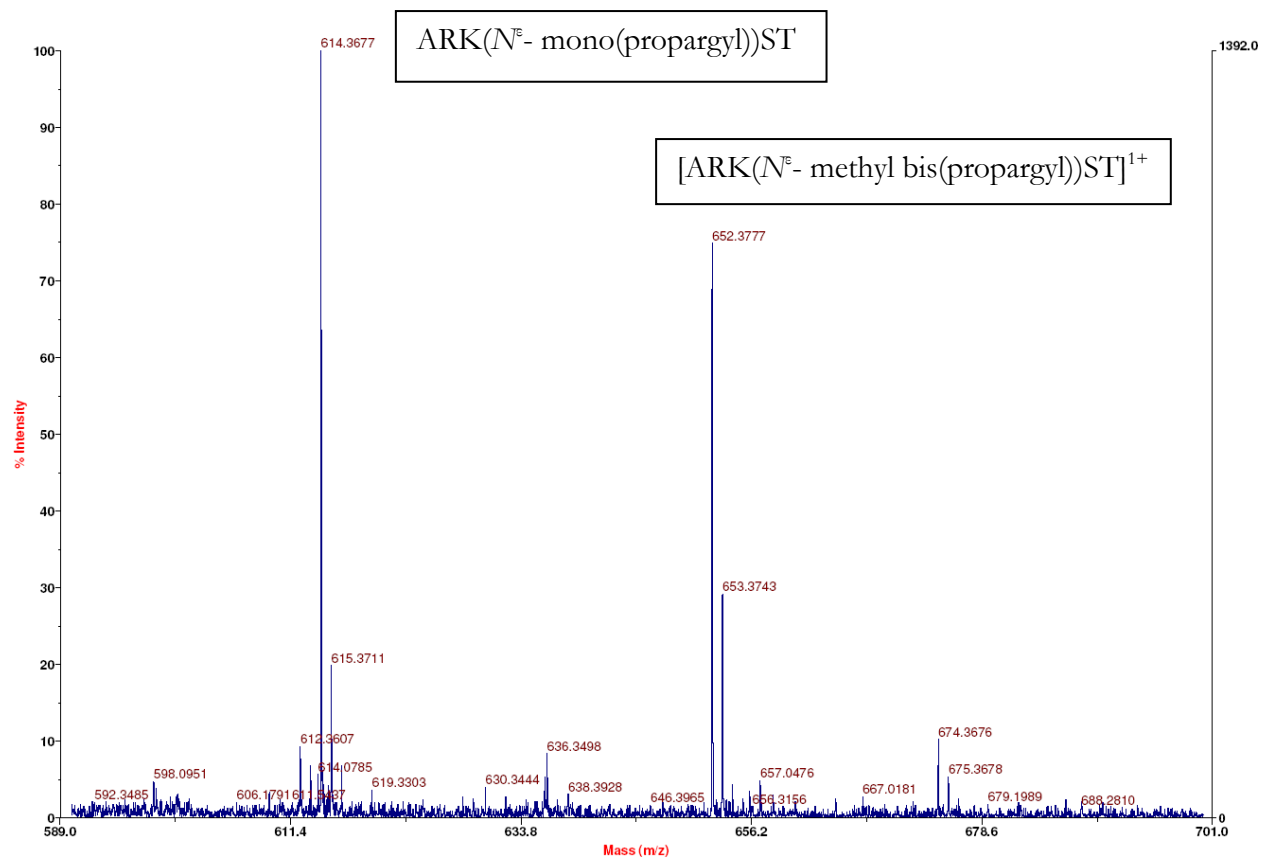
06262014-Barrie-peptide-MS2 #630-650 RT: 3.65-3.88 AV: 19 NL: 4.74E4
F: ITMS + p ESI Full ms2 326.82@cid25.00 [85.00-20



06262014-Barrie-peptide-MS2 #630-650 RT: 3.65-3.88 AV: 19 NL: 1.92E4
F: ITMS + p ESI Full ms2 326.82@cid25.00 [85.00-20



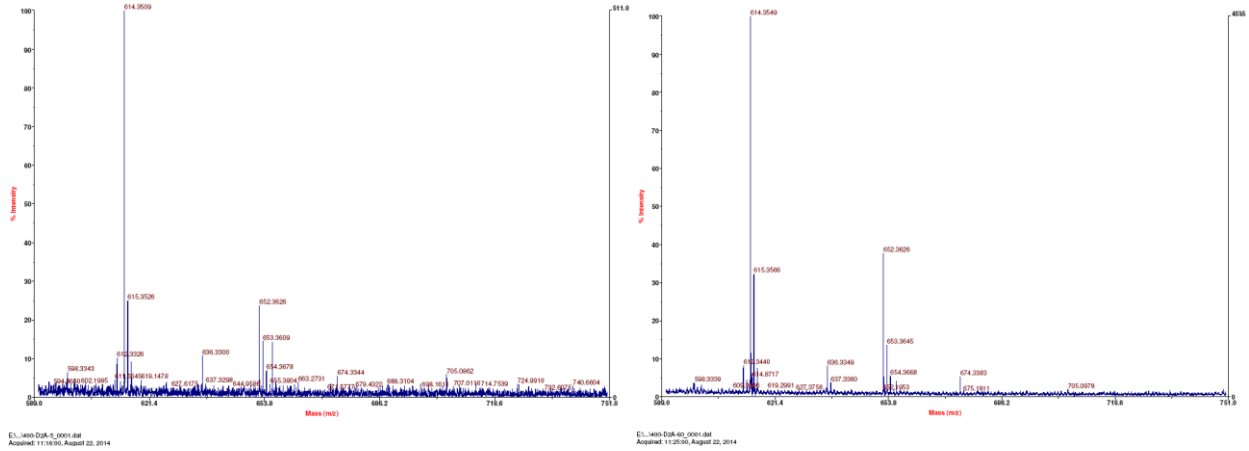
MALDI-TOF MS of ARK⁺(N^ε-methyl bis(propargyl))ST:



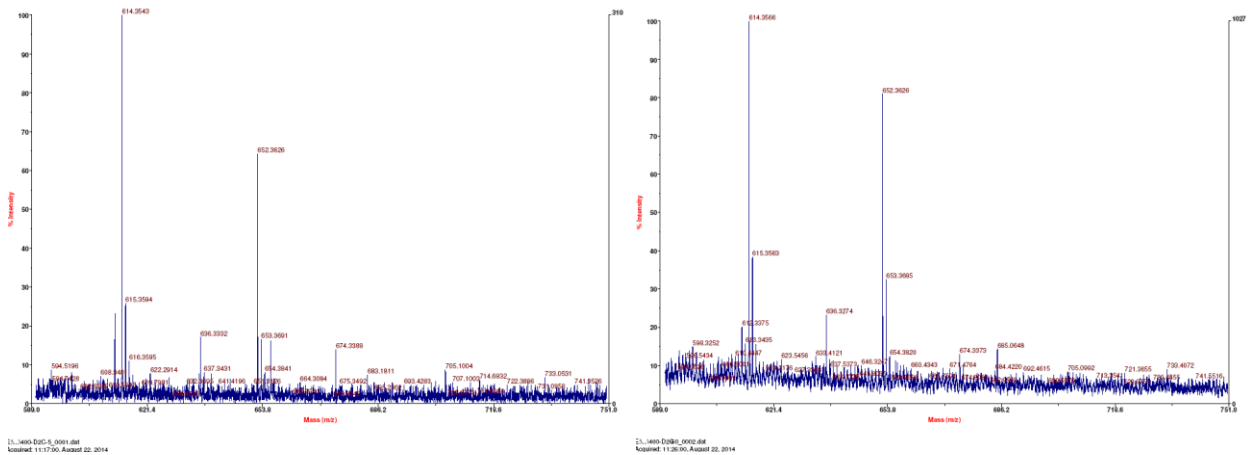
EA...ARKmethylbispropST 100uM_0008.dat

KDM4A, KDM4C, KDM4E Demethylation of ARKST experiment: we find no demethylation of the peptide by any enzyme up to 60 minutes

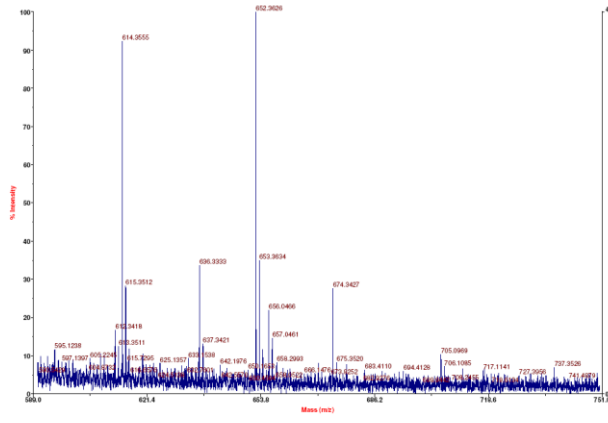
KDM4A at 5 minutes (left), at 60 minutes (right)



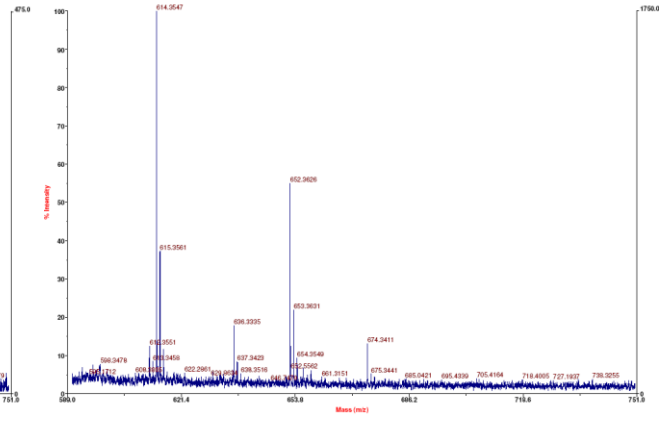
KDM4C at 5 minutes (left), at 60 minutes (right)



KDM4E at 5 minutes (left), at 60 minutes (right)



15_1460.D\\E-6_0062.D\\M
Acquired: 11/27/06, August 22, 2014



15_1460.D\\E-60_0062.D\\M
Acquired: 11/27/06, August 22, 2014

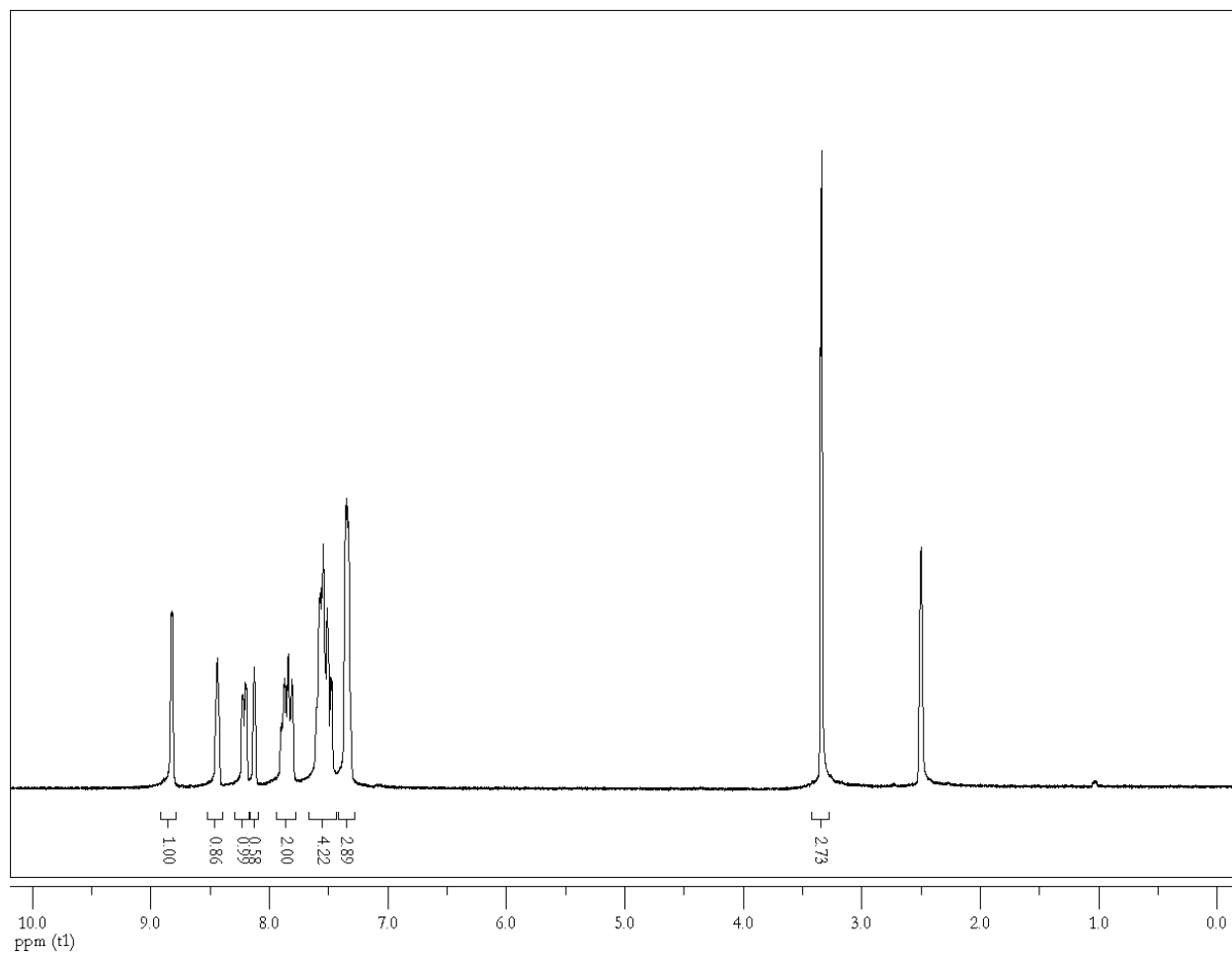
Appendix C: Supplementary Information for
Chapter 5

Table C.1. Data collection and refinement statistics for KDM4A/Ni²⁺/JIB-04.^a

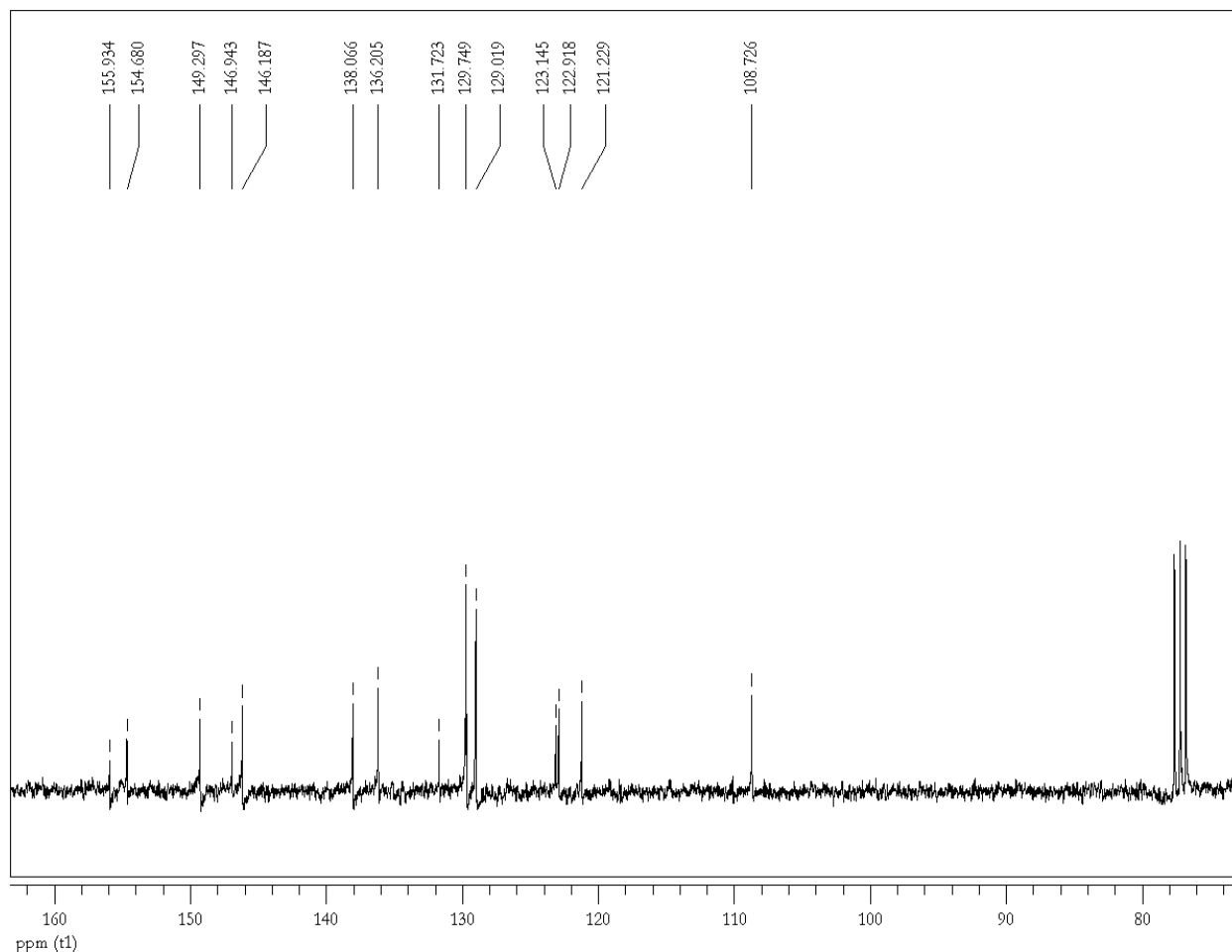
Resolution range (Å...)	35.31 - 3.207 (3.321 - 3.207)
Space group	P 2 21 21
Unit cell	57.611 101.219 149.417 90 90 90
Unique reflections	14068 (1164)
Completeness (%)	94.23 (79.73)
Mean I/sigma(I)	8.24 (2.88)
Wilson B-factor	70.80
R-work	0.2182 (0.2676)
R-free	0.2909 (0.3966)
Number of non-hydrogen atoms	5694
Macromolecules	5674
Ligands	20
Water	0
Protein residues	692
RMS(bonds)	0.007
RMS(angles)	1.26
Ramachandran favored (%)	93
Ramachandran outliers (%)	1.7
Clashscore	18.35
Average B-factor	72.80
Macromolecules	72.70
ligands	80.90

^a Statistics for the highest-resolution shell are shown in parentheses.

$^1\text{H-NMR}$ of JIB-04 in $(\text{CD}_3)_2\text{SO}$:



¹³C-NMR of JIB-04 in CDCl₃:



KDM4A inhibition by JIB-04 was tested without pre-incubation of the holoenzyme and inhibitor using the discontinuous MALDI-TOF MS assay. First, the inhibition was tested using an HDM : Fe^{II}(NH₄)₂SO₄·6H₂O of 1:5, and only mild inhibition of KDM4A up to 500 μM JIB-04 was found. As the excess iron in solution could be interacting with JIB-04, the inhibition was next tested using 1:1 KDM4A:Fe(II), with the results shown in Figure C.1. Again, we find only mild inhibition of KDM4A up to 500 μM JIB-04.

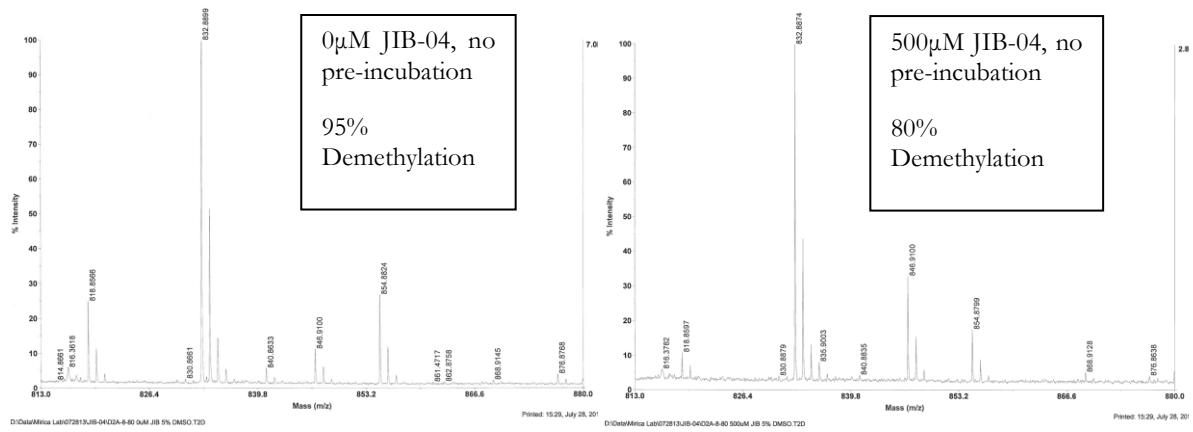


Figure C.1. Mild inhibition of KDM4A by JIB-04 as found by MALDI-TOF MS.

BARBARA GORDON CASCELLA

St. Louis, Missouri · (314) 308-7514 · gordonbs@go.wustl.edu

EDUCATION

Ph.D., Chemistry, Washington University in St. Louis, St. Louis, MO (2008-2014)
A.M., Chemistry, Washington University in St. Louis, St. Louis, MO (2008-2012)
B.S., Chemistry (ACS certified), Rhodes College, Memphis, TN (2004-2008)

RESEARCH EXPERIENCE

Doctoral Research: Laboratory of Professor Liviu M. Mirica, Washington University in St. Louis

- Kinetically characterized three JmjC-domain containing histone demethylases (JmjC-HDMs) with respect to primary and secondary substrates.
- Discovered JmjC-HDMs have markedly low affinities for dioxygen through the development of a new in vitro oxygen consumption assay.
- Designed, synthesized, and tested a library of compounds as potential specific inhibitors of JmjC-HDMs.

Undergraduate Research: Laboratory of Dr. Loretta Jackson-Hayes, Rhodes College

- Identified two novel genes, *gmtA* and *gmtB*, as encoding putative GDP-mannose transporters in the filamentous fungus *Aspergillus nidulans*.
- Generated a stable *gmtA-GFP* expression construct used to determine the cellular localization of GmtA.

SKILLS AND TECHNIQUES

- *Protein chemistry:* protein expression; purification by affinity column, ion exchange, and size exclusion chromatography; western blotting
- *Enzymology:* enzyme kinetics; assay development and optimization; inhibitor design and synthesis; molecular modeling
- *Characterization:* UV-VIS, NMR, fluorometry, ESI-MS, and MALDI-TOF MS
- *Software:* KaleidaGraph, Prism, Origin, OpenEye, PyMol, ChemDraw

HONORS AND AWARDS

Teaching Citation Certification, Washington University in St. Louis	(2011-2014)
Dean's Dissertation Fellowship, Washington University in St. Louis	(2014)
Departmental Teaching Award, Washington University in St. Louis	(2009)
Senior Research Award, Rhodes College	(2008)
Department of Defense Breast Cancer Research Program	(2010-2012)
Undergraduate Research Fellowship, Merck Institute for Higher Education	(2007-2008)
Vice President, Iota Sigma Pi, Rhodes College	(2006-2007)

TEACHING EXPERIENCE

- *Teaching Citation Certification*, issued to graduate students who seek to gain teaching expertise through seminars, workshops, and additional teaching experiences than those required by the graduate department (Teaching Center at Washington University in St. Louis).
- *Teaching assistant* and POGIL recitation leader, Organic Chemistry I & II (Washington University in St. Louis).
- *Teaching assistant* and POGIL recitation leader, General Chemistry (Chem 112, Washington University in St. Louis).
- *Guest lecturer*, Inorganic Biochemistry (Chem 464, Washington University in St. Louis)
- *Teaching assistant and co-lecturer*, Chemical Safety (Chem 599, Washington University in St. Louis).
- *Head teaching assistant* and supervisor of eight graduate teaching assistants, Organic Chemistry Laboratory (Chem 262, Washington University in St. Louis).
- *Biology teacher* of high school students, Honors- and Regular-level Biology (Westminster Christian Academy, Town and Country, MO).
- *Teaching assistant* and recitation leader, General Chemistry (Chem 112, Washington University in St. Louis).
- *Teaching assistant* and recipient of the Outstanding Teaching Award, Organic Chemistry Laboratory (Chem 252, Washington University in St. Louis)
- *Bench mentor* of four undergraduate research assistants (Washington University in St. Louis)

PUBLICATIONS

Cascella, B.G. and Mirica, L.M. Survey of Simple Primary- and Secondary- Substrate Analog Inhibitors of Iron-Dependent Histone Demethylases. *In preparation.*

Cascella, B. G. and Mirica, L. M. Kinetic Analysis of Iron-Dependent Histone Demethylases: α -Ketoglutarate Substrate Inhibition and Potential Relevance to the Regulation of Histone Demethylation in Cancer Cells. *Biochemistry* 2012 51(44): 8699-8701

Jackson-Hayes, L., Hill, T.W., Loprete, D.M., **Gordon, B.S.**, Groover, C.J., Johnson, L.R., Martin, S.A. GDP-mannose transporter paralogues play distinct roles in polarized growth of *Aspergillus nidulans*. *Mycologia* 2010 102(2): 305-310

Jackson-Hayes, L., Hill, T.W., Loprete, D.M., Fay, L.M., **Gordon, B.S.**, Nkashama, S.A., Patel, R.K., Sartain, C.V. Two GDP-mannose transporters contribute to hyphal form and cell wall integrity in *Aspergillus nidulans*. *Microbiology* 2008 154: 2037–2047

PRESENTATIONS

(* denotes presenter)

Cascella, B.G.* and Mirica, L. M. Kinetic Analysis and α -Ketoglutarate Substrate Inhibition of Iron-Dependent Histone Demethylases”, **poster presentation**. Washington University Graduate Research Symposium, 2014. St. Louis, MO.

Cascella, B.G.* and Mirica, L.M. “Kinetic Analysis and α -Ketoglutarate Substrate Inhibition of Iron-Dependent Histone Demethylases”, **oral presentation**. Washington University Biochemistry and Molecular Biophysics Retreat, 2013. Cedar Creek, MO.

Cascella, B.G.* and Mirica, L.M. “Design of Specific Inhibitors for Histone Demethylases”, **poster presentation**. ACS Midwest Regional Meeting, 2011. St. Louis, MO.

Gordon, B.S.* and Mirica, L.M. “Development of Specific Inhibitors of JmjC-Domain Histone Demethylases”, **poster presentation**. Washington University Biochemistry and Molecular Biophysics Retreat, 2010. Cedar Creek, MO.

Gordon, B.S.*, Jackson-Hayes, L., Hill, T.W., Loprete, D.M. “Roles of two GDP-mannose transporters in cell wall stability in the filamentous fungus *Aspergillus nidulans*”, **poster presentation**. ASBMB Annual Meeting, 2008. San Diego, CA.

VOLUNTEER AND LEADERSHIP ACTIVITIES

- Volunteer at **Grace and Peace Women’s Shelter**, a refuge for homeless women in University City (Winter 2013, Winter 2014)
- Volunteer at **Catalysts for Change**, an outreach program that seeks to inspire interest in STEM fields among young females from St. Louis city schools (2012, 2014)

